

AD-A081 908

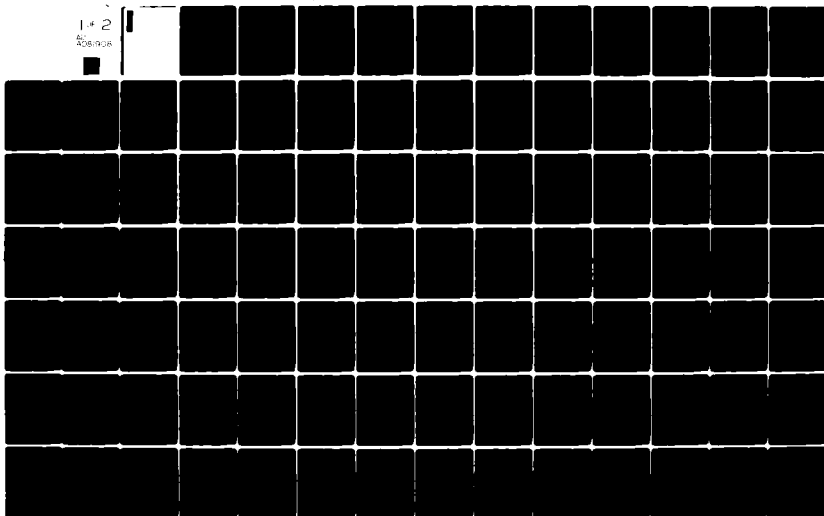
AIR FORCE INST OF TECH WRIGHT-PATTERSON AFB OH SCHOOL--ETC F/8 11/4
INVESTIGATION OF SAINT VENANT'S PRINCIPLE AS RELATED TO LAMINAT--ETC(U)
DEC 78 S R SMITH
AFIT/8AE/AA/78D-13

UNCLASSIFIED

NR

1-2

AL
208/008



AFIT/GAE/AA/78D-13

(1)

INVESTIGATION OF SAINT VENANT'S
PRINCIPLE AS RELATED TO
LAMINATED COMPOSITE PLATES

THESIS

AFIT/GAE/AA/78D-13 / Steven R. Smith
Capt. USAF

Approved for public release; distribution unlimited.

14

INVESTIGATION OF SAINT VENANT'S PRINCIPLE
AS RELATED TO LAMINATED
COMPOSITE PLATES

THESIS

Presented to the Faculty of the School of Engineering
of the Air Force Institute of Technology

Air University

in Partial Fulfillment of the
Requirements for the Degree of
Master of Science

by
Steven R. Smith, B.S.E.
Capt. USAF

Graduate Aeronautical Engineering

11 December 1978

Approved for public release; distribution unlimited.

Preface

In this thesis, I have analyzed the effects of three end conditions on laminated plates made of orthotropic plies. The behavior of orthotropic plates with a single fiber orientation were also considered to give the reader a point of reference as some work in this area has already been accomplished. The point of Saint Venant's validity was found in each case in order to show the region where this principle can be applied.

Completion of this study has required many hours of assistance from other individuals, and I would like to specifically acknowledge a few at this point. I am indebted to Capt. William Witt for sharing his knowledge and experience in the use of the finite element program employed in this study. I would also like to acknowledge Capt. Jerry Stinson for his helpful comments and guidance in the use of the CDC Cyber 74 Operating System. I must further acknowledge the comments and suggestions made by my thesis committee members, Dr. Ernest Dorko and Dr. Peter Torvik. As in any thesis work, the success and often the outcome depend largely on the guidance and assistance provided by one's thesis advisor. A mere acknowledgement cannot express the debt of gratitude I owe my thesis advisor, Dr. Anthony Palazoto for his valuable advice and direction given throughout this work. Finally, I must acknowledge my wife, Linda, for her encouragement and support through the many months of work represented here.

Contents

	<u>Page</u>
Preface	ii
List of Figures	iv
List of Tables	v
List of Symbols	vi
Abstract.	viii
I. Introduction	1
Problem Statement.	2
Background	2
II. Theory	7
Saint Venant's Principle	7
Two-Dimensional Model Implications	11
III. Numerical Analysis	14
General Comments	14
Parabolic Tension End Condition.	15
Parabolic Bending End Condition.	20
Clamped End Condition.	22
IV. Results.	24
Parabolic Tension End Condition.	25
Parabolic Bending End Condition.	28
Clamped End Condition.	29
V. Conclusions.	34
Bibliography.	37
Appendix A: Graphical Results of the Parabolic Tension End Condition.	39
Appendix B: Graphical Results of the Parabolic Bending End Condition.	55
Appendix C: Graphical Results of the Clamped End Condition.	71
Appendix D: Analytic Solution for the Orthotropic Plate.	94

List of Figures

<u>Figure</u>		<u>Page</u>
1	Elastic Body Considered by Zanaboni	9
2	End Perturbations Considered by Von Mises	9
3	End Conditions Investigated	16
4	Quarter Plate Convergence Study Meshes With Symmetry Conditions for Parabolic Tension End Conditions.	17
5	Full Plate Convergence Study With Parabolic Tension End Condition	19
6	Mesh Arrangements For Parabolic Bending and Clamped End Conditions.	21
Appendix A:	Parabolic Tension End Condition Results.	39
Appendix B:	Parabolic Bending End Condition Results.	55
Appendix C:	Clamped End Condition Results.	71

List of Tables

<u>Table</u>		<u>Page</u>
I	Graphite Epoxy Properties.	3
II	Parabolic Tension End Condition Uniform Stress Station	27
III	Parabolic Bending End Condition Uniform Stress Station	30

List of Symbols

A	area
C	arbitrary portion of a body
e_{ij}	strains
E_{11}	ply longitudinal modulus
E_{22}	ply lateral modulus
E_{xx}	plate longitudinal modulus (load direction)
F	force or a function
F_e	eigenfunction
G_{12}	ply shearing modulus
I	moment of inertia
M	moment
N_x	resultant force in x-direction (lb/in) on x plane
N_{xy}	resultant shear force in y-direction (lb/in) on x plane
N_o	average resultant force (lb/in)
P	load
P_i	arbitrary real number
q_i	arbitrary real number
Q	first statical moment area
R_1, R_2	surface regions
R	radius or distance
s	symmetric ply lay-up
S_1, S_2	surfaces
SIGMAX, SIGMAXY	normalized σ_x and σ_{xy} stresses
t	thickness

u_{ij}	displacements
V	shear force
x	longitudinal coordinate, along length of plate (in.)
y	lateral coordinate, along width of plate (in.)
β_{ij}	material constants
γ	arbitrary complex constant
ϵ	infinitely small dimension
μ	arbitrary complex constant
ν_{12}	Poisson's ratio
ϕ	Airy function
σ_x	stress in the x-direction
σ_{xt}	allowable tensile stress in the x-direction
σ_{xc}	allowable compressive stress in the x-direction
σ_{xy}	shearing stress
σ_y	stress in the y-direction
σ_{yt}	allowable tensile stress in the y-direction
σ_{yc}	allowable compressive stress in the y-direction
τ_{ij}	stress tension
ω	arbitrary complex constant

Abstract

The structural stiffness properties of composite laminated plates are experimental information needed in order to design aircraft components manufactured with composite materials. A common test used to obtain the necessary moduli is to apply a tension load on the ends of the specimen. Little study, if any, has been reported relating the application of the Saint Venant's principle within a multi-ply laminated plate.

Previously, researchers have shown that routine application of Saint Venant's principle in problems involving a single composite lamina is not generally justified. This study offers justification for using Saint Venant's principle in commonly laid-up graphite epoxy plate specimens. The boundary conditions considered are attempts at modeling varying end supports for an in-plane loading. The analysis has been carried out using a finite element model considering three aspect ratios: 3, 5, and 10.

INVESTIGATION OF SAINT VENANT'S PRINCIPLE
AS RELATED TO LAMINATED
COMPOSITE PLATES

I. Introduction

This thesis is an investigation of Saint Venant's principle in laminated composite plates by use of a finite element model. Saint Venant's principle has played a fundamental role in the application of classical elasticity theory to problems of practical interest. The statement of Saint Venant's principle does not lend itself to a concise formulation which can easily be translated into mathematical terms. The regions of validity of this principle in isotropic materials has been extensively studied and is readily available in literature [1]. However, the conquest of space and the rise in energy costs have made the Air Force, as well as the aerospace industry, very conscious of overall vehicle weights. This has lead to the use of lightweight laminated composite materials as primary load bearing structures. Advanced composite material use has prompted numerous studies of the behavior of orthotropic and anisotropic materials using either classical elasticity theory or experimental procedures to determine material properties. The use of the Saint Venant assumption is basic to the measurement of these material properties as well as to structural design.

Problem Statement

This investigation used the finite element analysis and classical laminated plate theory to model the stress gradients throughout plates with aspect ratios (i.e. length to width) of three, five, and ten. This modeling technique allows the monitoring of stress gradient propagation at discrete points within the plate. As the decay of the stress gradient would logically depend on the loading conditions, different loading conditions are considered. Detailed discussion of the loading conditions is found in the numerical analysis section. In addition, the material properties have a great bearing on the decay lengths. The anisotropic behavior of laminated plates is directly related to the ply orientations. In order to ascertain the effects of ply orientation (0, ± 45 , 90)s, (0, ± 45)s, (± 45)s, and (0, 90)s laminated plates are analyzed. The individual lamina characteristics were also investigated for 0deg, 90deg, and 45deg orientations. The analysis utilized the Control Data Corporation 6600/Cyber 74 computer system.

Throughout this study the material properties for graphite epoxy listed by Ashton, et al. [2] were used in calculating stresses. These properties are shown in Table I.

Background

An extended discussion of some of the theoretical formulations and further definitions of the Saint Venant's principle is presented in a subsequent section. For purposes of the

TABLE I
Graphite Epoxy Properties

Elastic Constants		* Allowable Stresses	
t	.1 in	σ_{xt}	70 ksi
E ₁₁	18.5 x 10 ⁶ psi	σ_{xc}	110 ksi
E ₂₂	1.54 x 10 ⁶ psi	σ_{yt}	6.5 ksi
G ₁₂	.85 x 10 ⁶ psi	σ_{yc}	15 ksi
ν_{12}	.25	σ_{xy}	8.5 ksi

NOTE: *Used as input parameter for OPSTAT only.

present discussion, Saint Venant's principle is assumed to be the ability to replace complicated end loads with statically equivalent loads. The errors caused by this assumption will die out or decay at a distance sufficiently far from the ends. This definition closely parallels those given in elementary solid mechanics texts such as reference [3]. The interpretation of this principle, as well as its application, is not entirely clear. The justifications for the use of this assumption are largely empirical; however, a large class of problems are idealized mathematically using this assumption. Many of these problems would be difficult, if not impossible, to solve using a classical elasticity approach. An example of a difficult problem which has been simplified by the use of this principle is the simple tension test in which the ends of the specimen are clamped. The Saint Venant's principle is invoked by assuming a uniform force distribution sufficiently

far from the clamping devices.

It is evident from the many formulations and examples given in the literature that the decay length or distance sufficiently far from the end forces in a body depends on the boundary conditions, body geometry, and material properties. It is reasonable to assume that the region of validity for the Saint Venant assumption will be different for isotropic, orthotropic and anisotropic materials.

Using classical elasticity theory, Horgan [4] has investigated the decay of end effects in anisotropic materials and has concluded that the end effects decay slowly in highly anisotropic materials. The slow decay of stresses with distance from the boundary of a body under the influence of self-equilibrating forces gives rise to questions about the measurement of elastic material properties. Folkes and Arridge [5] have shown experimentally that end effects in highly anisotropic polymers are very slow to decay and can give rise to erroneous material property measurements.

Choi and Horgan [6], again using classical theoretical elasticity, have investigated the decay lengths in an orthotropic material. Further detail of the mathematical solution employed by Choi and Horgan can be found in Appendix D. This analysis used a series representation of the solution to show that the decay lengths along the fiber axis of an orthotropic composite material is considerable in small aspect ratio plates.

The question of applications to multilayered composite plates of similar aspect ratios is prompted and is the subject

of this investigation. Also, questions are raised concerning orientations other than those along the fiber axis.

The study of off-axis behavior of composite materials has been reported by Pagano and Halpin [7]. This study indicates that significant shear and bending effects are present in tension tests which incorporate clamped ends. The experimental results show large, non-uniform displacements near the clamped edges and more uniform displacements near the center of an off-axis plate. Pagano and Halpin have shown large shear coupling effects in the off-axis specimens. Jones [8] has commented that these results indicate that a much longer gage length is needed in the off-axis tension specimen in order to reach a region in which Saint Venant's principle may be applied. Pagano and Halpin have further stated that a possible alternative is to test bidirectional ($\pm\theta$)s specimens for material properties.

Whitney [9] has shown that material properties measured in tensile tests of symmetric orthotropic laminates may be a function of the stacking sequence. He further notes that if end conditions due to clamping are neglected in off-axis tensile tests, erroneous values for E_{xx} will result. The magnitude of the error is inversely proportional to the aspect ratio of the plate. Wu and Thomas [10] have further pointed out that the clamped end condition induces a moment which is not a part of the Saint Venant effect. This further complicates the experimental study of this problem. Rizzo [11], using a finite element model, has pointed out that the rotation

of the specimen near the clamp is a function of the specimen aspect ratio and the rigidity of the clamp as well as material properties. He has concluded that rotating clamps would help reduce some of the end effects, and aspect ratios greater than six are needed. Richards, et al. [12] have confirmed the findings of Rizzo using another finite element model. This model utilized two-dimensional, constant strain triangles similar to the one used in this study.

Although much can be found in the literature about the orthotropic composite plate under end loads, little has been said about the laminated plate under similar loads. It is hoped that this study will help bridge that gap.

II. Theory

The theoretical considerations in this study may be summed up by answering the following questions. What is the generalized Saint Venant's principle? Where is this principle valid? Does the model used correctly transfer the load? When does laminated plate theory apply? The first two questions are discussed in the following subsection. The last two questions have to do with the implications of a two-dimensional model and are discussed in a separate subsection.

Saint Venant's Principle

In 1855 Saint Venant stated the principle of elastic equivalence of statically equal systems of forces. This principle was stated in justification of a result which applied rigorously to a load condition other than the one under study. The original statement of the principle has been greatly generalized to include all types of loading systems. Because of the fundamental nature of this principle in solid mechanics, further study of its application in orthotropic and anisotropic materials is needed, but a solid understanding of the basic concepts related to the principle is required.

One formulation of Saint Venant's principle, attributed to Zanaboni by Fung [13], considers strain energy density as a measure of the region of validity in an arbitrary body. This density is shown to decrease in cross sections farther removed from the surface where a generalized force distribution anomaly

occurs. If one is sufficiently removed from the force anomaly, the strain energy density is negligible. The region of validity of Saint Venant's principle under this formulation is that region where the strain energy density to the force anomaly is negligible. The Zanaboni formulation is now as follows:

Let S_1 and S_2 be two nonintersecting sections of a body outside the sphere shown in Fig 1. If the section S_2 lies at a greater distance than the section S_1 from the sphere in which a system of self-equilibrating forces acts on the body, then the strain energy density caused by surface tractions at R_2 is less than the strain energy density caused by surface tractions at R_1 , where R_1 and R_2 are the surface areas at cross sections S_1 and S_2 , respectively.

The significance of this result is that at some point sufficiently far from the sphere, the effects of the force system is negligible. The effect of the true end condition load is unimportant if Saint Venant's principle is applicable. This can be further generalized to justify assuming a uniform edge loading where a non-uniform edge loading occurs.

Another formulation of Saint Venant's principle due to Von-Mises is presented to give further insight; details can be found in Fung. Von-Mises considered four examples of forces on the boundary of a half space. The forces, F , acted on a small circle of diameter, ϵ , as shown in Fig 2. The order of magnitude of the largest stress component at an arbitrary point which lies a distance R from the circle

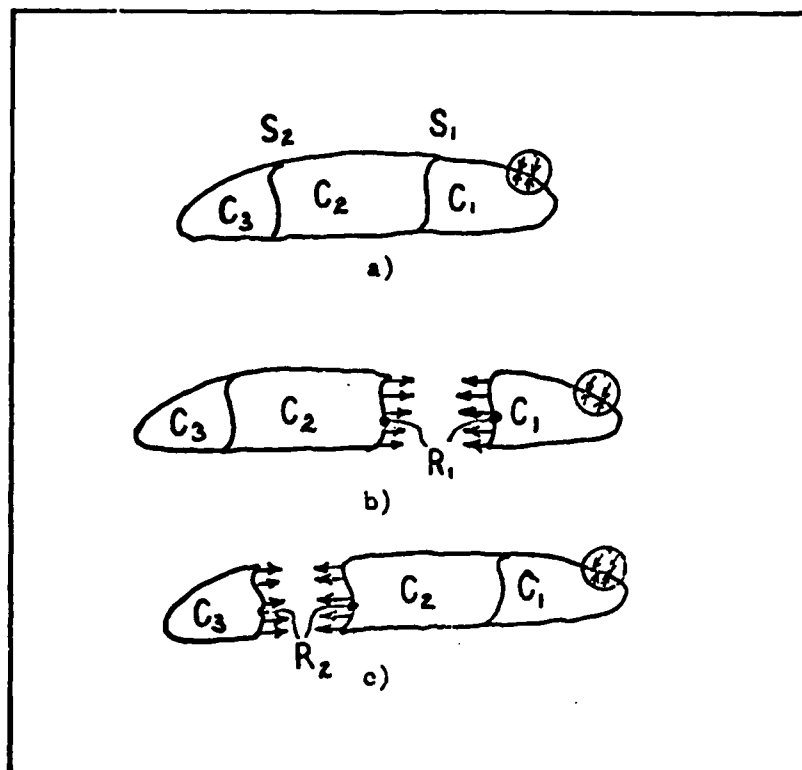


Fig 1. Elastic Body Considered by Zanaboni

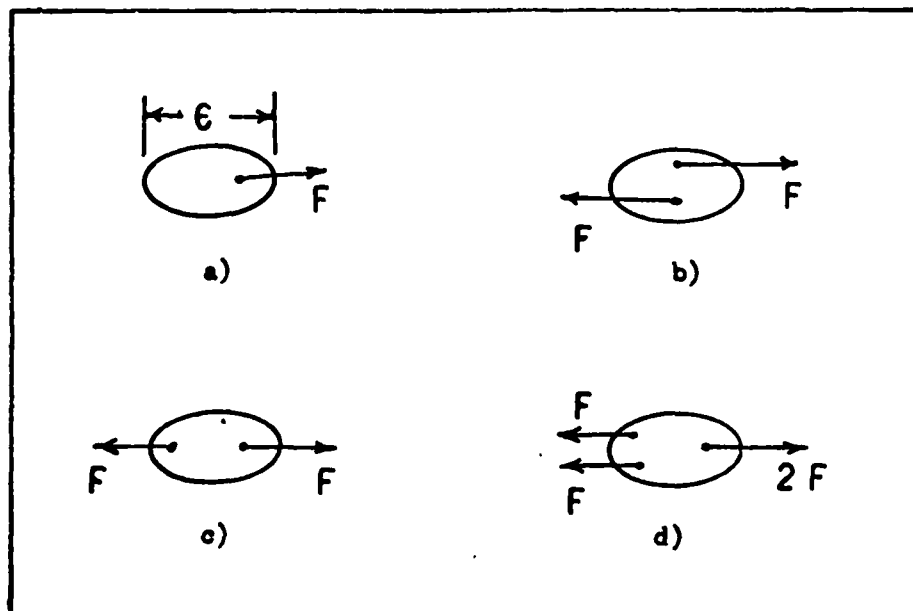


Fig 2. End Perturbations Considered by Von Mises

is $\sigma_{\text{MAX}} = F/R^2$ for case a, and on the order of $(\epsilon/R)\sigma_0$ for cases b through d where σ_0 is the uniform stress value that would be assumed at a suitable distance. This leads to the conclusion that end effects and surface stress variations become negligible at some point sufficiently far from the edge.

Another example of the decrease in the end condition force has been demonstrated by Timoshenko and Goodier [1] for an isotropic plate using a classical elasticity series solution. This example shows a plate under a single point compressive load P at the center of the short ends. The stress at cross-sections along the plate length are shown to uniformly approach P/A , where A is the cross-sectional area at a distance equivalent to the width of the plate. At this distance, the load could be assumed equal to a uniform stress, $\sigma_0 = P/A$. This example is considered as justification in using a simple equivalent stress for other loading conditions by invoking Saint Venant's principle at a particular distance [4]. In general, this is not true for orthotropic composite materials, as shown by Choi and Horgan. Thus, the question is raised pertaining to the region of validity in laminated composite plates. The study of this region has obvious utility in design and measurement of material properties.

The author has found several practical descriptions of Saint Venant's principle in the literature of which two are mentioned here. The first is due to Filonenko-Boradich [14] and is repeated here: "At points in a solid which are sufficiently far from the surfaces of application of external loads,

stresses depend very slightly on the particular manner in which the loads are applied." One drawback in this definition of Saint Venant's principle is the lack of load definition. A better definition, and the one which has been used in this study, has been offered by Sokolnikoff [15]. His statement of Saint Venant's principle is as follows:

If some distribution of forces acting on a portion of the surface of a body is replaced by a different distribution of forces acting on the same portion of the body, then the effects of the two different distributions on the parts of the body sufficiently far removed from the region of application of the forces are essentially the same, provided that the two distributions of forces are statically equivalent.

Here static equivalence refers to equivalent resultant forces and moment. This definition gives the necessary equivalence of force guidelines.

The previous definitions and concepts have answered the first two questions raised at the opening of this section. The previous discussion has given some insight into how the Saint Venant assumption was originally employed and how it has been generalized into a fundamental building block of solid mechanics. This study has applied the same definitions to the laminated composite plates to give examples and to determine the appropriate decay lengths of specific end condition effects.

Two-Dimensional Model Implications.

The application of Saint Venant's principle in an elastic solid has to be three-dimensional for complete validity. In order for a two-dimensional model to be valid, the state of

stress in the third dimension must be shown to have negligible affect on the stress gradients in the plane of the two dimensions modeled. Filonenko-Boradich has stated that the surface of force application must be small compared to the overall dimensions of the body, and the surface of force application must be at least of the same order as the smallest body dimension for validity of the Saint Venant assumption. This implies that Saint Venant's principle cannot be applied across the thickness of a plate. However, classical elasticity theory has modeled thin plates as a two dimension body with great success. The Timoshenko and Goodier plate example previously discussed uses this two-dimensional model with very good results. This raises the question of validity in the laminated composite plate and plane stress modeling in such plates.

In the work of Pipes and Pagano [16], the interlamina stresses were studied. These stresses were found to be significant only in regions near the free edge approximately equal to the laminate thickness where the thickness was at least an order of magnitude smaller than the other dimensions. Justification for the plane stress model and for the invocation of Saint Venant's principle in the third dimension exists if that dimension is small compared to the other two dimensions.

If one examines classical laminated plate theory [3], it is found that the stress gradient across the lamina thickness is averaged out of the problem and only the two-dimensional portion of the problem is considered. If the interlamina stresses are not significant, one might also ask if the

averaging of the stress across a lamina as in classical laminated plate theory has an appreciable affect on the validity of solutions. The analysis of Rizzo and that of Richards, et al., are essentially dealing with a plate of a single off-axis lamina. The two-dimensional models used in these studies showed a high correlation with experimental results.

Probably the most attractive reason for using a two-dimensional model is the level of computational difficulty compared to the three-dimensional problem. The two-dimensional solution has given good results in the isotropic case and in the laminated composite examples cited, with less computation. The level of computational difficulty in many cases can be directly tied to the cost of computer time and ultimately, in some cases, to the ability to obtain a solution for a particular problem.

III. Numerical Analysis

The finite element method was used to generate the data obtained in this thesis. The finite element models incorporated in the numerical analysis are discussed herein.

General Comments

In the previous sections, it was pointed out that a point exists sufficiently far from the end conditions where the stress no longer becomes affected by the loading conditions. In order to locate this point, an exact solution becomes necessary. Since exact solutions are difficult, if not impossible to obtain for composite material problems, it is useful to carry out approximate numerical solutions and place a level of confidence on the results obtained.

The level of confidence placed on a given solution obtained due to a particular finite element model may be associated with the error involved in the technique used to obtain the solution. Durocher and Palazotto [17] have pointed out that the sources of error can be classed as idealization, discretization and manipulative errors. Replacing an anisotropic or orthotropic material with a homogeneous continuum is a typical example of the idealization error. Errors of this type are common to all engineering models. The discretization error is due to replacing the continuous medium with finite elements. The manipulative errors are associated with truncation and round off produced by computer programming. The latter sources of

error are not inherent to the engineering model. Thus, a convergence study is required to guarantee the numerical solution approaches the exact or idealized solution. The convergence of the chosen numerical models will be discussed in subsequent sections.

The finite element program used in this analysis was developed by Venkayya [18] of the Air Force Flight Dynamics Laboratory. Classical laminated plate theory and the displacement method of finite element is used in this program. The program can be utilized to analyze plates with several combinations of ply orientations as well as orthotropic plates. This study employed $(0, \pm 45, 90)_s$, $(0, 90)_s$, $(0, \pm 45)_s$, and $(\pm 45)_s$ oriented plates along with plates of 0deg, 90deg, and 45deg fiber orientations. The program incorporated several standard elements, including the constant strain triangle which was exercised in this study. Relative percentage of ply orientations contained in the laminate and element material properties were applied in calculating the elemental stiffness matrix.

The necessary characteristics of proper convergence is noted by Durocher and Palazotto. Mesh refinement has been carried out to enforce convergence. The specific end conditions will now be addressed using Fig 3.

Parabolic Tension End Condition

The parabolic tension end condition is an attempt to model a non-uniform tensile end force in which the edges of the plate are allowed to slip. The plate is loaded at the ends with a

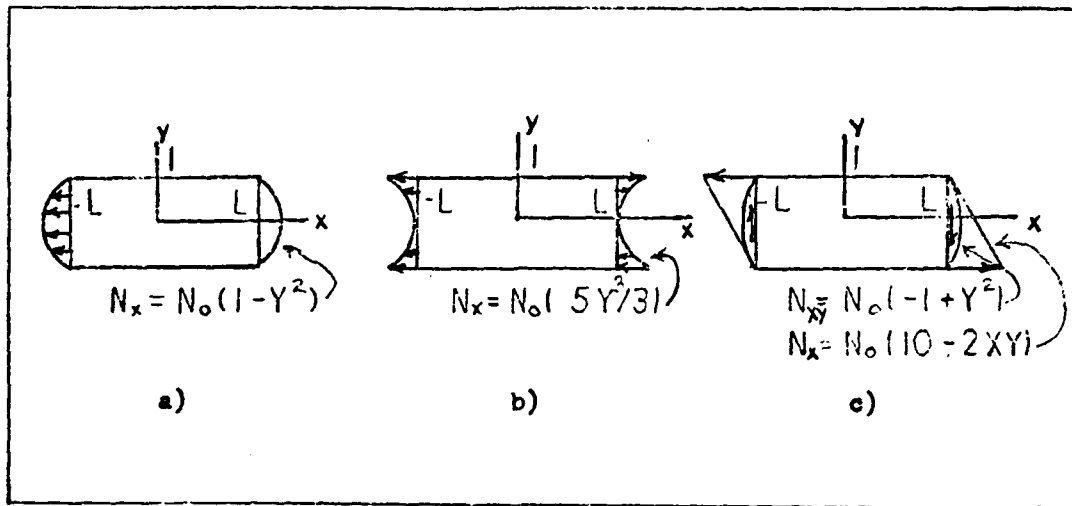


Fig 3. End Conditions Investigated

force distribution per unit thickness given by the equation

$$N_x = N_0(1 - y^2) \quad (\text{III-1})$$

where N_x is the end force, N_0 is the normalization force, and y is the coordinate across the width of the plate with zero at the center. The load is symmetric about the x -axis and the y -axis, thus only a quarter of the plate need be modeled. The material properties for all the laminated plate orientations and the 0deg and 90deg fiber oriented plates are symmetric about these axes also. The exception to this is the 45deg fiber oriented plate which will be discussed separately. The first quadrant meshes used for these cases are shown in Fig 4.

In order to model the high stress gradients with constant strain triangles, a more refined mesh is needed over those areas. This dictates a larger number of elements near the

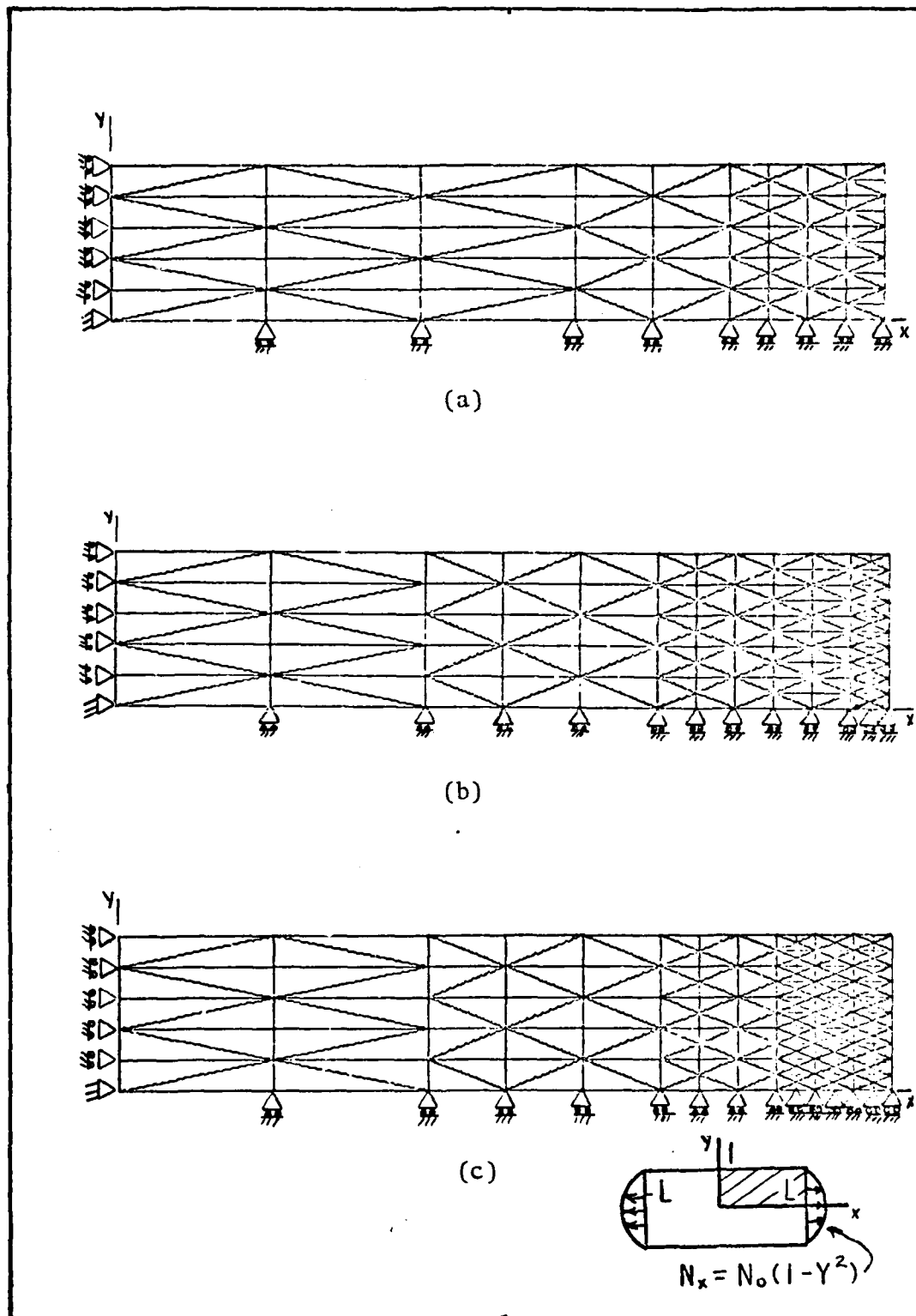


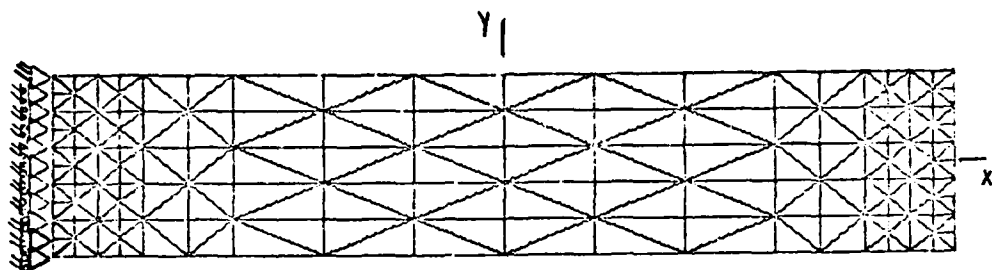
Fig 4. Quarter Plate Convergence Study Meshes With Symmetry Conditions for Parabolic Tension End Conditions

loads. The symmetry conditions require restraints as shown in Fig 4 along the quadrant boundaries.

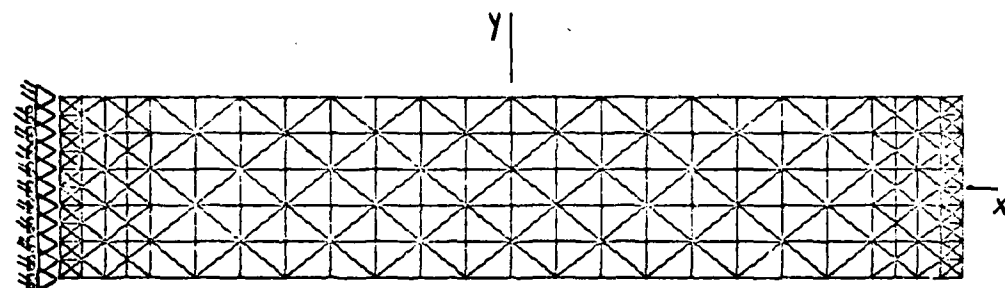
As constant strain triangles were used, the centroid coordinates of the triangle are employed for stress comparison and the loci of points must be established in the analysis for convergence to a particular solution. The end condition under study was also investigated by Choi and Horgan in their analysis of an orthotropic graphite epoxy plate. The series solution obtained by Choi and Horgan was compared to the results in the convergence study.

Three mesh arrangements were studied in order to estimate convergence. Stresses were checked along the width of the plate at various stations on the x (length) axis. The σ_x stress across width sections must average to 2/3 of the stress normalization factor σ_0 , and σ_y stresses must average to zero. This was the case in the three mesh arrangements to within five percent. The fine mesh arrangement shown in Fig 4-C had average stresses σ_x values within one percent of 2/3 σ_0 . All three solutions compared favorably with the Choi and Horgan solutions.

As previously touched on, the 45deg oriented fiber plate could not be considered symmetrical because of material properties. This is in contrast to the ± 45 deg combination as in these laminates the plies act together as one material. Figure 5 depicts the boundary conditions utilized for the 45deg fiber oriented plate and the mesh arrangements which were used for the full plate convergence study. Two mesh arrangements were



(a)



(b)

Diagram of a rectangular plate with rounded ends, showing the coordinate system and the equation $N_x = N_0(1 - y^2)$.

Fig 5. Full Plate Convergence Study With Parabolic Tension End Condition

employed in this convergence study and the results were similar to those obtained with the quarter plate mesh arrangements. In both the quarter plate and full plate mesh arrangements, the loads were applied to the end along $X = L$.

Parabolic Bending End Condition

The parabolic bending end condition was considered to find the effects of end rotations on the decay lengths for Saint Venant's assumption. This represents a pure bending load which is not found in practical application, but this condition gives insight to the in-plane rotational problem found in rotating clamping devices. The force distribution per unit width is given by

$$N_x = N_o (5y^3/3) \quad (\text{III-2})$$

It should be noted that the term parabolic bending refers to the shape of the loading curve as shown in Fig 6-a. Again, N_x is the end force, N_o is the normalization force, and y is the coordinate across the plate. As the full plate is modeled, all laminates and single fiber oriented plates were analyzed using this mesh arrangement. This mesh is the same as that applied to the parabolic tension case. Timoshenko and Goodier have shown that this loading condition produces a straight line function when the point of Saint Venant's principle validity is reached.

The average σ_x stress for this case is zero. All loci of centroid points across the width of the plate averaged to zero

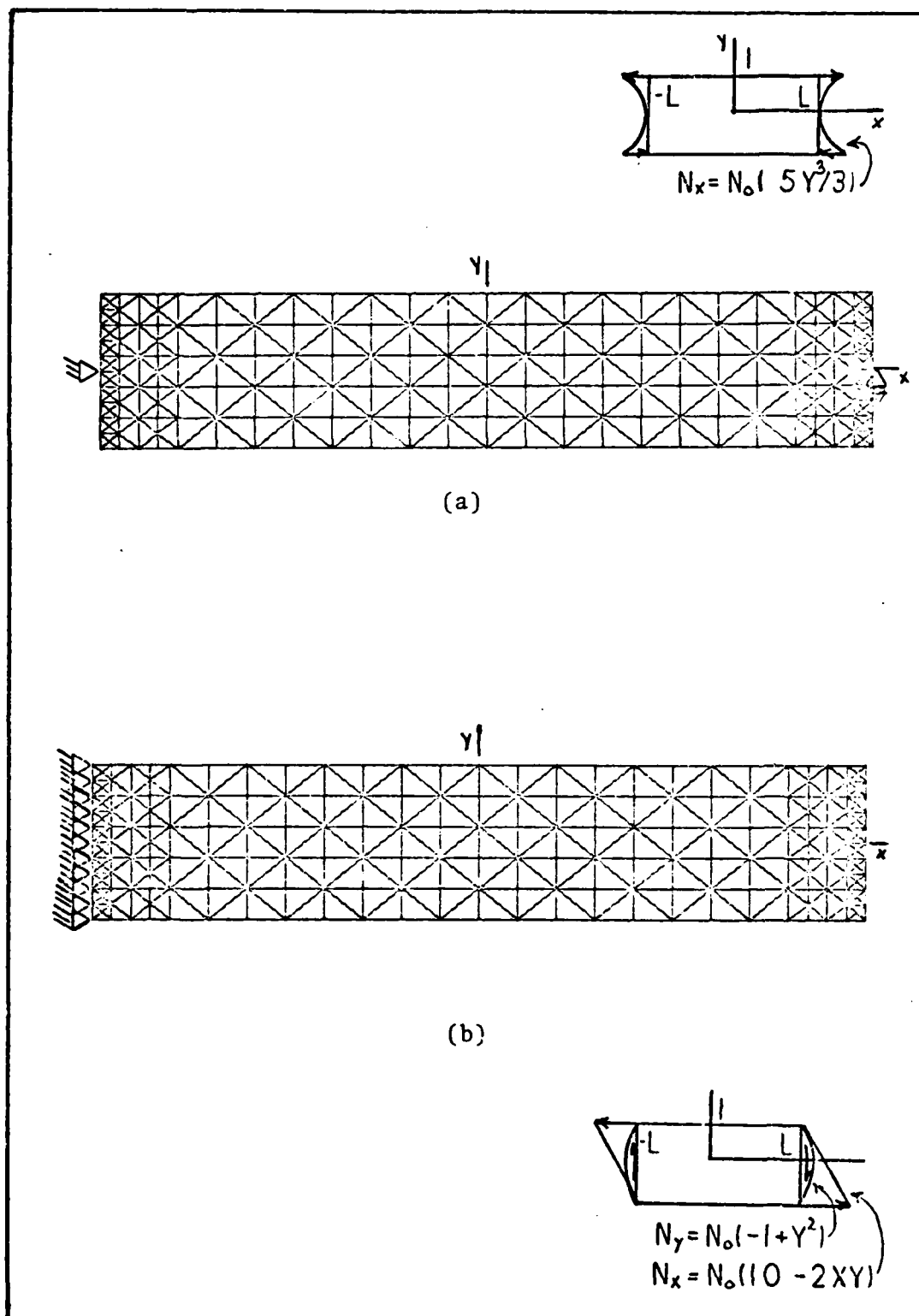


Fig 6. Mesh Arrangements For Parabolic Bending and Clamped End Conditions

within one percent. This load was positioned on both ends of the plate.

Clamped End Condition

The final end condition considered was the clamped end condition. This is a condition normally associated with experimental tension specimens. The shear-moment coupling is inherent in off-axis plate tests and would only be present in symmetric laminated composite plates if rotating clamping devices were used with an eccentric load. This loading was investigated primarily to show the effects of shear on the finite element model and to specifically point out difficulties encountered in using the constant strain triangle. Wu and Thomas call attention to the fact that bending and shear coupling effects are not Saint Venant type problems but do exist in real clamped end tension test. The end condition load functions are

$$N_x = N_o(10 - 2XY) \quad (III-3)$$

and

$$N_{xy} = N_o(-1 + Y^2) \quad (III-4)$$

Here again, N_x is the end force in the x direction, N_o is the normalization factor and X and Y are the plate coordinates. N_{xy} is the end force in the y direction and provides the shear to compensate for the moment produced by the 2XY term in N_x . The same full plate mesh was utilized in this analysis as was employed in the previous end condition cases.

The load functions given above are more simple than those

used by Rizzo and can be derived by an Airy type function

$$\phi = bxy + \frac{c}{2}y^2 + \frac{d}{6}xy^3 \quad (\text{III-5})$$

where b, c, and d are arbitrary constants. The resulting load functions are a uniform tension added to a uniform in-plane bending moment and a parabolic shearing force which is required for moment equilibrium. These loads will give insight into the actions of various plies and the dependence on ply lay-up for strength measurements in laminated plates.

Although the uniform loading in the x direction and the parabolic shear loading representation of the clamped end problem is simplistic, the insight gained from this end condition will give the reader some feeling for the difference between the Saint Venant decay length problem and the moment-shear coupling problem in a true clamped end plate.

IV. Results

The results of the finite element analysis of the three end conditions will be discussed in this section. Graphical representation of the normalized stress dissipation across the width of the plate at specific stations along the length of the plate are included in Appendices A through C. The normalized stress values are given by

$$\text{SIGMAX} = \sigma_x / \sigma_0 \quad (\text{IV-1})$$

and $\text{SIGMAXY} = \sigma_{xy} / \sigma_0$

where SIGMAX and SIGMAXY are normalized stresses, σ_x and σ_{xy} are the stress in the x direction and shearing stress respectively, and σ_0 is the stress normalization factor computed by dividing the resultant force normalization factor, N_0 , by the width of the plate.

The point of Saint Venant's principle validity is described by a constant uniform state of stress in each case. The decay length of the σ_x stresses were chosen by comparing the σ_x values along a particular loci of mesh element centroids, across the width of the plate, with the constant state of stress for the particular end condition. The station or x-coordinate which defined the region of Saint Venant's principle validity was chosen as that station where the locus of stress values was within ten percent of the constant state of stress. The ten

percent margin is consistent with the mesh size, the program round-off error, and the ability to practically measure stress in an actual application.

In all cases, the σ_x and σ_y direct stresses acted similarly in that the constant stress value was reached at the same station. The σ_x stresses were highest in the 0deg plies, followed by the ± 45 deg plies. The lowest σ_x stress values were evidenced in the 90deg ply. This is due to the relative stiffness properties. Discussion of the individual end conditions follows.

Parabolic Tension End Condition

The 0deg fiber oriented plate results, shown in Fig A-1, agree closely with the results obtained by Choi and Horgan. It was found that this case produced one of the longest decay lengths and, thus, one of the smallest areas for use of the Saint Venant's principle. Larger areas of Saint Venant's principle validity were found for the 90deg and 45deg fiber oriented plates.

The laminated plates were investigated for three aspect ratios (length to width, L/W). The constant uniform state of stress for this end condition averaged across the plies of the laminate is $\frac{2}{3}\sigma_0$. However, a different value for the constant uniform stress was found for each ply according to the relative stiffness of the ply. All laminas had the same percent thickness for a given ply lay-up, and all plates had the same total thickness. Thus, plates with less laminas had thicker laminas

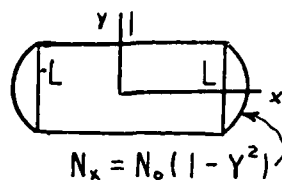
than plates with more laminas and exhibited lower stress gradients.

As shown in Table II, the percent of the plate length where the stresses reach a value within ten percent of the uniform value is on the order of one plate width for aspect ratios of five and ten, with the exception of the (0, 90)s plate. In this plate the same regions of constant uniform stress were not exhibited for both plies in the three and five aspect ratio cases, and the decay length is much longer in the $L/W = 10$ case as compared to the other laminates. This is attributed to the greater stiffness of the 0deg ply in tension. The stress values differ in this case by a factor equal to the ratio of E_{11} to E_{22} , which would be expected for a pure tension loading.

The aspect ratio of three had regions of stress values within ten percent of the constant uniform stresses for the (± 45)s and the (0 ± 45)s plates. The (0, ± 45 , 90)s case exhibited dissimilar ply actions. Again, this is attributed to the stiffness properties. The (0, 90)s plate did not reach a uniform stress value for the aspect ratio of three. It must be pointed out that if a margin of less than ten percent were used for the aspect ratio of three, none of the plates would reach the uniform stress value for this end condition.

As shown in Fig A-3, the stress values for the 45deg fiber oriented plate had a certain amount of variation about the mean value. This phenomena is specifically pointed out since all off-axis plies exhibited this variation in stress values.

The variation appears to be related to the shear stresses in the problem as is later evidenced in the clamped end condition.



$$N_x = N_o(1 - y^2/h^2)$$

TABLE II			
Parabolic Tension End Condition			
Uniform Stress Station			
Orientation	L/W = 3	L/W = 5	L/W = 10
0	--	.43L	--
90	--	.86L	--
45	--	.73L	--
(±45)s	.63L	.77L	.87L
(0,±45)s	.43L	.63L	.82L
(0,90)s	¹	.26L ⁴ , .43L ⁵	.63L
(0,±45,90)s	.47L ² , .57L ³	.77L	.88L
Note: ¹ No uniform stress value ² ±45 plies ³ 0 and 90 plies ⁴ 90 plies ⁵ 0 plies			

Graphical results for this end condition can be found in Appendix A.

Parabolic Bending End Condition

This end condition reaches a constant straight line stress value for σ_x as shown by the figures in Appendix B. This agrees with the results Timoshenko and Goodier predicted for isotropic materials. This constant straight line stress value was utilized to define the region of Saint Venant's principle validity. As in the previous end condition, the single fiber orientation plates were investigated for the aspect ratio of five. Again, the 0deg fiber oriented plate has the longest decay length due to the relative orientation stiffness properties along the load axis. The role played by the relative stiffness properties can be seen in Fig B-4 thru 5 for the (0, ± 45 , 90)s plate. This is similar to what was found in the parabolic tension cases. As in the previous end condition, all of the decay lengths are within one plate width along the length for all cases considered with exception to the (± 45)s plate with aspect ratio of three. In the aspect ratio of the three, the higher stress gradients created by the end loads start to interfere with one another before a uniform load can be reached. This caused the drastic decrease in the region of Saint Venant's validity for the (± 45)s plate.

The (0, 90)s plate displayed a much different behavior under this loading than under the parabolic tension action. This is attributed to the stiffness properties of each ply. The 0deg ply is much stiffer in tension than compression due to the values of the moduli, E_{11} and E_{22} . The 90deg ply has the same moduli, but the role of each is reversed. Due to

Poisson's ratio effects, the 90deg ply carries more of the load in this case than in the parabolic tension loading. However, the stress values in the 90deg ply is still less than those in the 0deg ply.

The graphical results of Appendix B, once again, depict variations in normalized stress values for different ply lay-ups due to differences in ply stiffness properties, as all plies have the same relative thicknesses for a given laminated plate. The 0deg lamina carried most of the stress in the plate, as was found in all end conditions investigated. This is due to the increased stiffness properties of this orientation in the direction of the loads. A tabulation of the uniform stress positioning for this end condition can be found in Table III.

Clamped End Condition

The clamped end condition was investigated to show constant strain triangle modeling difficulties and the difference between Saint Venant end effects and the moment-shear coupling found in a truly clamped end with rotating clamping devices and eccentric loading. The clamped effect is a displacement end condition. The program used in this investigation did not have provisions for end displacements; however, the resultant force end condition produced displacements which agree with those reported by Pagano and Halpin. The clamped end condition was examined for the aspect ratio of five in the single fiber oriented plates. The laminated plate cases were analyzed for aspect ratios of three and five. The graphical

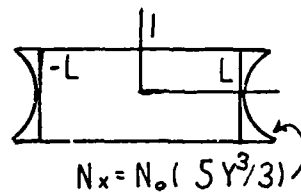


TABLE III			
Parabolic Bending End Condition			
Uniform Stress Station			
Orientation	L/W = 3	L/W = 5	L/W = 10
0	--	.76L	--
90	--	.93L	--
45	--	.83L	--
(±45)s	.17L	.76L	.87L
(0,±45)s	.73L	.82L	.92L
(0,90)s	.67L	.76L	.92L
(0,±45,90)s	.56L ¹ .76L ²	.76L	.83L
Note: ¹ ±45 plies ² 0 and 90 plies			

results are presented in Appendix C.

From elementary theory, one would expect constant shearing forces throughout the length of the plate and decreasing stresses due to moment as the center is approached. The center σ_x stress should be the constant tension stress value. The results for this end condition generally bears this out with variations due to material stiffness. The exception is the

off-axis plies. As displayed in Fig C-3, the off-axis plate shearing stresses did not reproduce the loading condition curve as would be expected. In checking the average stress values at a given station along the x-axis, poor agreement was found with the input load function. In the multilayered plate, the -45deg ply complements the 45deg ply such that, when considered together, the σ_{xy} curve has a similar shape as the shear end loading curve. In all of the laminated plate graphical results of Appendix C, the action of the ± 45 plies are considered as acting together and the averaged finite element points are shown to depict the stress variations per ply.

As the aspect ratio was increased from three to five in the course of this investigation, the variation of shearing stresses mentioned under the parabolic tension discussion increased. The variation affected the mean value of the shearing stress curves from station to station as displayed in the figures of Appendix C. The variation appears to be related to the orientation of the fibers within a given constant strain triangle. The ± 45 deg plies were affected more than the other orientations as the off-axis orientation is more sensitive to shear loads. A possible problem with modeling off-axis materials with a constant strain triangle is that the element load conditions are not the same as found in the continuum. In all cases, the σ_y stresses varied with the shearing stresses as to keep the constant strain triangle in equilibrium. Richards, et al., experienced variations in off-axis stress results and used averaging over a very refined mesh to compensate for the

variations. Further mesh refinement was prohibited in this study because of computational storage requirements. The variation of the mean value of shearing stresses for the $\pm 45\text{deg}$ plies is on the order of ten percent and for the 0deg and 90deg plies about two percent. It is felt that this is the order of error induced by this phenomena. The σ_x stresses did not exhibit the above mentioned variations. If variations were present in the σ_x results, it was within the accuracy of the computations.

The practical insight given is that the stress measurement in off-axis plies can be drastically different than would be expected from elementary theory, discounting the variations mentioned above. This has implications for instrumenting laminated plates for stress measurements. As shown by the figures in Appendix C, the variations in stress values per ply in a laminated composite plate can be considerable. The exception to this is the $(0, 90)_s$ plate shear stress results which indicate an equal division of the load between the plies. The clamped end effects are totally unrelated to the Saint Venant end effect and must be accounted for in material property measurements. This is born out in the $\pm 45\text{deg}$ ply results as the end load causes a constantly changing σ_{xy} shear stress in addition to the constantly σ_x direct stress. In this case a region of Saint Venant's principle validity could be found if the σ_x stress reached a uniform $\frac{My}{I} + \frac{P}{A}$ distribution and the σ_{xy} stress reached a uniform $\frac{VQ}{It}$ stress value. However, no such station was found as the Saint

Venant σ_x and σ_{xy} stress distributions were the input functions at the loaded edge.

In all the figures in Appendices A through C, the four stations depicted are on the positive half-length. The percentage of plate half-length is shown in each figure.

V. Conclusions

The basic conclusions of this investigation is that material properties of laminated composite plates can be measured with some degree of confidence in plates with aspect ratios greater than five, but some striking differences exist from one lamina to another in a multi-layered plate. The relative stiffness properties of a given lamina greatly affect the stresses measured. In some ply lay-up and end condition combinations, the difference in lamina stresses affects the decay lengths. These differences in lamina stresses could give rise to erroneous stress measurements if strain gages are employed only on the outer lamina of a plate. In most cases with aspect ratios of five or greater, the region of Saint Venant's validity was reached at a distance equal to one plate width from the edge. Caution should be exercised, however, in applying this result to other end conditions as the lamina stresses vary greatly with ply lay-up and end condition.

In general, for the parabolic tension and parabolic bending condition, the region of Saint Venant's principle validity can be found. The clamped end condition points out the further complications incurred in a tension test of the laminated plate. This end condition affects laminated plates in a manner similar to the results reported by Wu and Thomas for off-axis plates. The stress gradient due to moment does not

dissipate to a uniform stress except at the center of the plate, and shearing stresses are always present. If one examines the direct σ_x and σ_y stresses, a similar dissipation pattern is found. The highest stress gradients are found in the stiffer laminas (i.e., the 0deg ply exhibits higher direct stresses than the ± 45 deg plies, and the 90deg plies exhibit the smallest stress values). This is in contrast to the shearing stresses where the ± 45 deg plies exhibit the highest stress magnitudes, and the 0deg and 90deg plies act together.

The aspect ratio of three in all cases may not give a region of Saint Venant's validity depending on the accuracy required. For this investigation, the ten percent uniform stress region was only a small region in the center, and for uniformity of stress less than ten percent, there is no region of Saint Venant's validity.

More can be drawn from this study if one thinks of the possibility of superimposing the stress fields produced by the three stress fields. This would model a non-uniformly clamped end with a rotating grip. In this case, the Saint Venant end effects would decay at about one plate width from the loaded edge, but the stress field due to the moment-shear coupling effects would not dissipate. The simple load per unit area, P/A , stress field would only be realized at the center of the plate, regardless of aspect ratio. In addition to the P/A stress field for σ_x , a parabolic shearing stress would be present. This leads to the conclusion that

meaningful σ_x stress measurement can only be made at the center of the plate in material property calculations. Shearing stress measurements would be greatly influenced by the shear-moment coupling. In addition, the stress gradients per ply orientation are not the same. This can lead to erroneous stress measurements if only the outer plies are instrumented.

It is further concluded that not enough data has been gathered to adequately investigate the variation in stress values found in the off-axis plate cases and in the clamped end condition where shear loading is used. The effects of using constant strain triangles with off-axis orthotropic materials needs further study. It is felt that further mesh refinement and averaging stresses across several triangles would produce better results; however, computer storage limitations are a problem with the program utilized herein. This aspect of finite element analysis merits further study.

Bibliography

1. Timoshenko, S.P. and J.N. Goodier. Theory of Elasticity. Third Edition. New York: McGraw-Hill Book Company, 1970.
2. Ashton, J.E., J.C. Halpin, and P.H. Petit. Primer on Composite Materials: Analysis. Westport, CT: Technomic Publishing Co., Inc., 1969.
3. Popov, E.P. Introduction to Mechanics of Solids. Englewood Cliffs: Prentice-Hall, Inc., 1968.
4. Horgan, C.O. "The axisymmetric End Problem for Transversely Isotropic Circular Cylinders." International Journal of Solid Structures, 10:837-852 (1974).
5. Folkes, M.J. and R.G.C. Arridge. "The Measurement of Shear Modulus in Highly Anisotropic Materials: The Validity of St. Venant's Principle." Journal of Physics D: Applied Physics, 8:1053-64 (1975).
6. Choi, I. and C.O. Horgan. "Saint Venant's Principle and End Effects in Anisotropic Elasticity." Transaction of the American Society of Mechanical Engineers: Journal of Applied Mechanics: 424-430 (September 1977).
7. Pagano, N.J. and J.C. Halpin. "Influence of End Constraint in the Testing of Anisotropic Bodies." Journal of Composite Material, 2:18-31 (January 1968).
8. Jones, R.M. Mechanics of Composite Materials. Washington, D.C: Scripta Book Company, 1975.
9. Whitney, J.M. Testing and Characterization of Composite Materials. Technical Report AFML-TR-71-124. Wright-Patterson AFB, OH: Air Force Materials Laboratory, June 1971.
10. Wu, E.M. and R.L. Thomas. "Off-Axis Test of a Composite." Journal of Composite Materials, 2:523-56 (October 1968).
11. Rizzo, R.R. "More on the Influence of End Constraints on Off-Axis Tensile Tests." Journal of Composite Materials, 3:202-19 (April 1969).
12. Richards, G.L., T.P. Airhart, and J.E. Ashton. "Off-Axis Tensile Coupon Testing." Journal of Composite Materials, 3:586-89 (July 1969).

13. Fung, Y.C. Foundations of Solid Mechanics. Englewood Cliffs: Prentice-Hall, Inc., 1965
14. Filonenko-Boradich, M. Theory of Elasticity. New York: Dover Publications, Inc., 1965.
15. Sokolnikoff, I.S. Mathematical Theory of Elasticity. New York: McGraw-Hill Book Company, 1956.
16. Pipes, R.B. and N.J. Pagano. "Interlaminar Stress in Composite Laminates Under Uniform Axial Extension." Journal of Composite Materials, 4:538-548 (October 1970).
17. Durocher, L.L. and A.N. Palazotto. "Notes For Computer Methods in Stress and Structural Analysis." Lecture material used in MC6.41, Fundamentals of Matrix Structural Analysis. School of Engineering, Air Force Institute of Technology, Wright-Patterson AFB, Ohio.
18. Venkayya, V.B. Finite element program OPSTAT, written at the Air Force Flight Dynamics Laboratory, Wright-Patterson AFB, Ohio.

Appendix A

Graphical Results of the Parabolic

Tension End Condition

The following figures resulted from the use of the quarter plate mesh shown in Fig 4-C with the exception of Fig A-3, which utilized the full plate mesh of Fig 5-b. All stresses in the figures are normalized to the average stress σ_0 as follows:

$$\text{SIGMAX} = \frac{\sigma_x}{\sigma_0} \quad (\text{A-1})$$

where SIGMAX is the normalized stress value, σ_x is the stress in the x-direction and σ_0 is the average stress computed from N_0 , the average resultant force. In all figures the four stations depicted are on the positive half length of the plate. The percentage of the half length is noted in the legend for the station plotted.

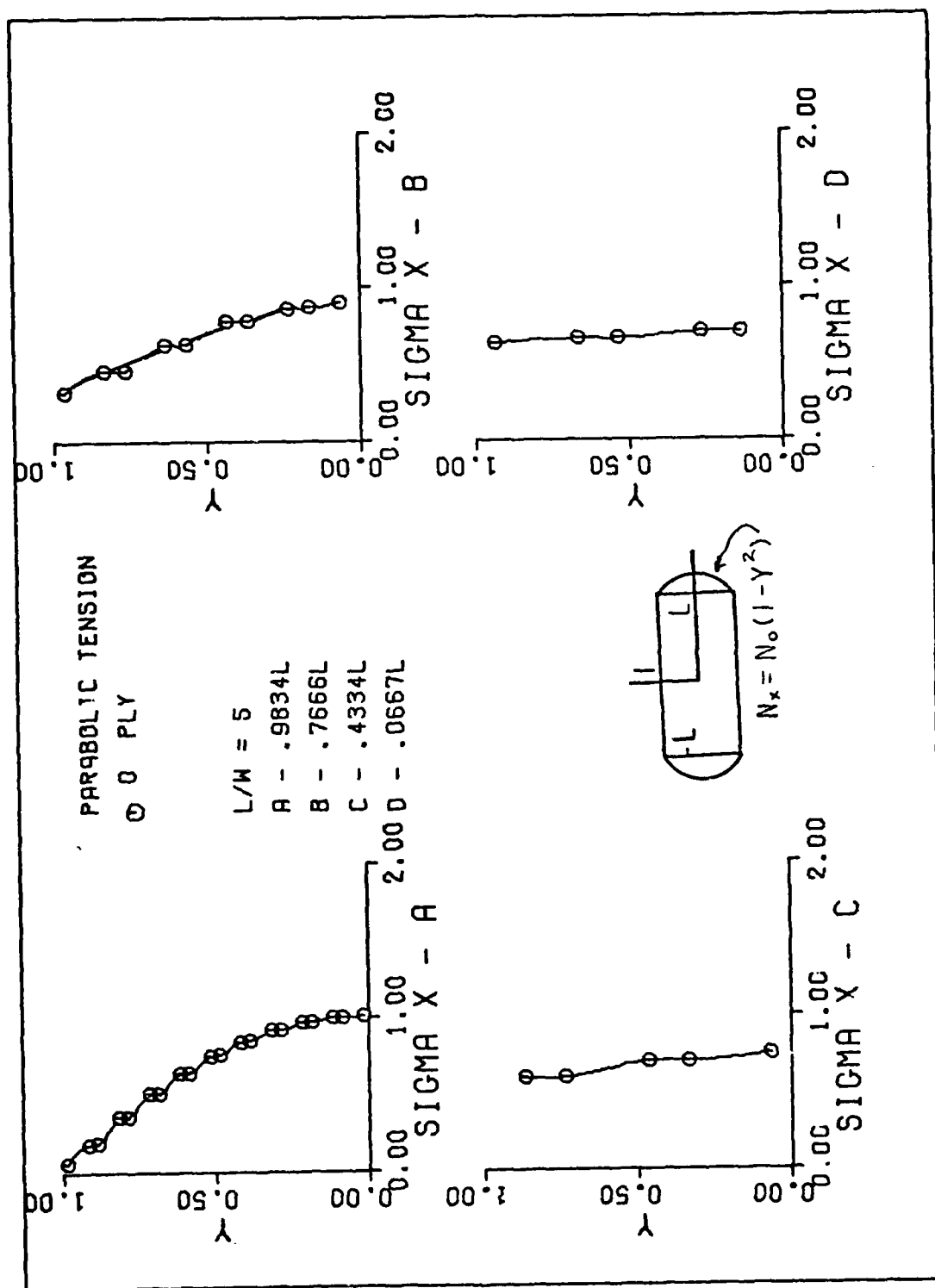


Fig A-1. Single 0 Degree Fiber Oriented Plate Results for Aspect Ratio of Five

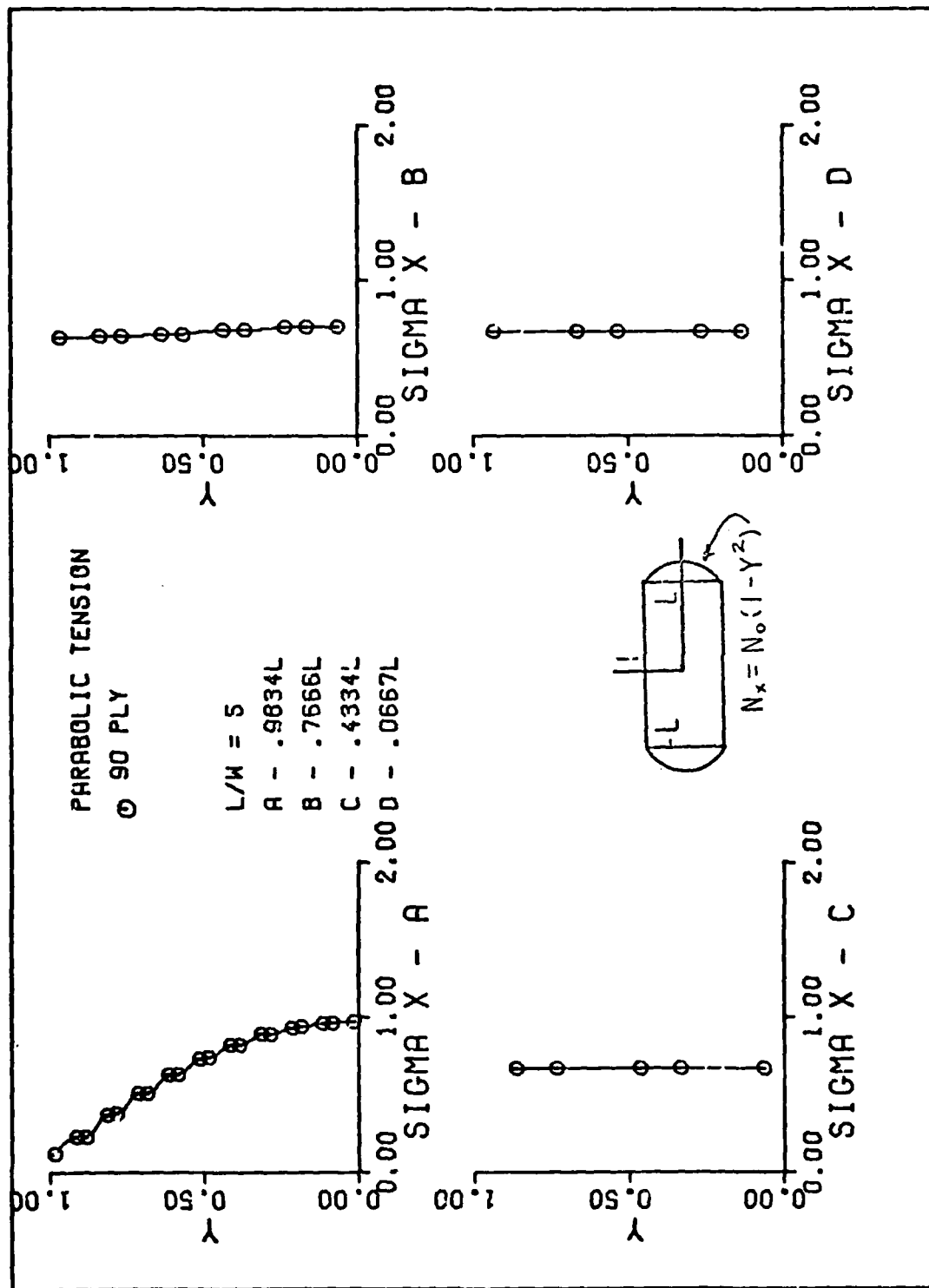


Fig A-2. Single 90 Degree Fiber Oriented Plate Results for Aspect Ratio of Five

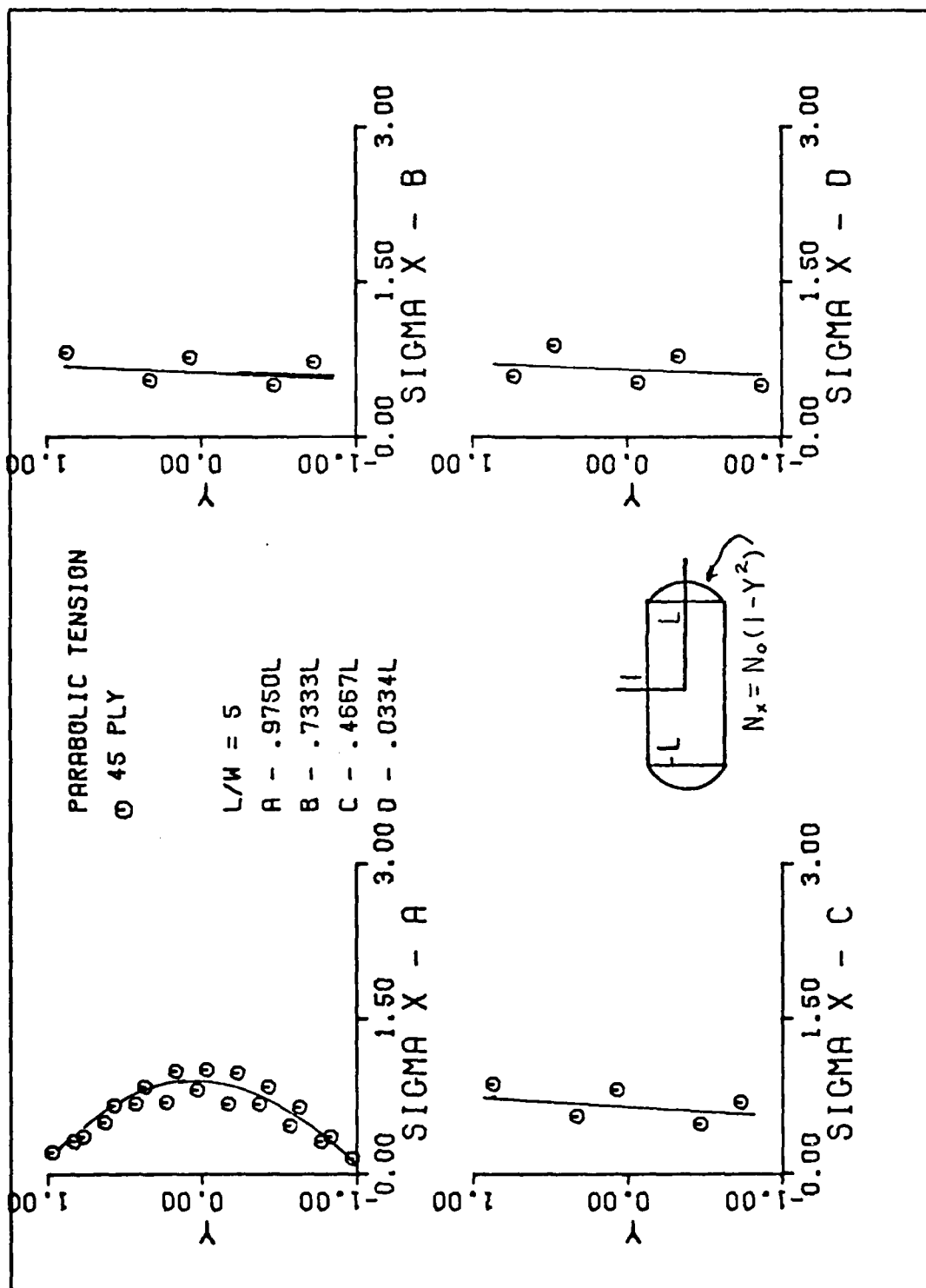


Fig A-3. Single 45 Degree Fiber Oriented Plate Results for Aspect Ratio of Five

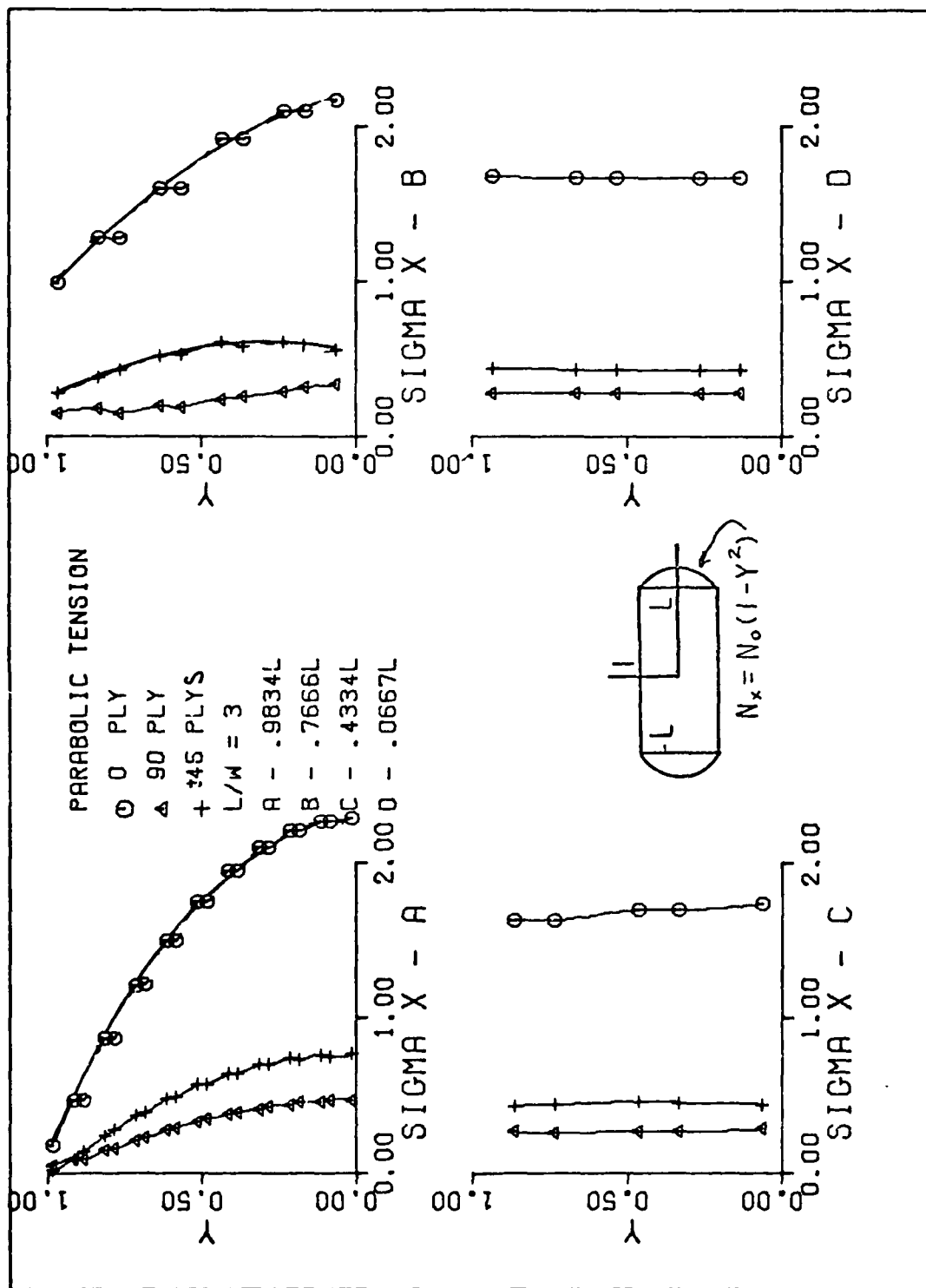


Fig A-4. (0,±45, 90)s Plate Results for Aspect Ratio of Three

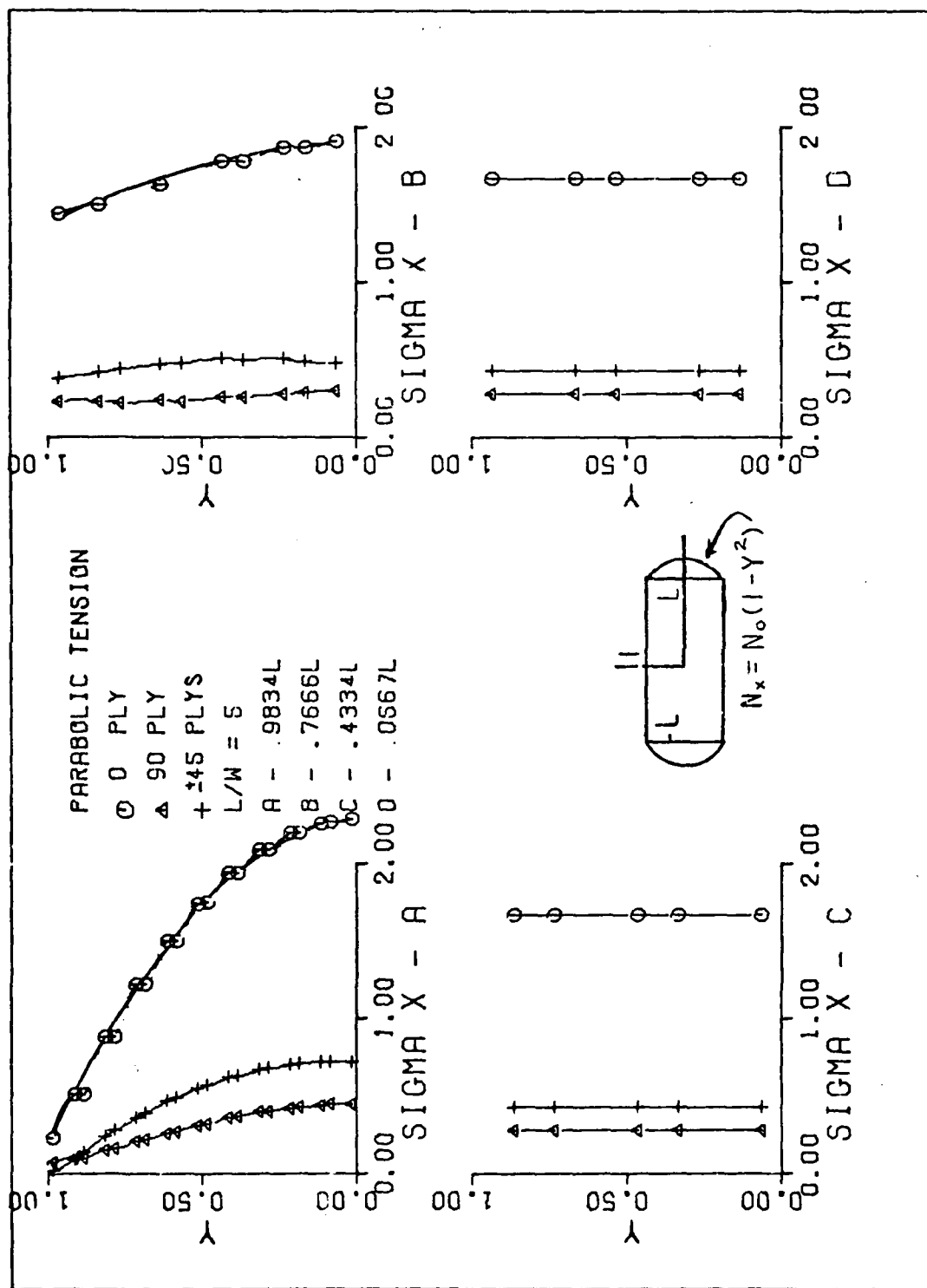


Fig A-5. (0, ±45, 90)s Plate Results for Aspect Ratio of Five

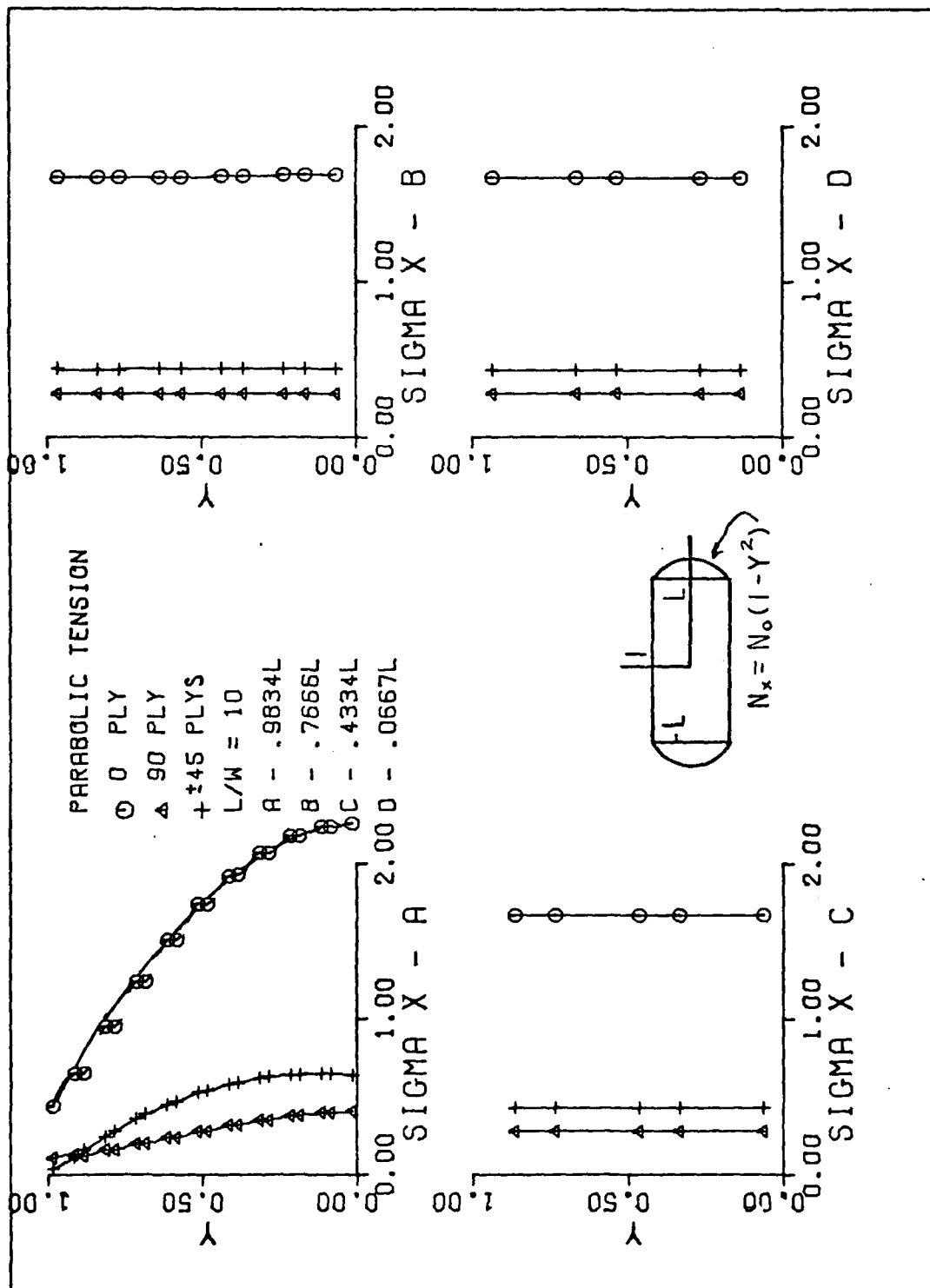


Fig A-6. (0, ±45, 90)s Plate Results for Aspect Ratio of Ten

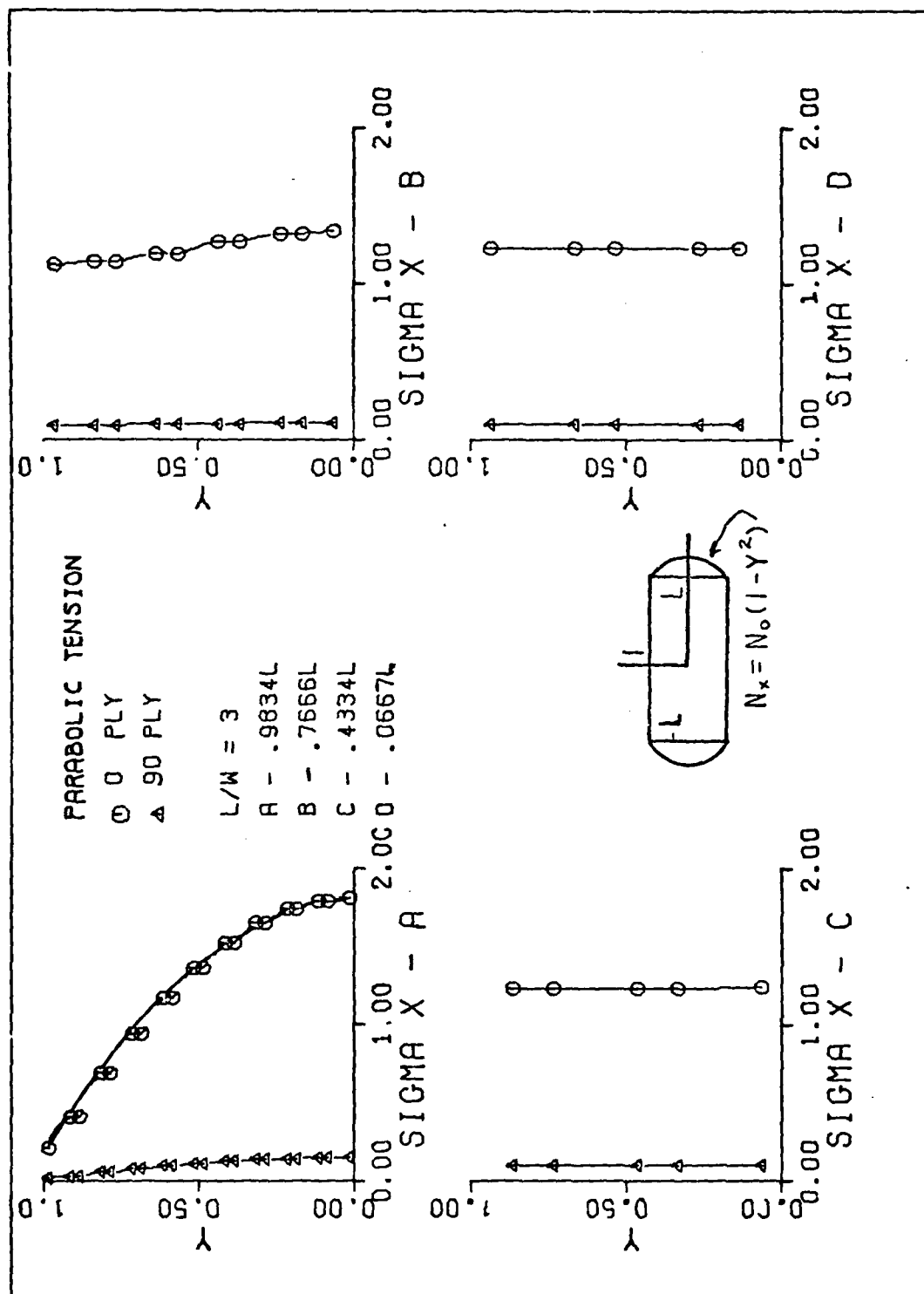


Fig A-7. (0, 90)s Plate Results for Aspect Ratio of Three

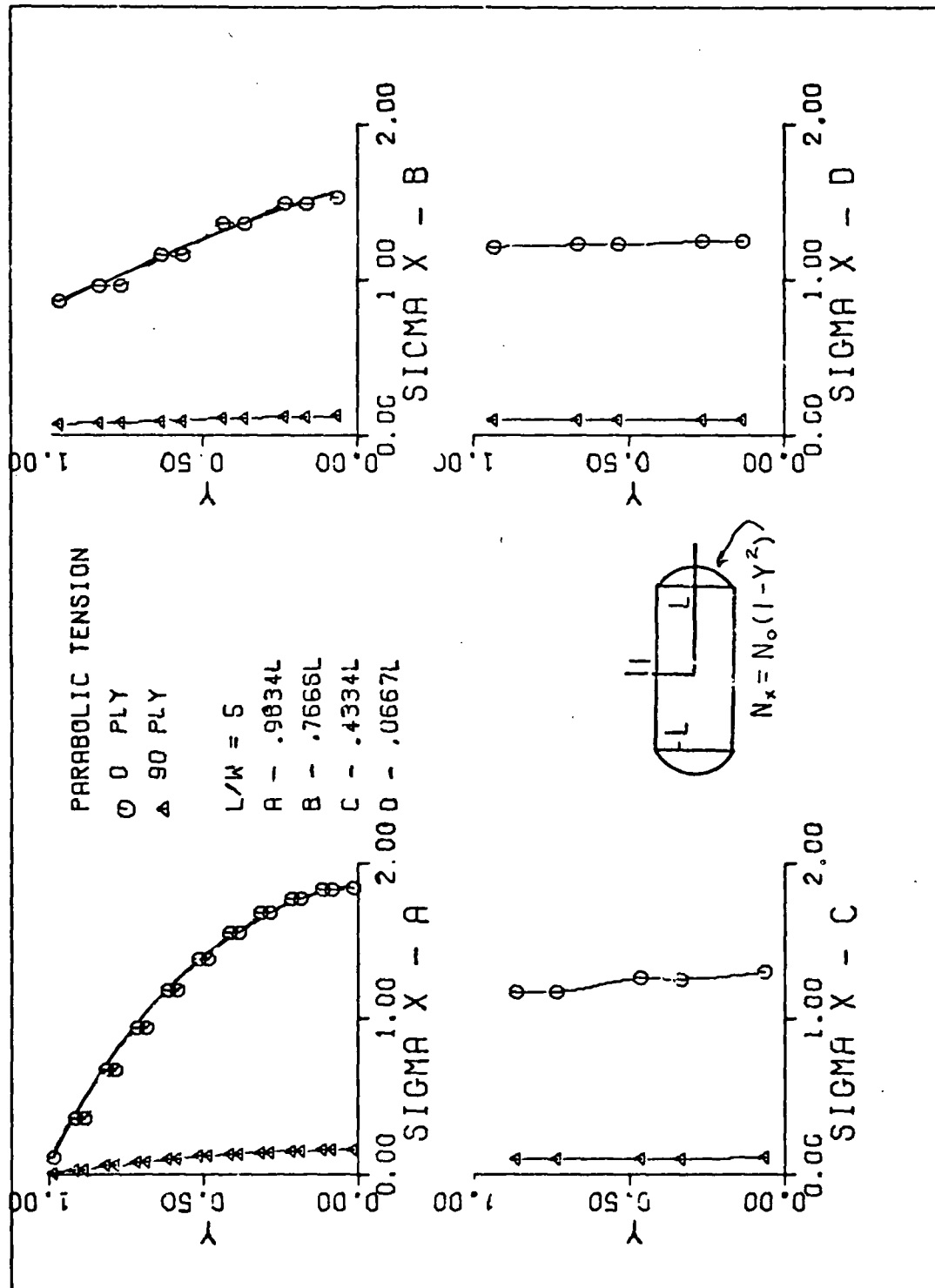


Fig A-8. (0, 90)s Plate Results for Aspect Ratio of Five

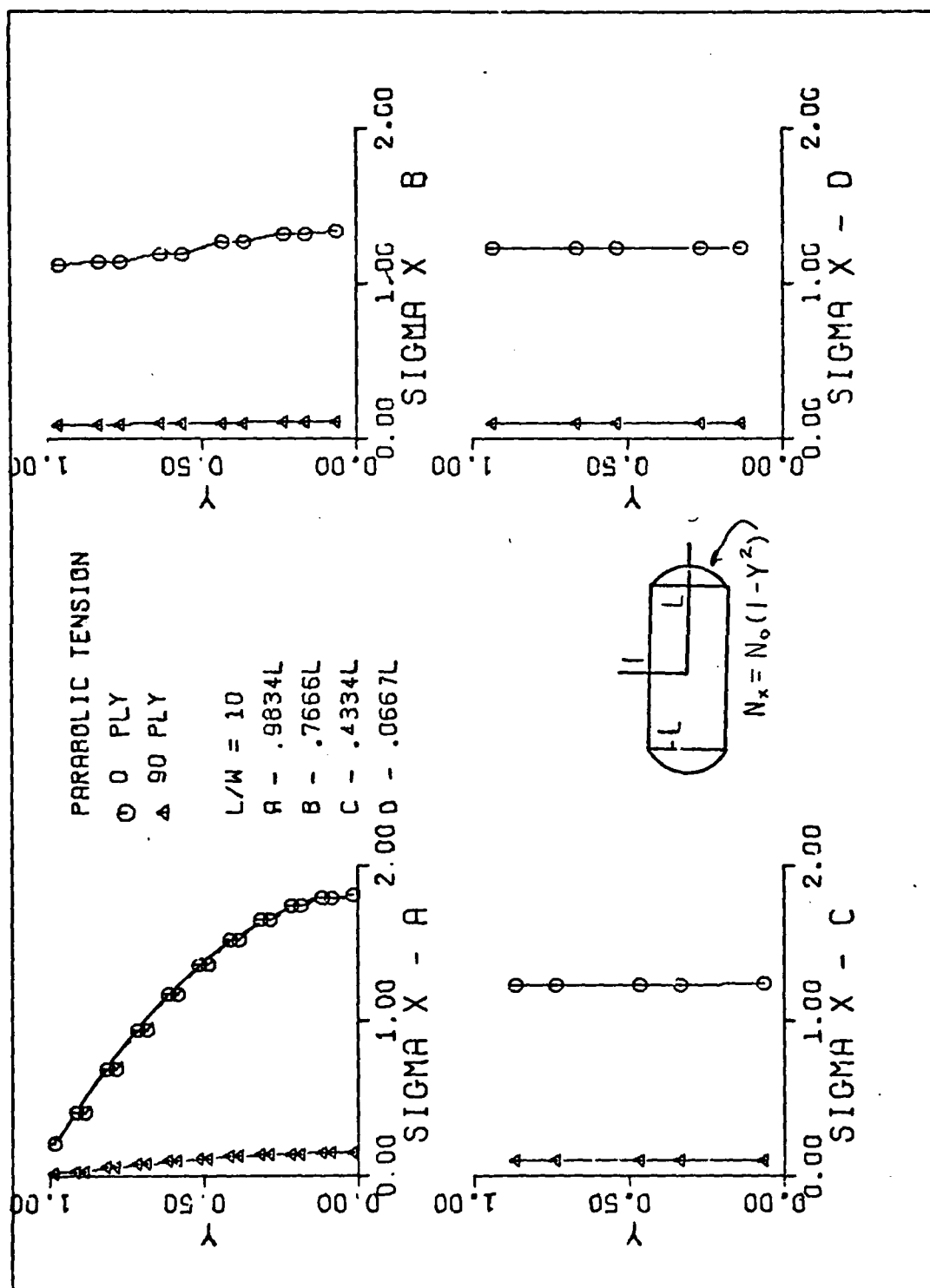


Fig A-9. (0, 90)s Plate Results for Aspect Ratio of Ten

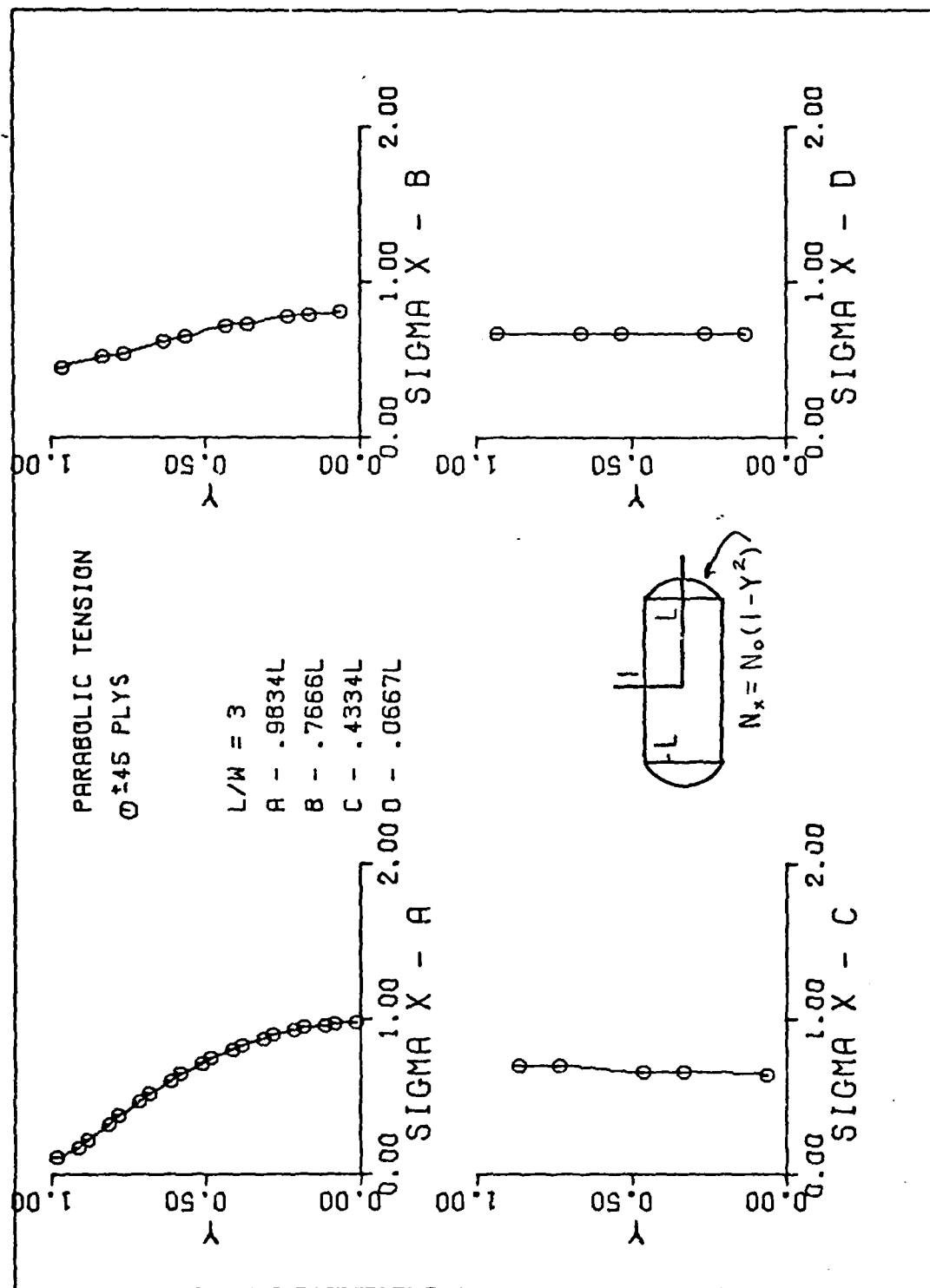


Fig A-10. (± 45)s Plate Results for Aspect Ratio of Three

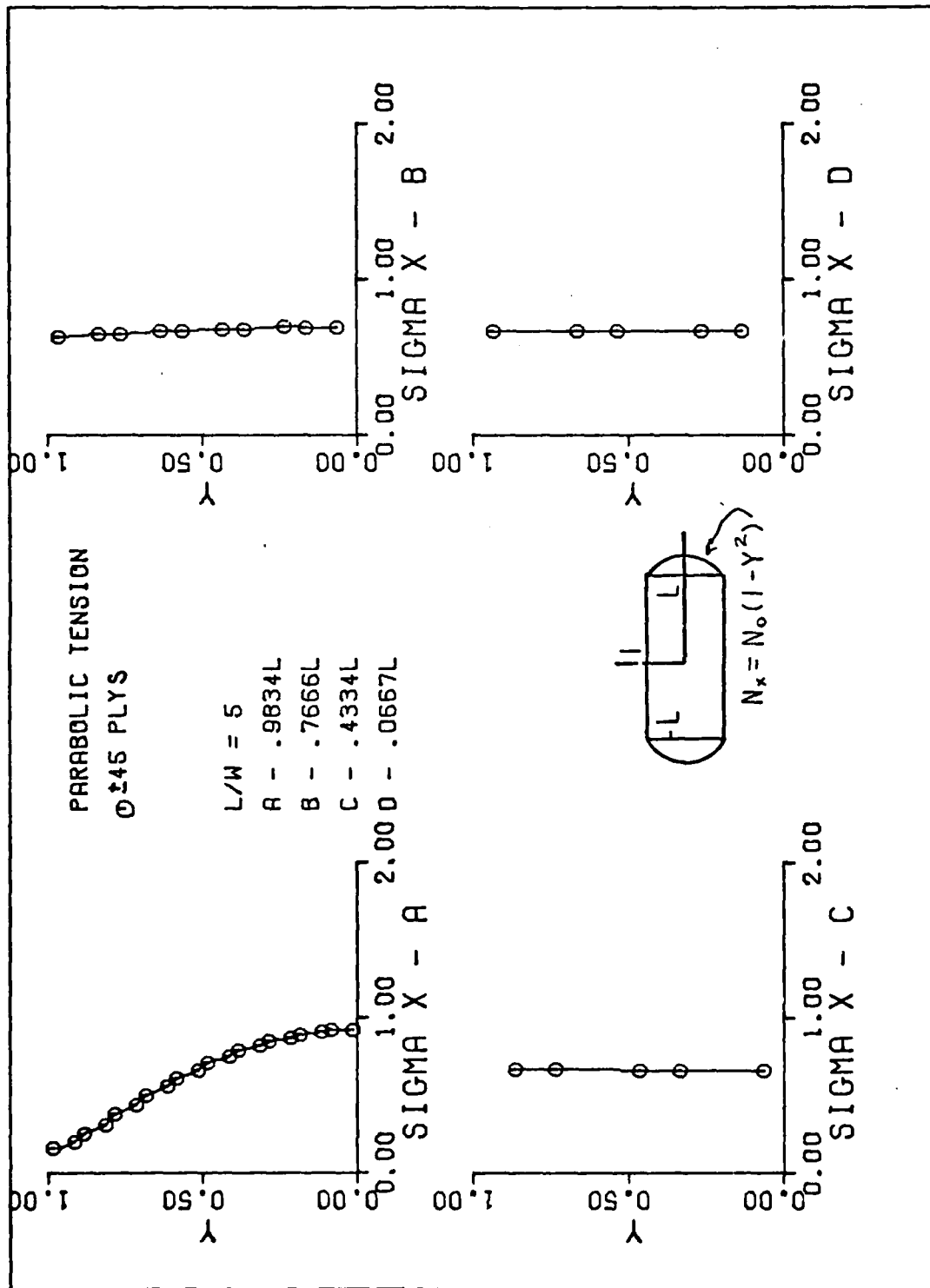


Fig A-11. (± 45)s Plate Results for Aspect Ratio of Five

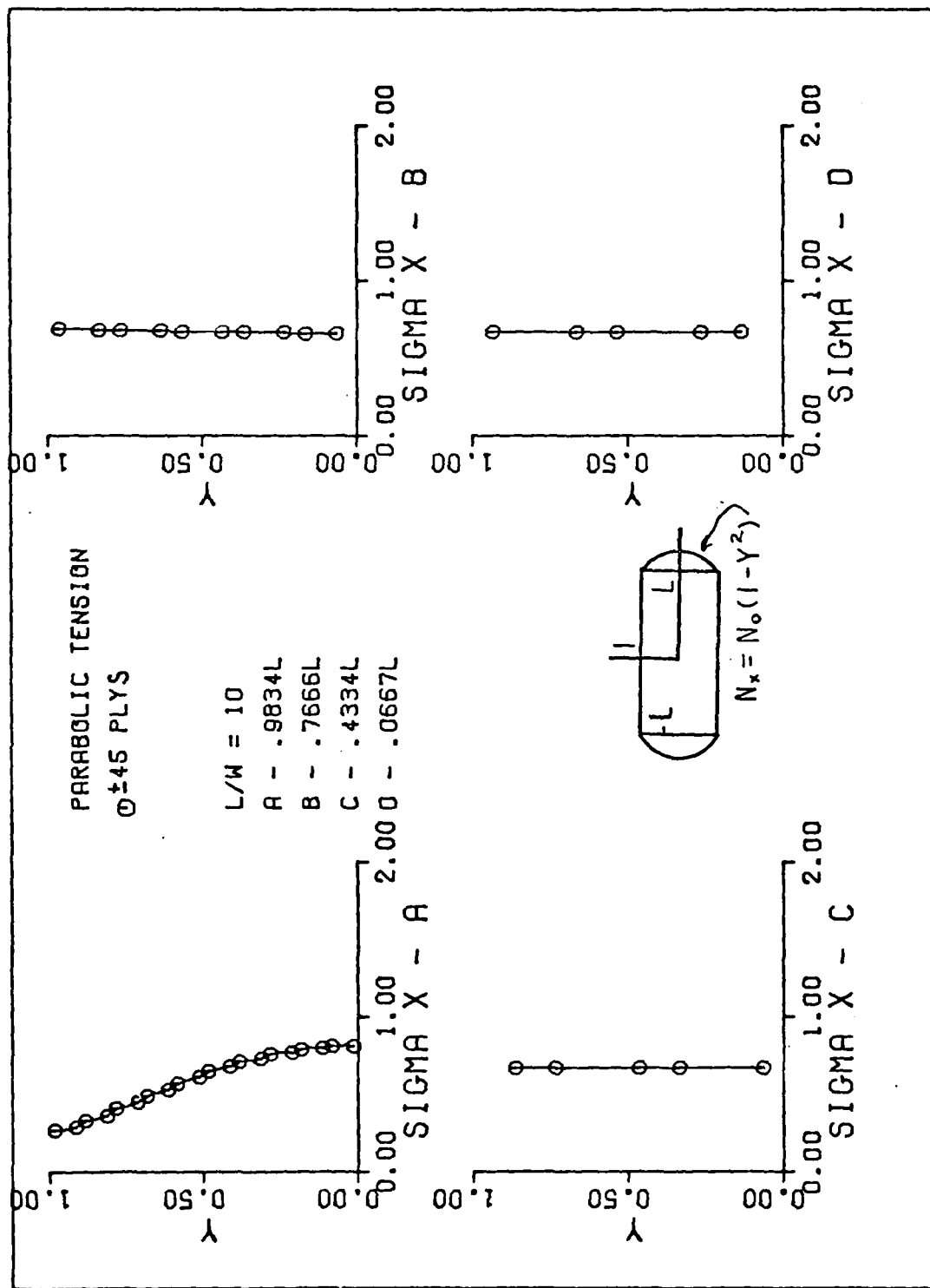


Fig A-12. (± 45) s Plate Results for Aspect Ratio of Ten

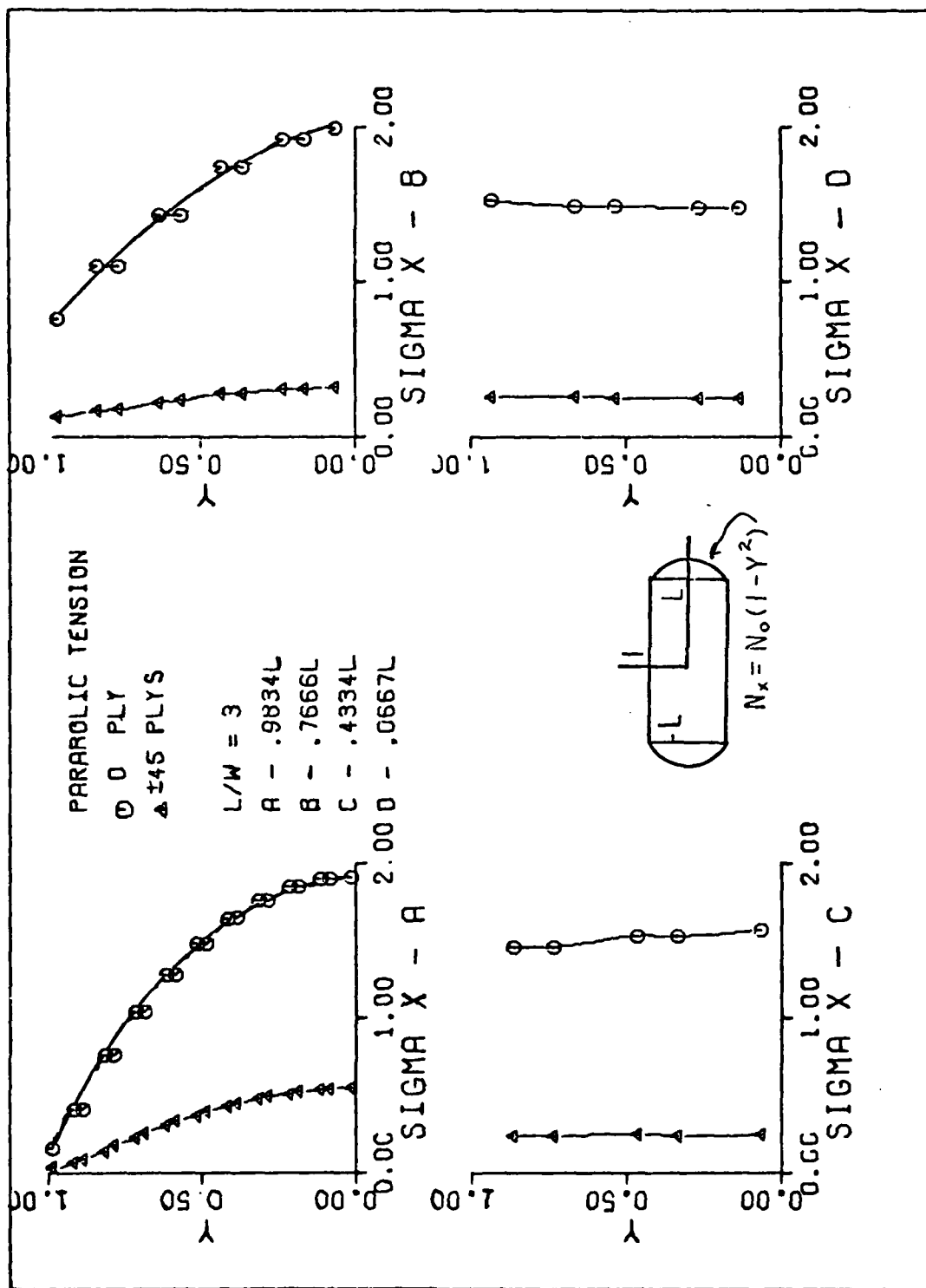


Fig A-13. (0, ±45)s Plate Results for Aspect Ratio of Three

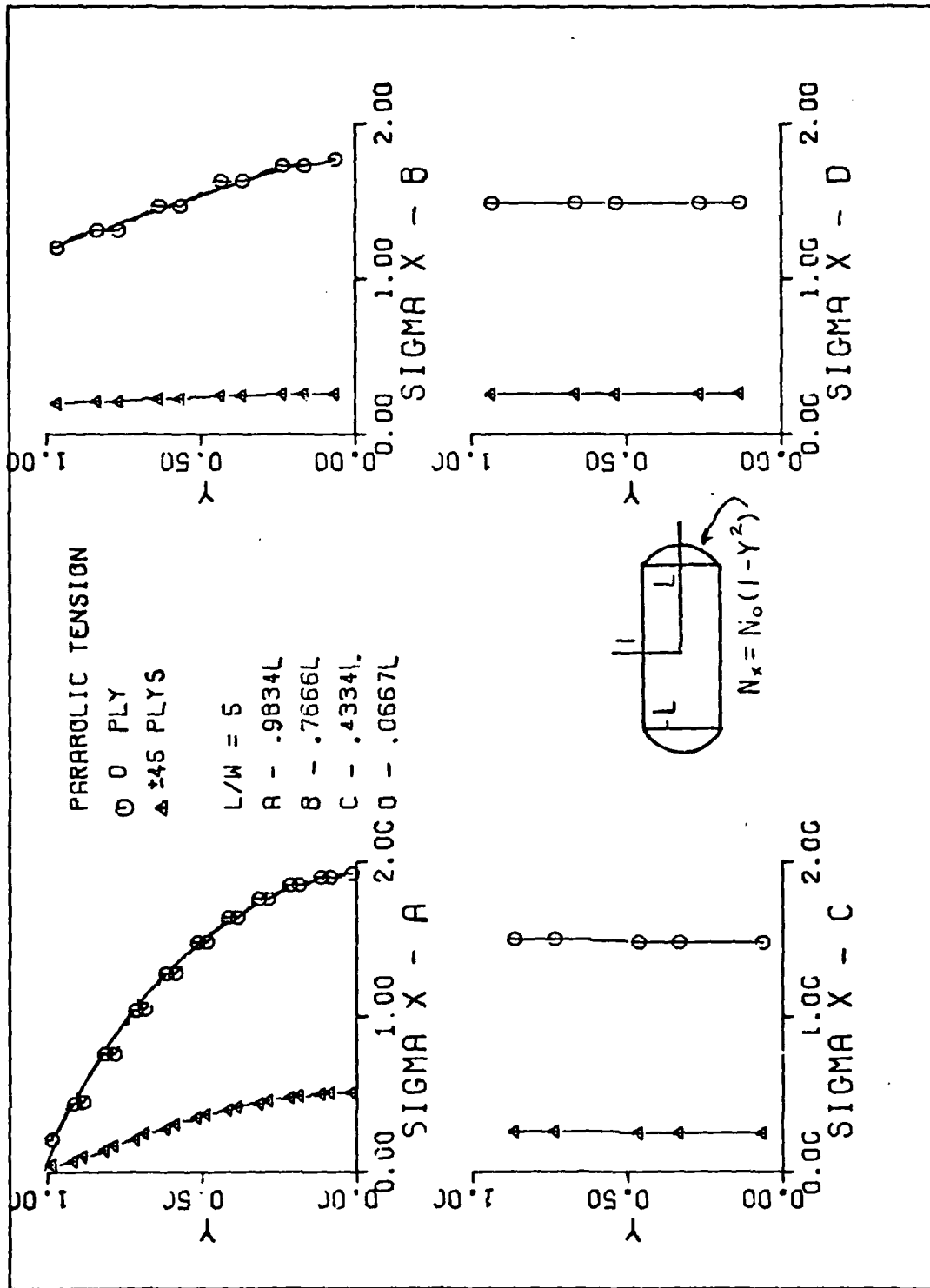


Fig A-14. (0, ±45)s Plate Results for Aspect Ratio of Five

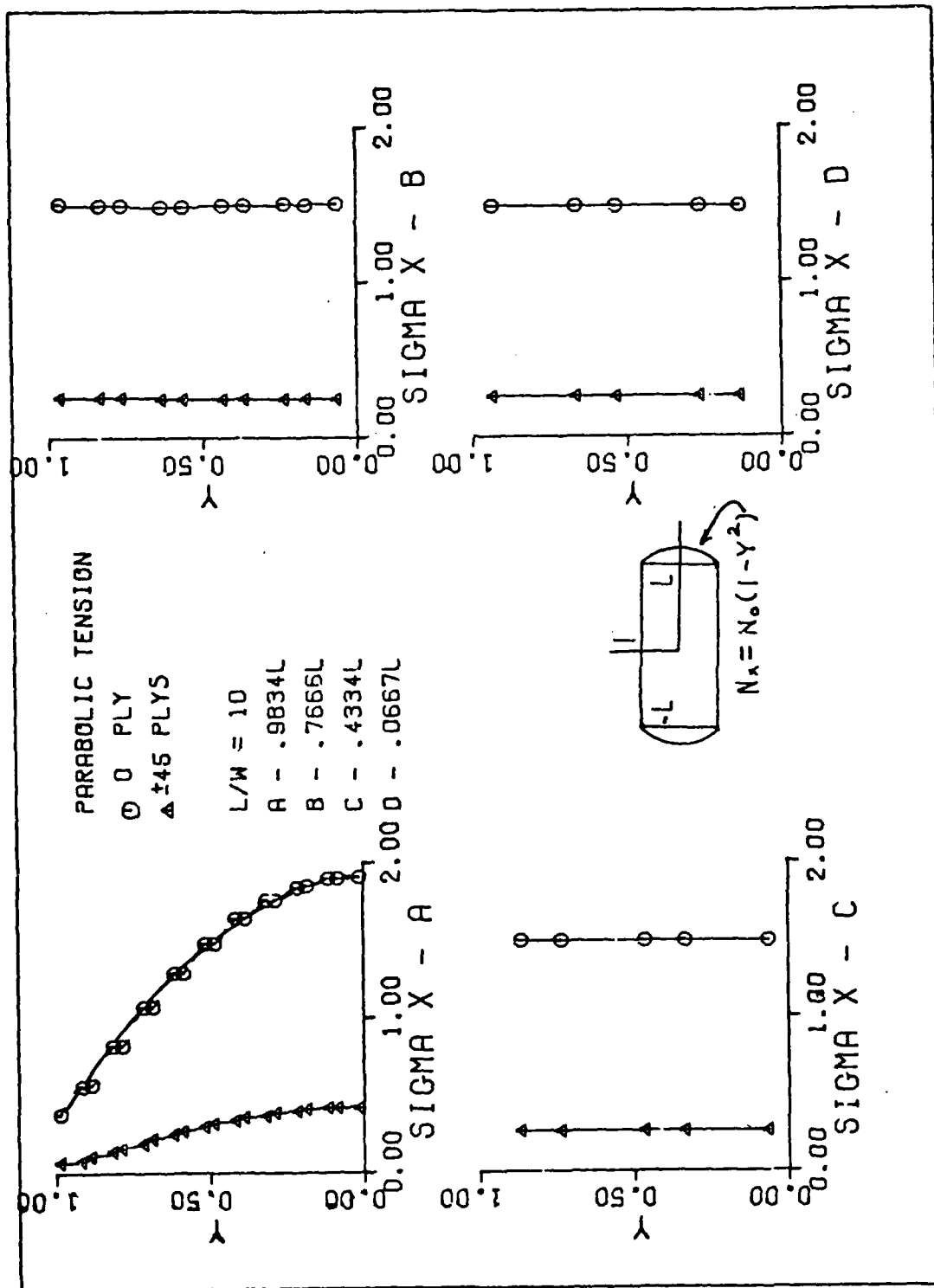


Fig A-15. (0, ±45)s Plate Results for Aspect Ratio of Ten

Appendix B

Graphical Results of the Parabolic

Bending End Condition

The following figures resulted from the use of the full plate mesh shown in Fig 6-A. All stresses in the figures are normalized to the average stress σ_0 given by Eq (A-1). Legend comments found in Appendix A apply.

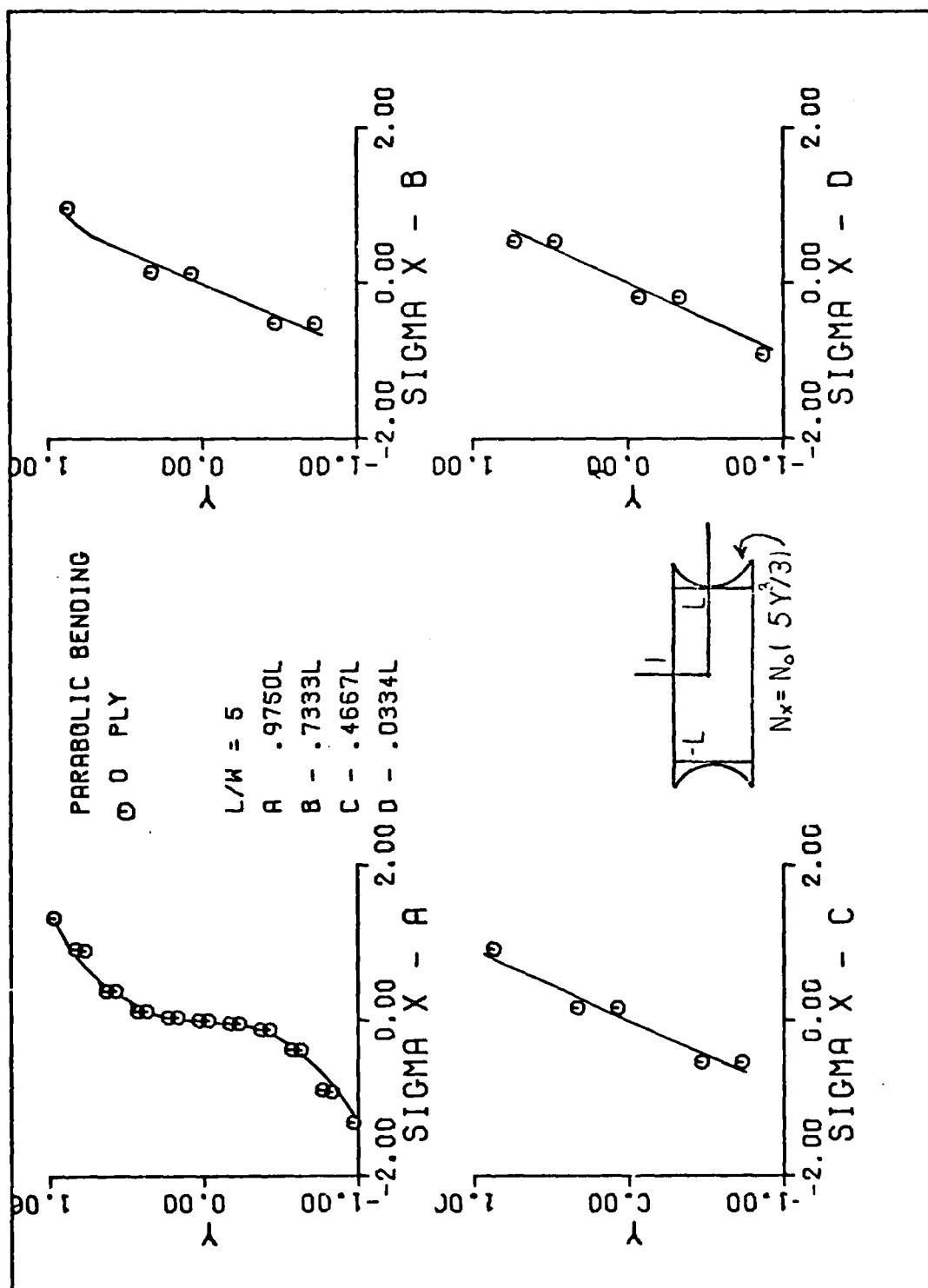


Fig B-1. Single 0 Degree Fiber Oriented Plate Results for Aspect Ratio of Five

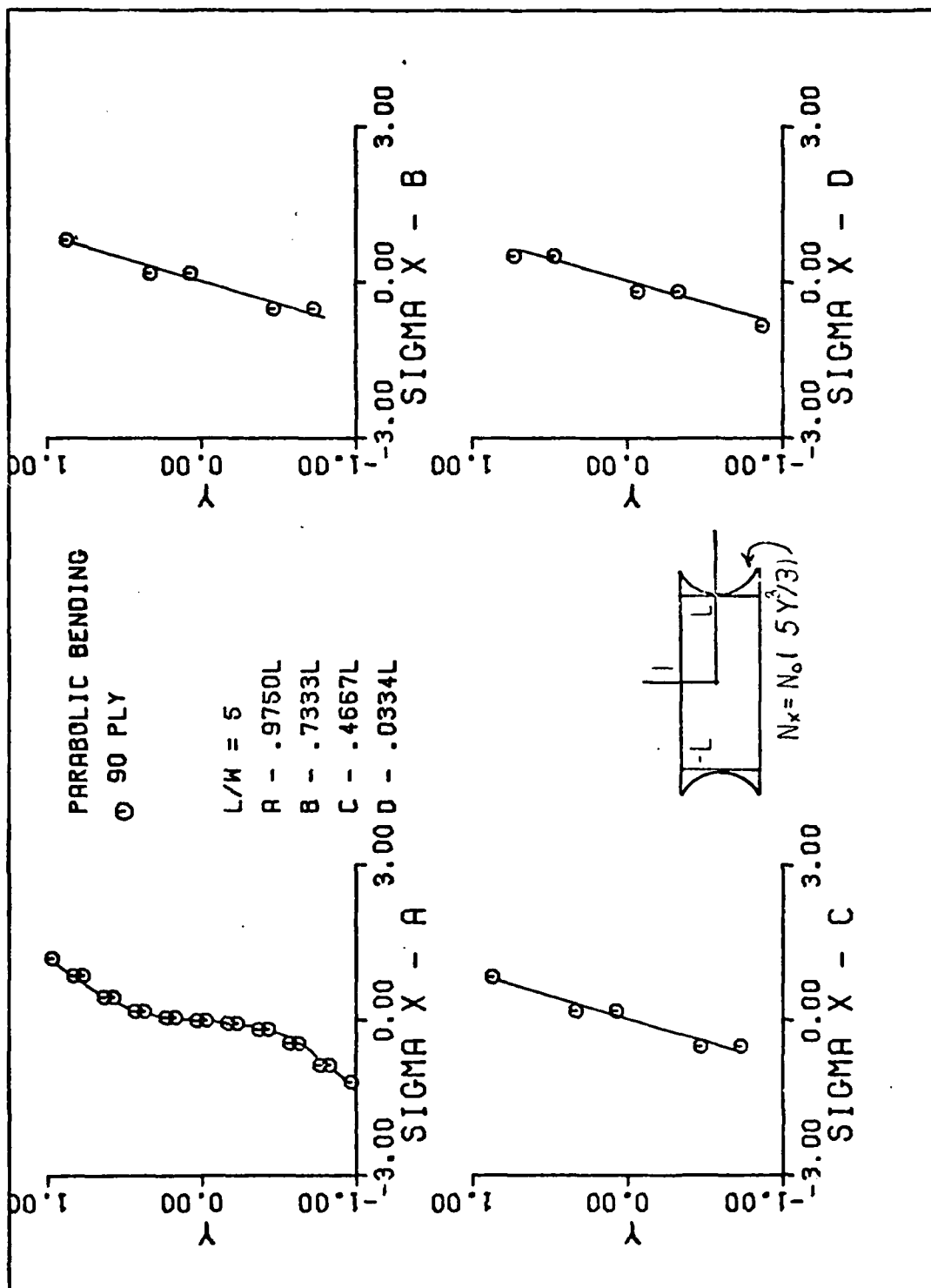


Fig B-2. Single 90 Degree Fiber Oriented Plate Results for Aspect Ratio of Five

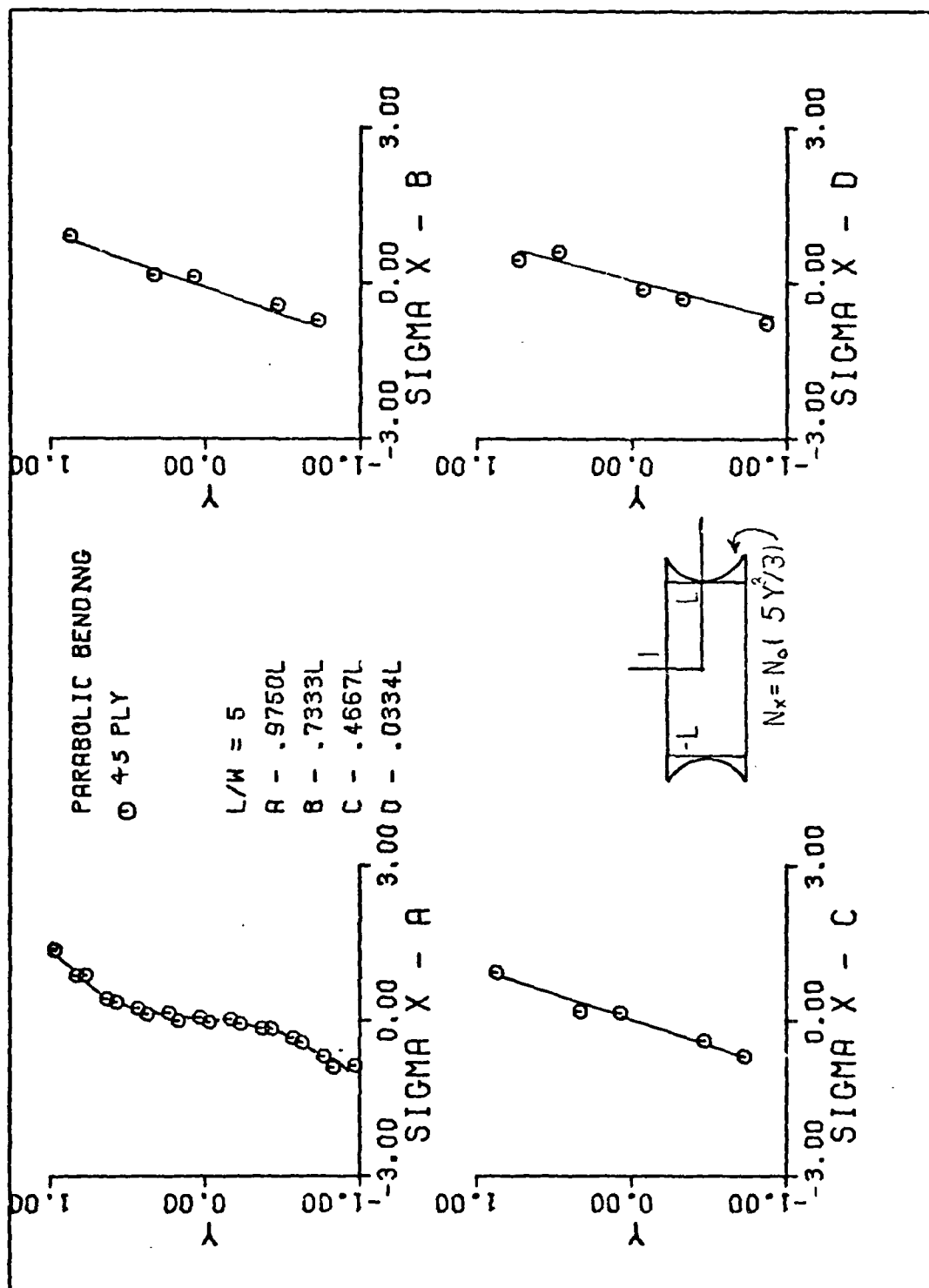


Fig B-3. Single 45 Degree Fiber Oriented Plate Results for Aspect Ratio of Five

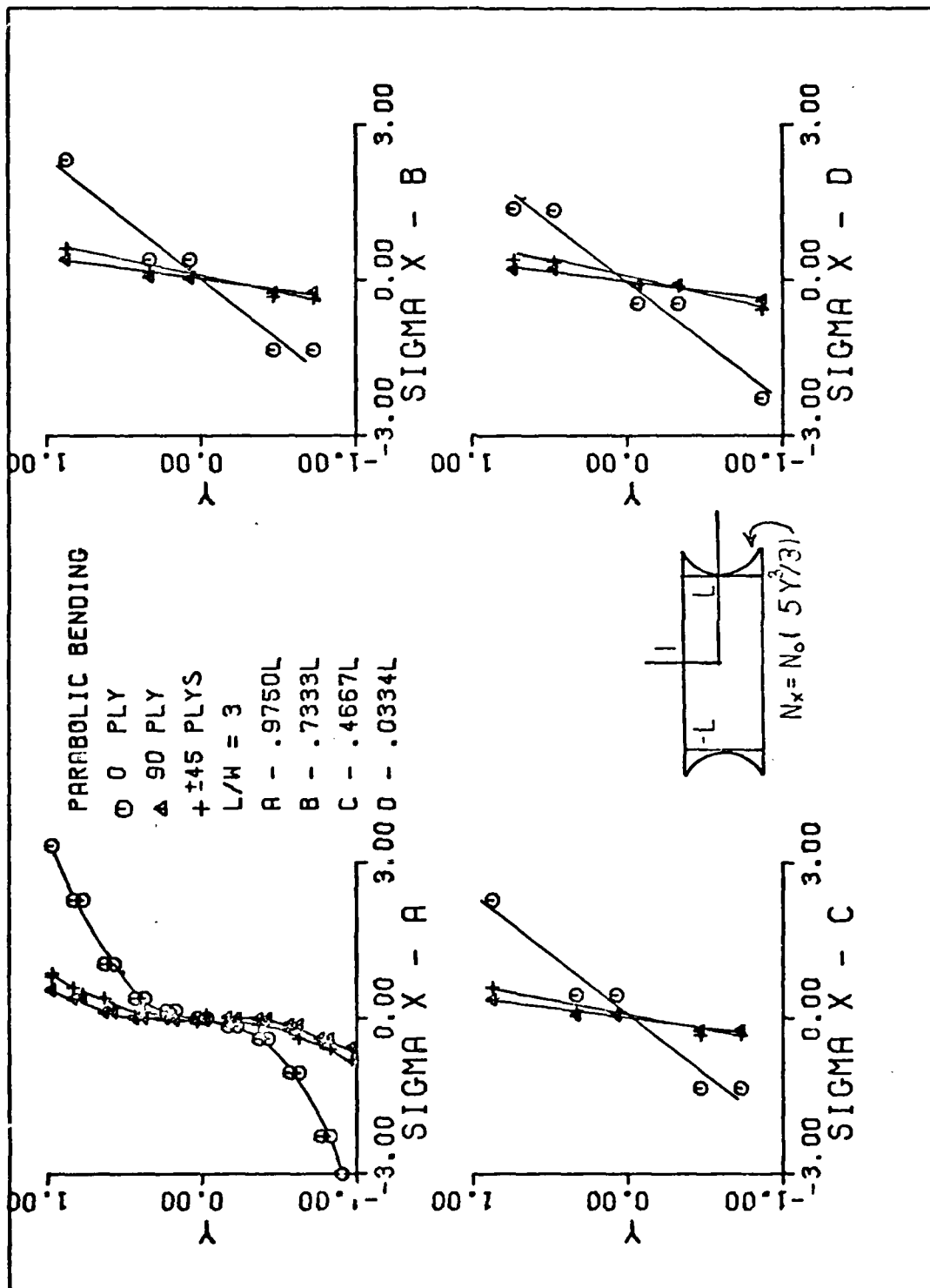


Fig B-4. (0, ±45, 90)s Plate Results for Aspect Ratio of Three

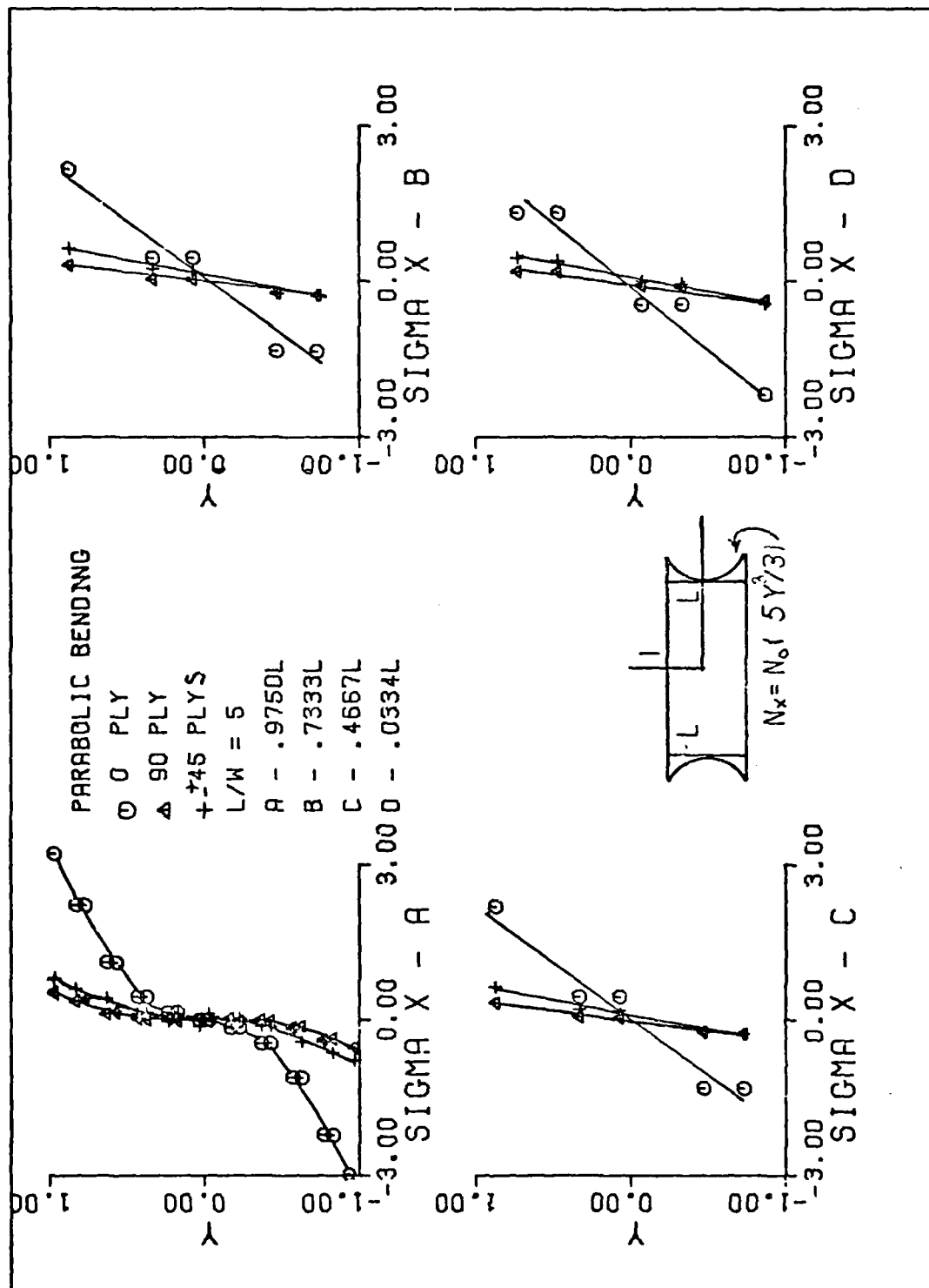


Fig B-5. (0, ±45, 90)s Plate Results for Aspect Ratio of Five

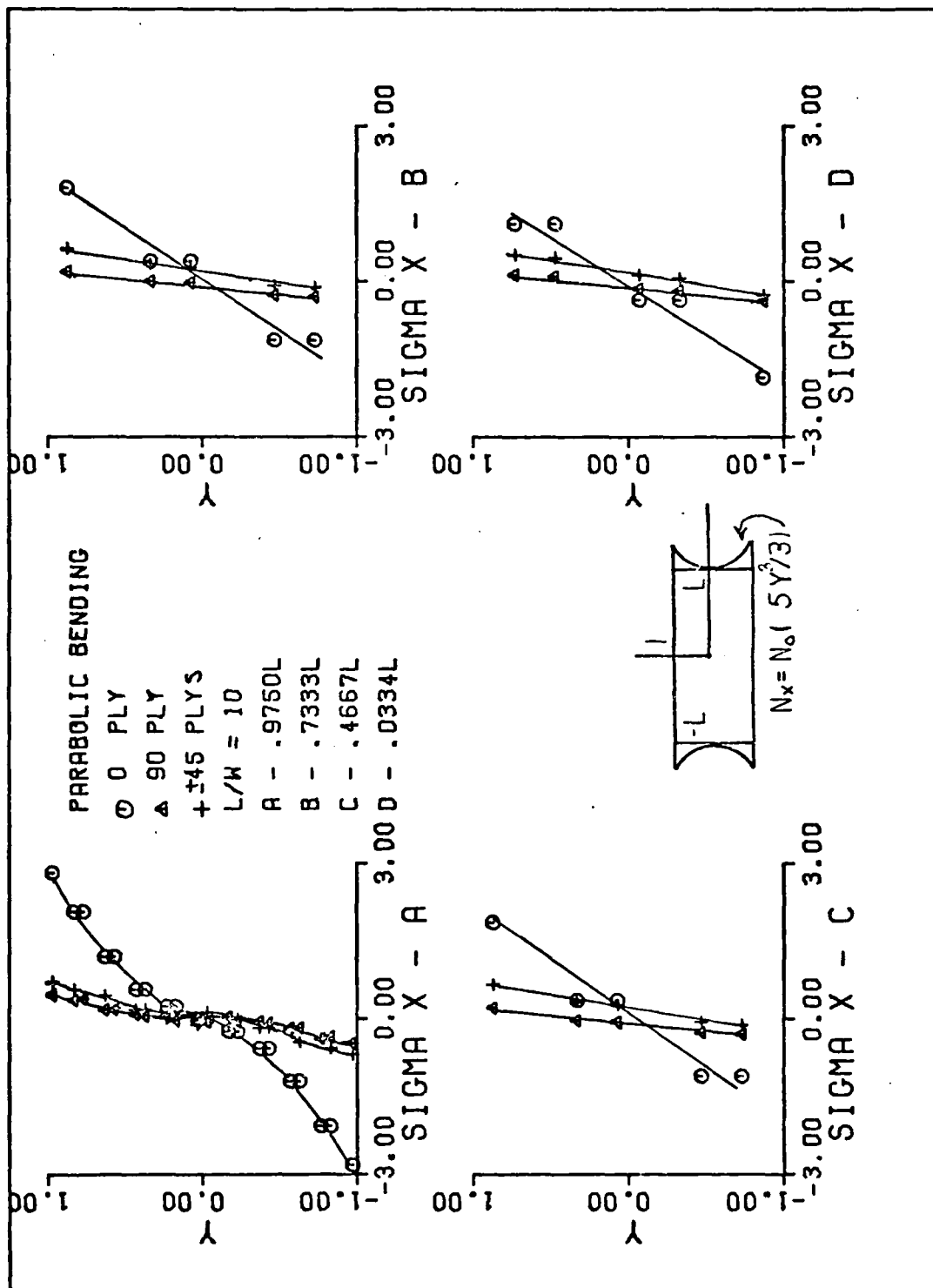


Fig B-6. (0, ±45, 90)s Plate Results for Aspect Ratio of Ten

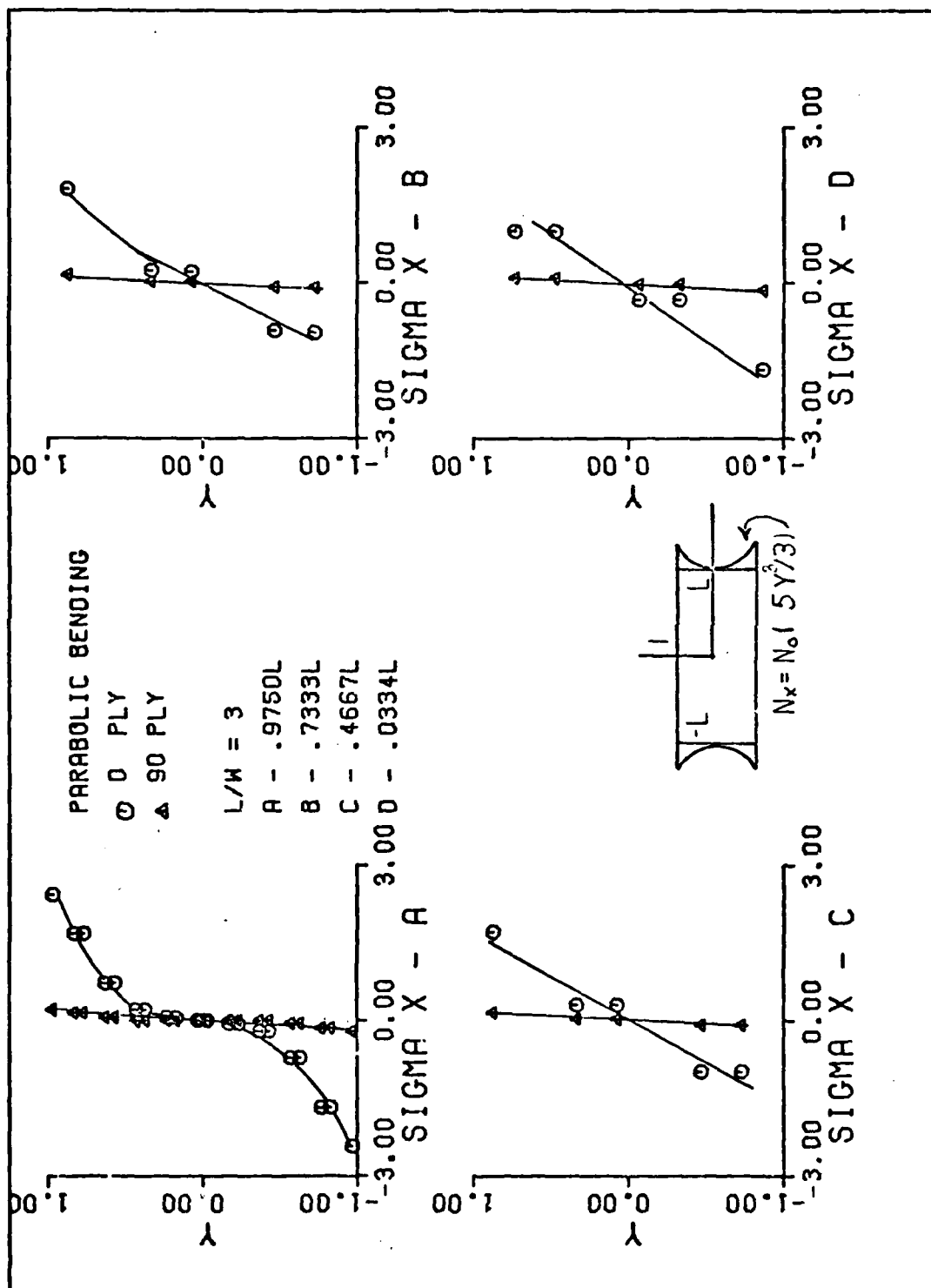


Fig B-7. (0, 90)s Plate Results for Aspect Ratio of Three

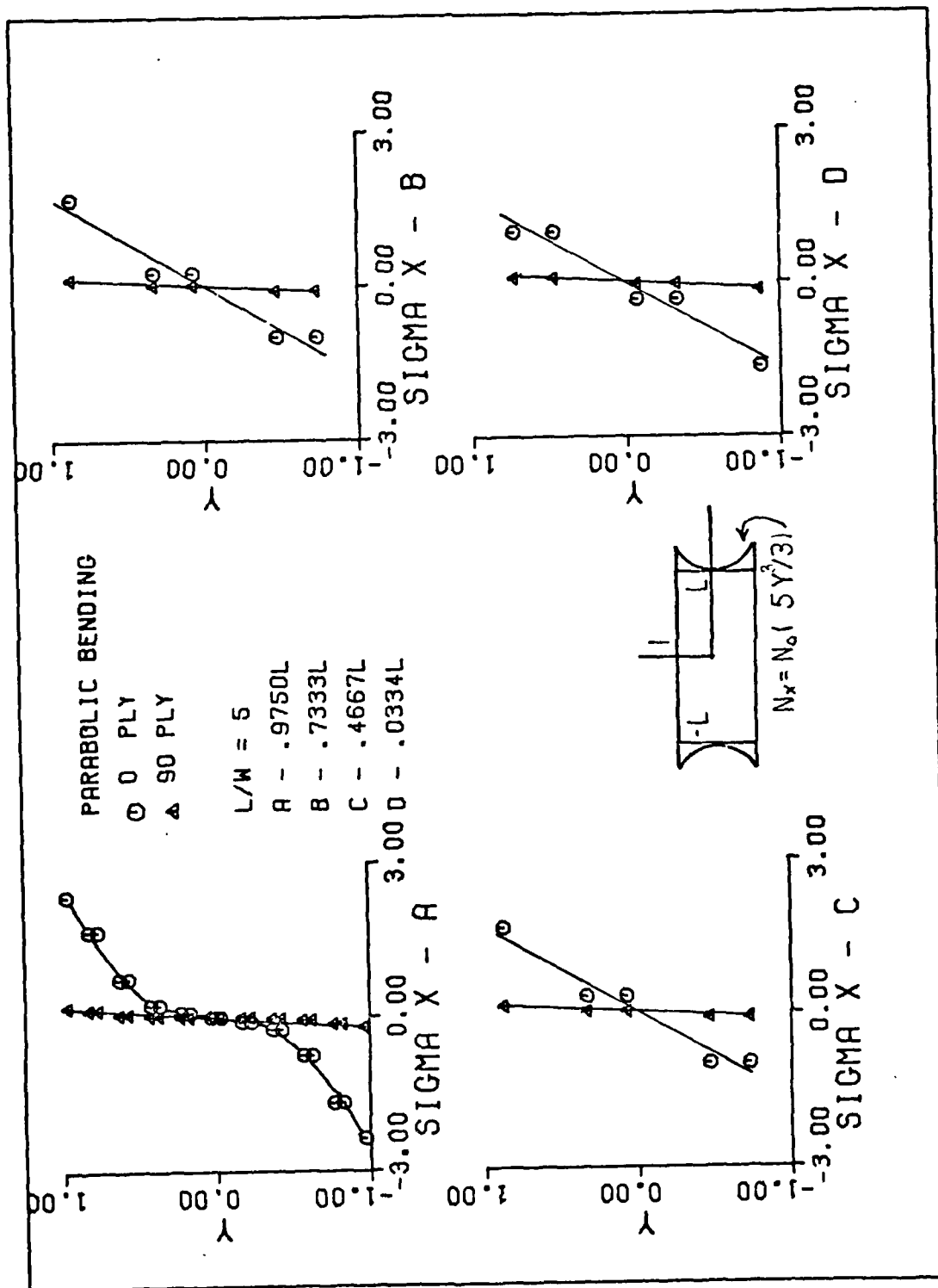


Fig B-8. (0, 90)s Plate Results for Aspect Ratio of Five

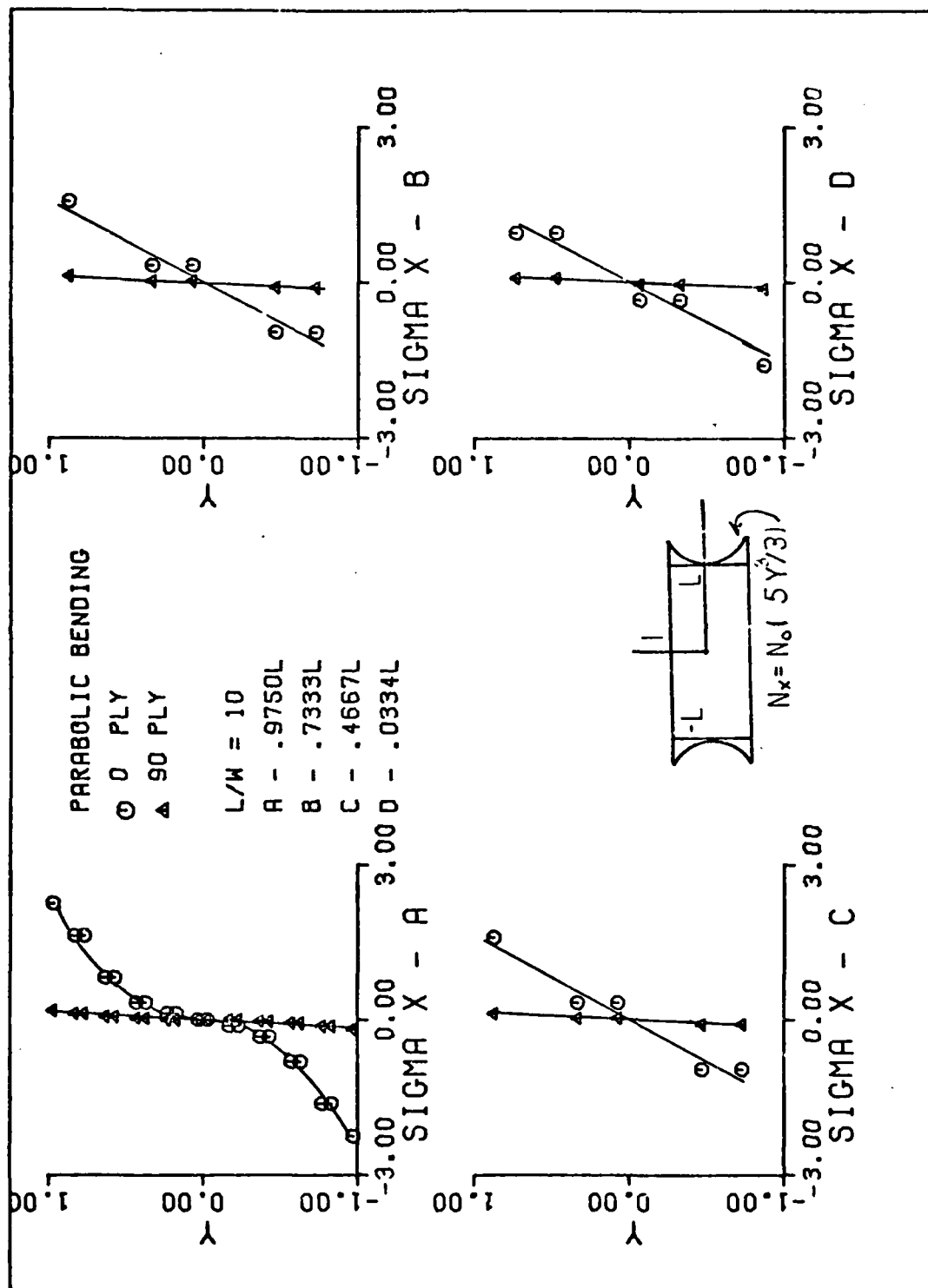


Fig B-9. (0, 90)s Plate Results for Aspect Ratio of Ten

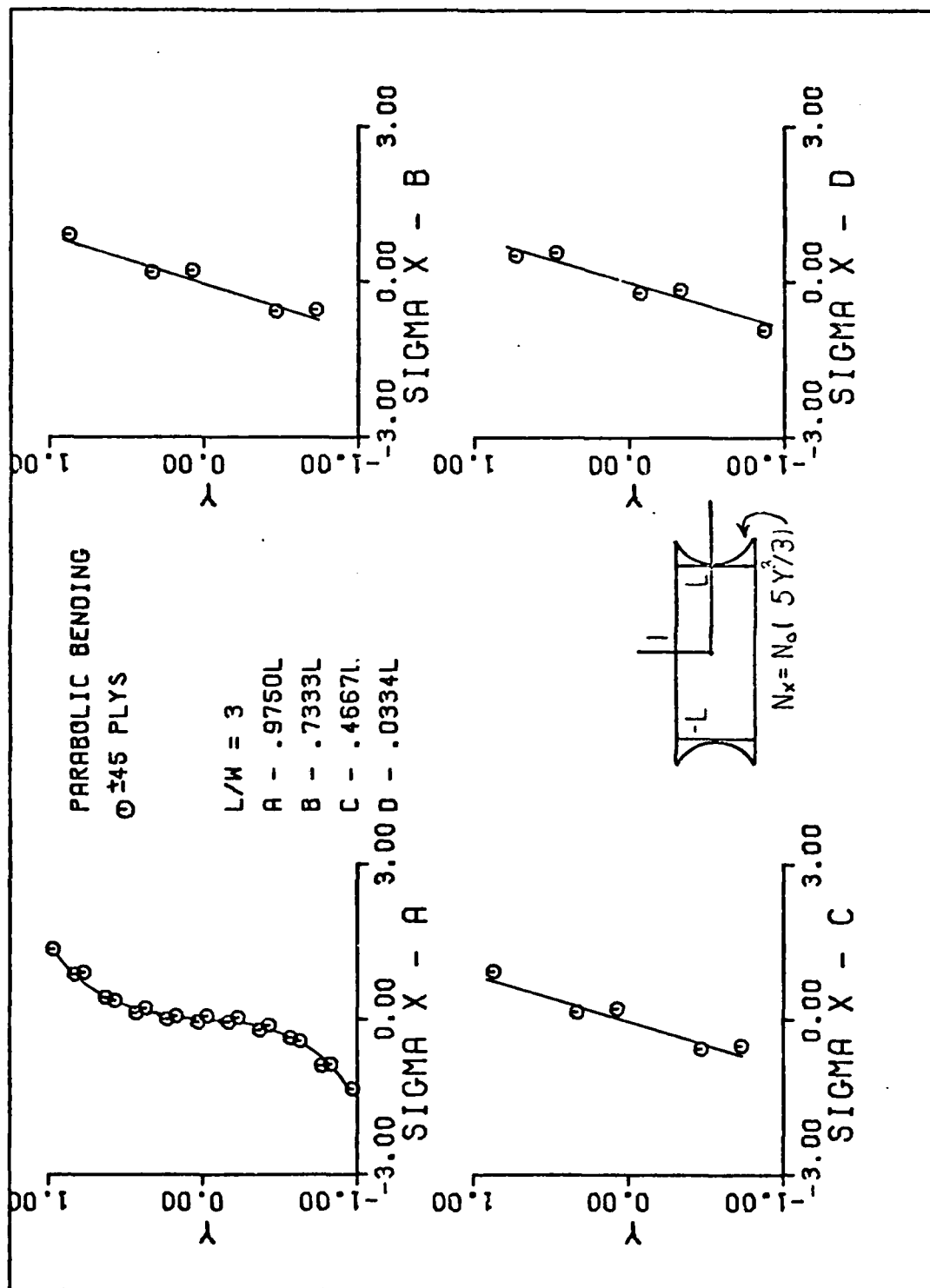


Fig B-10. (± 45) s Plate Results for Aspect Ratio of Three

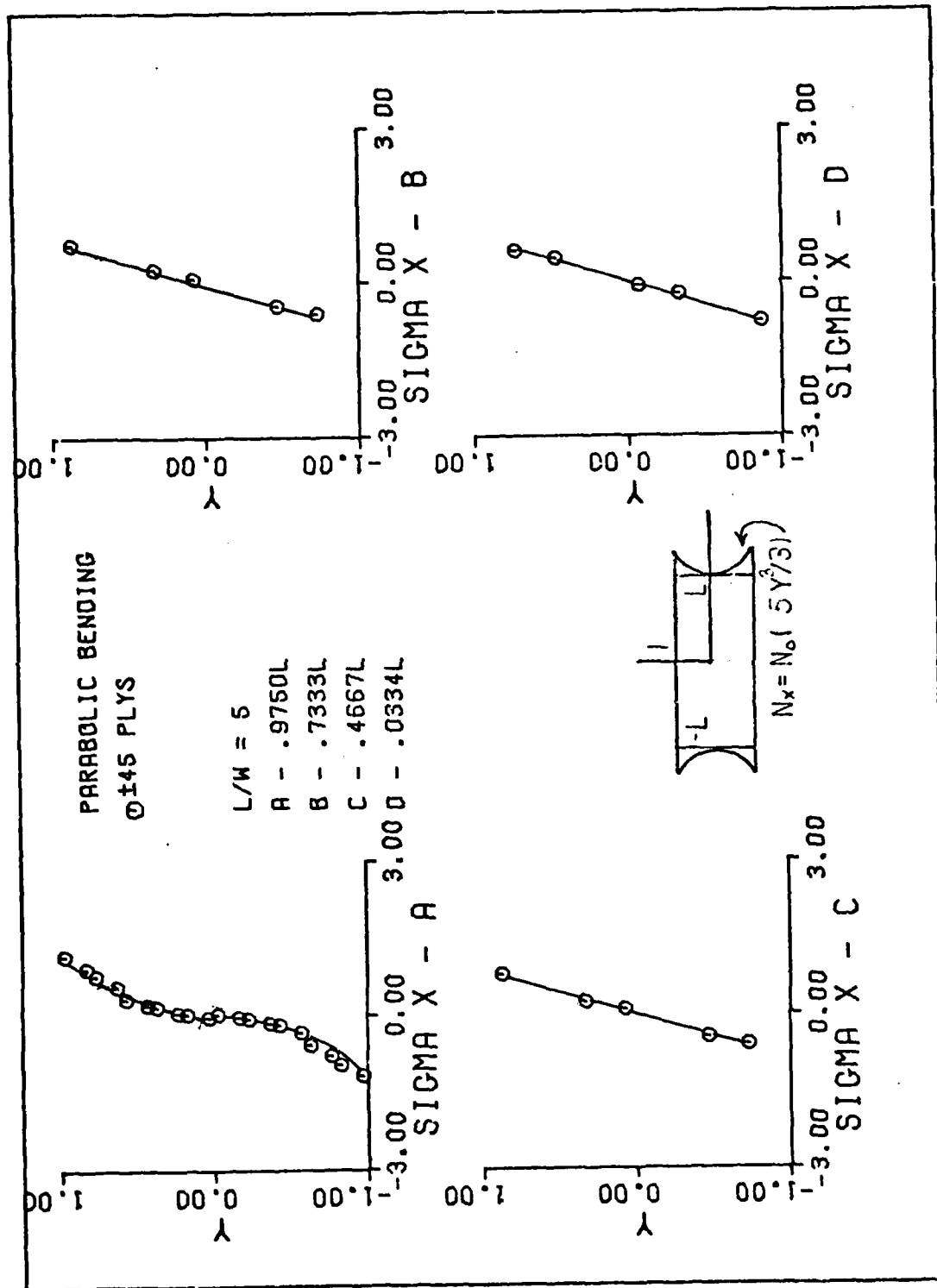


Fig B-11. (+45)s Plate Results for Aspect Ratio of Five

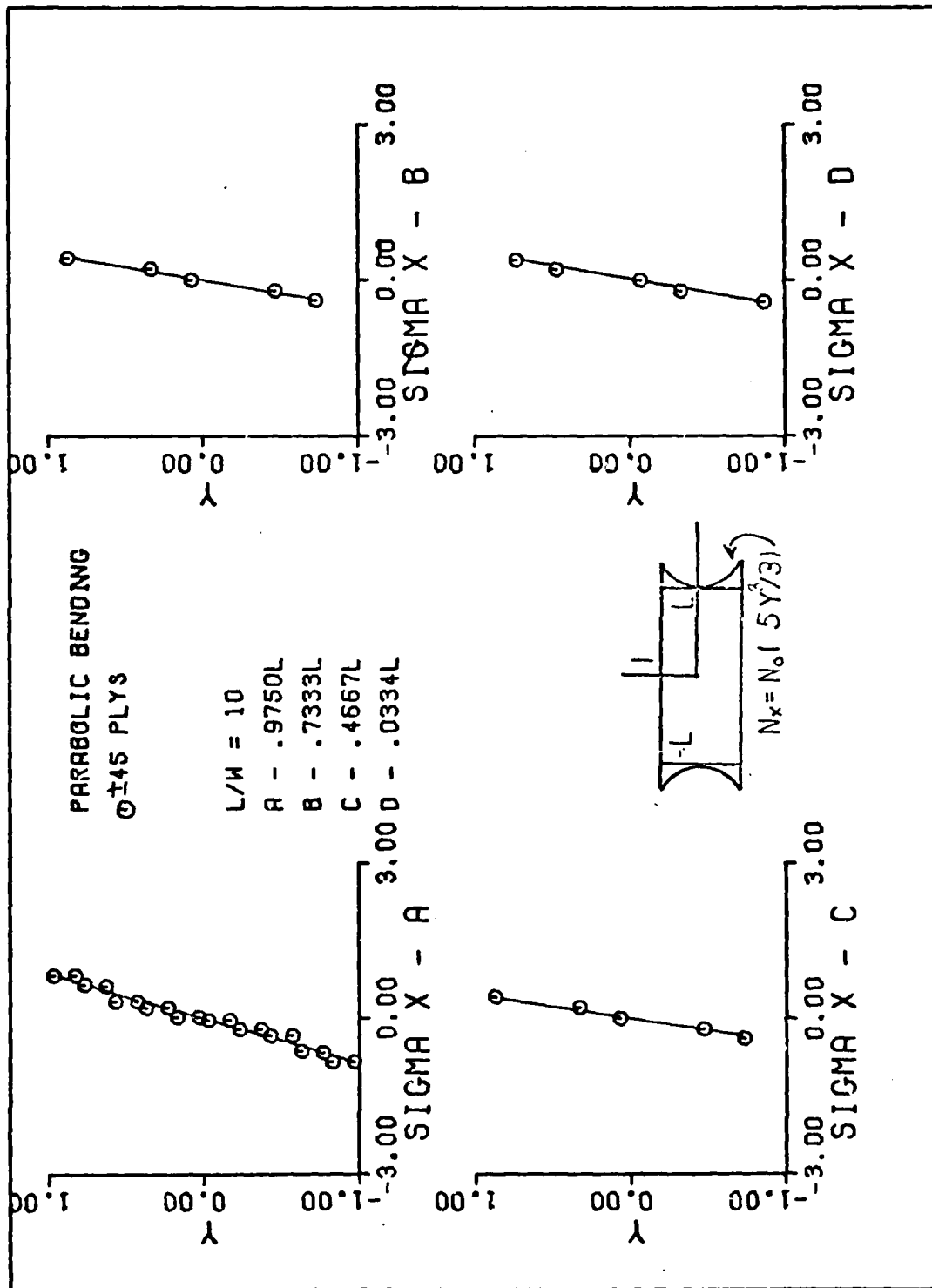


Fig B-12. (±45)s Plate Results for Aspect Ratio of Ten

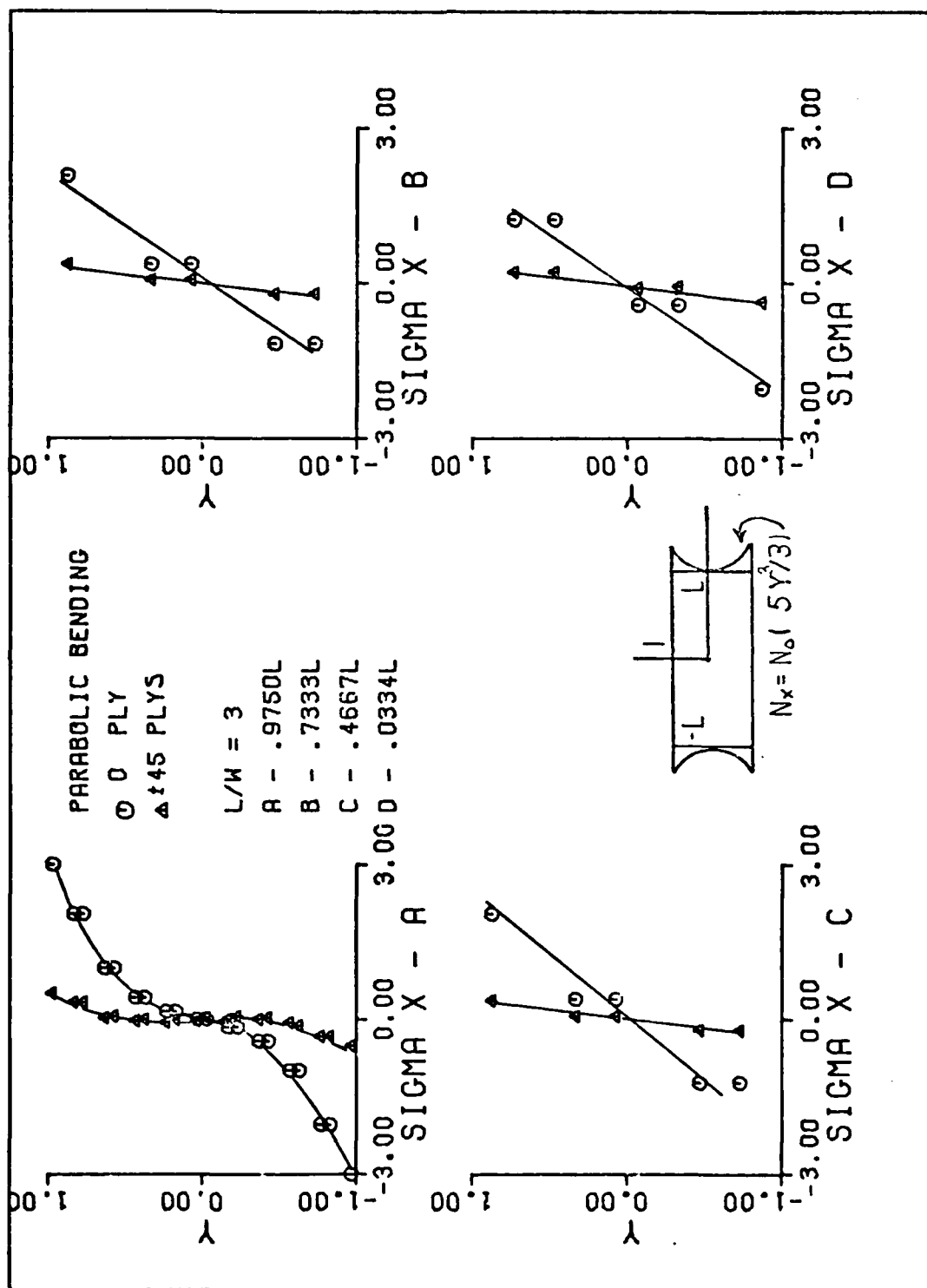


Fig B-13. (0, ±45)s Plate Results for Aspect Ratio of Three

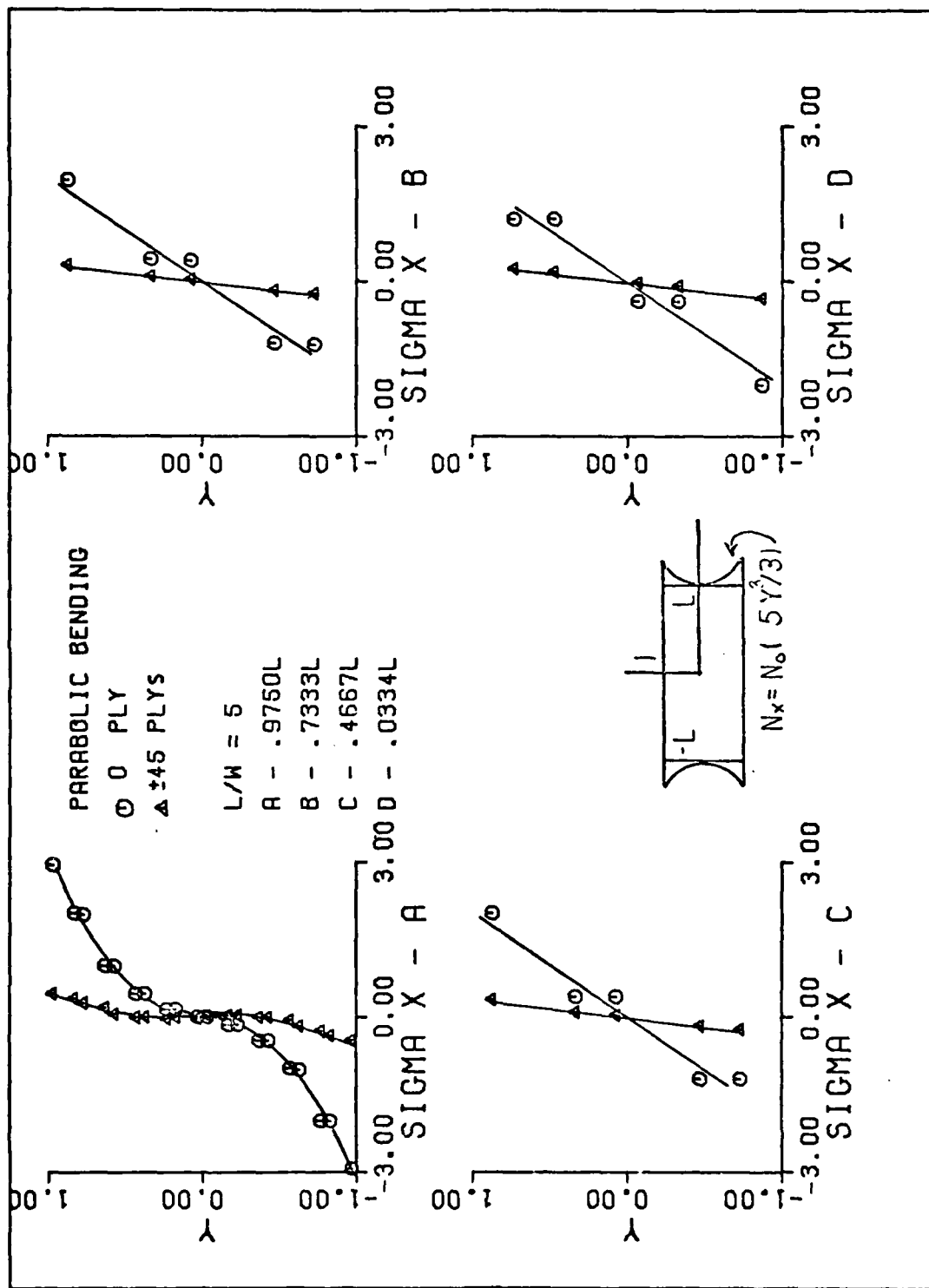


Fig B-14. (0, ±45)s Plate Results for Aspect Ratio of Five

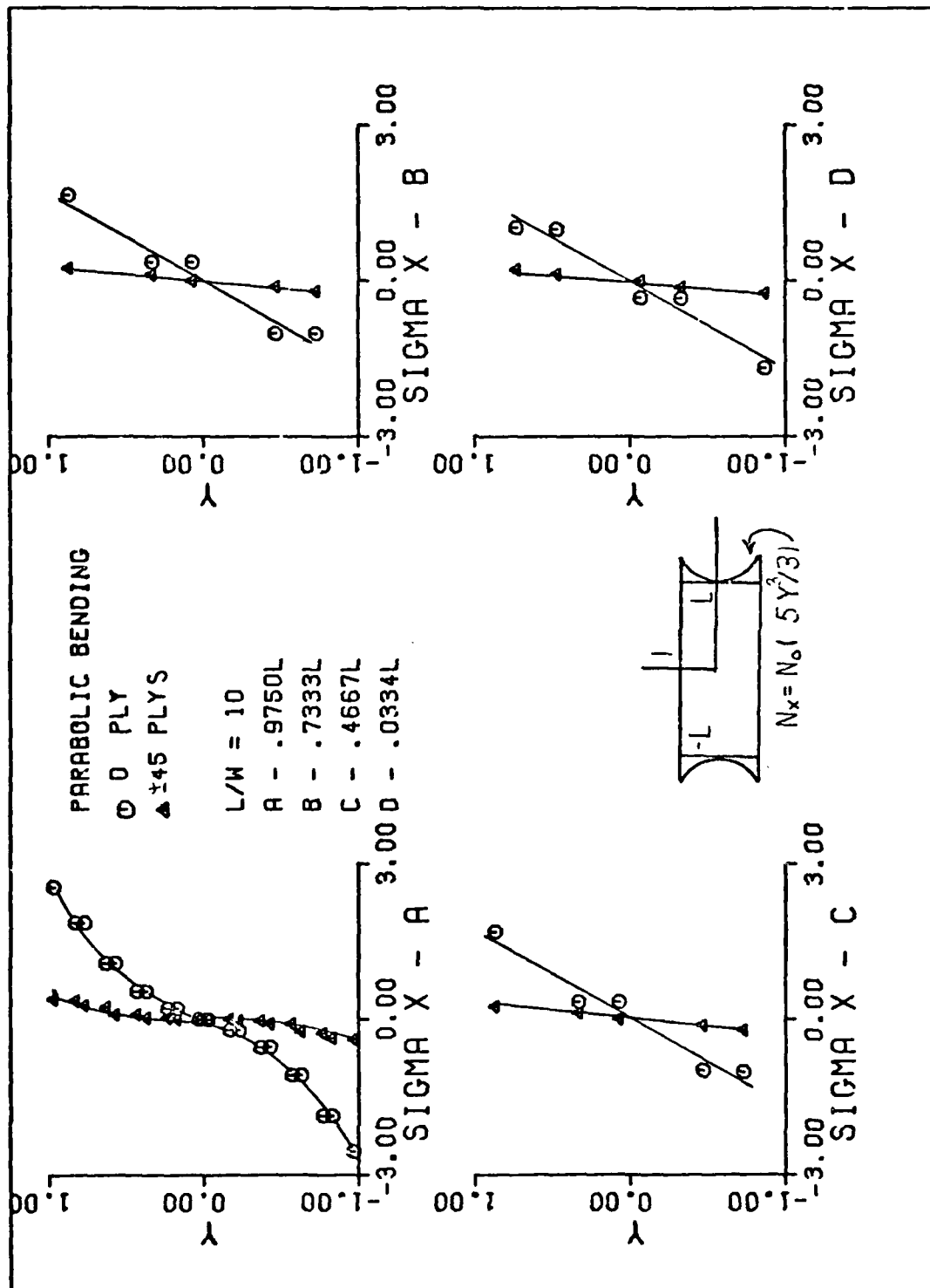


Fig B-15. (0, ±45)s Plate Results for Aspect Ratio of Ten

Appendix C

Graphical Results of the Clamped End Condition

The following figures resulted from the use of the full plate mesh shown in Fib 6-B. All stress in the figures are normalized to the average stress σ_o given by

$$\text{SIGMAX} = \frac{\sigma_x}{\sigma_o} \quad (\text{C-1})$$

and

$$\text{SIGMAXY} = \frac{\sigma_{xy}}{\sigma_o}$$

where σ_x is the stress in the x-direction, σ_{xy} is the shearing stress, SIGMAX is the normalized σ_x stress, SIGMAXY is the normalized σ_{xy} stress, and σ_o is the average stress computed from N_o , the average resultant force. Legend comments of Appendix A apply.

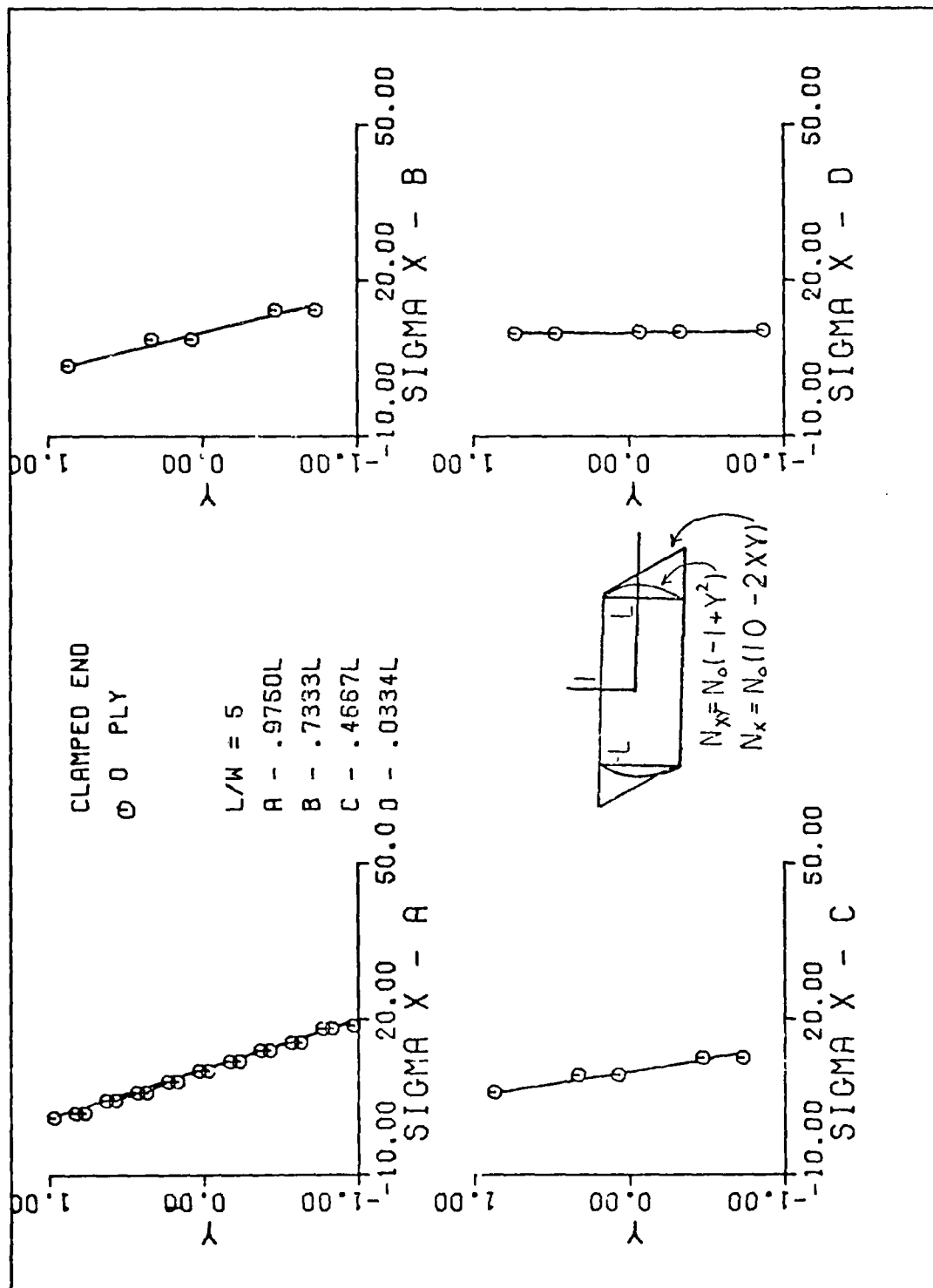


Fig C-1. Single 0 Degree Fiber Oriented Plate SIGMAN Results for Aspect Ratio of Five

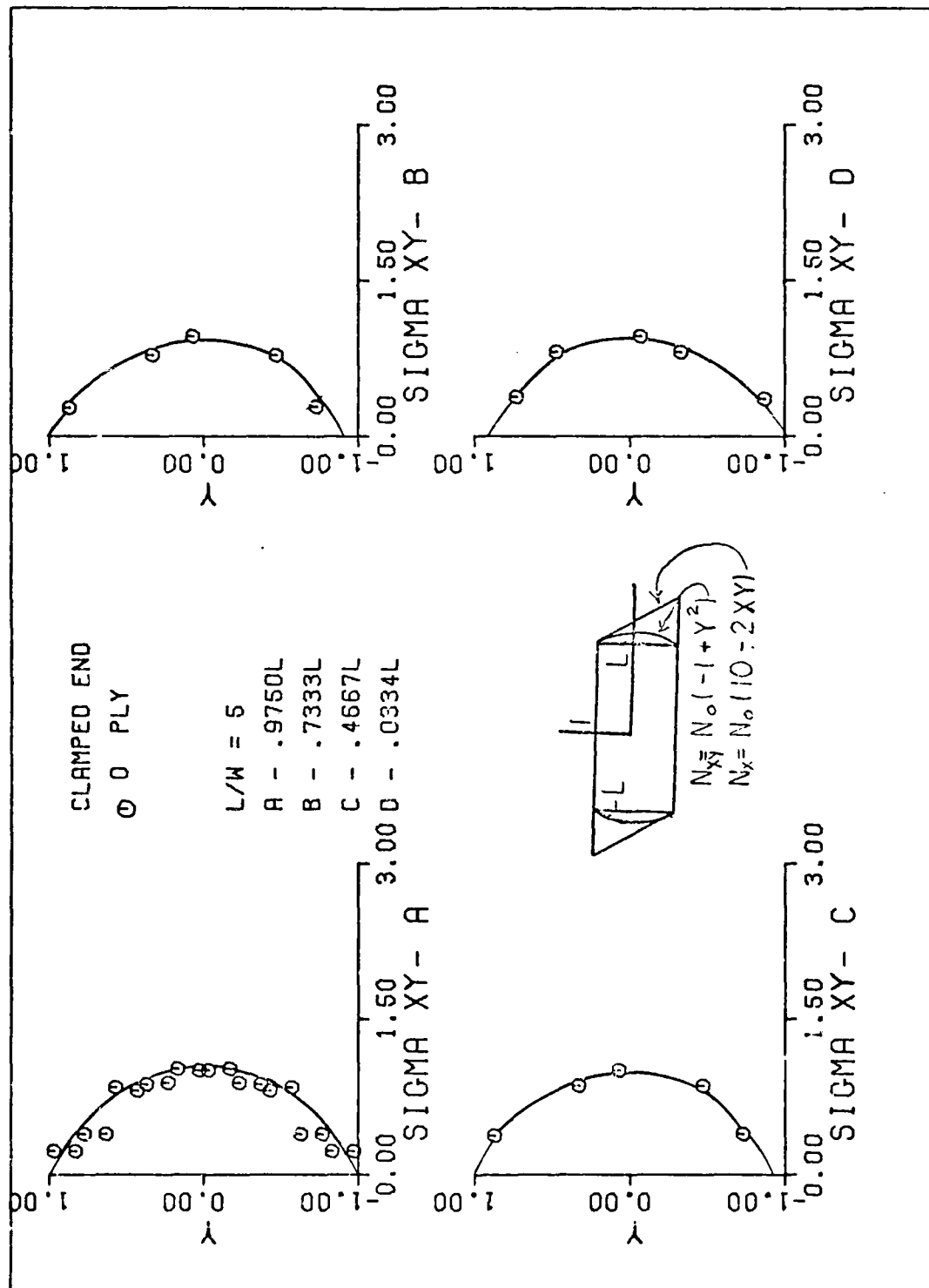


Fig C-2. Single 0 Degree Fiber Oriented Plate SIGMAXY Results for Aspect Ratio of Five

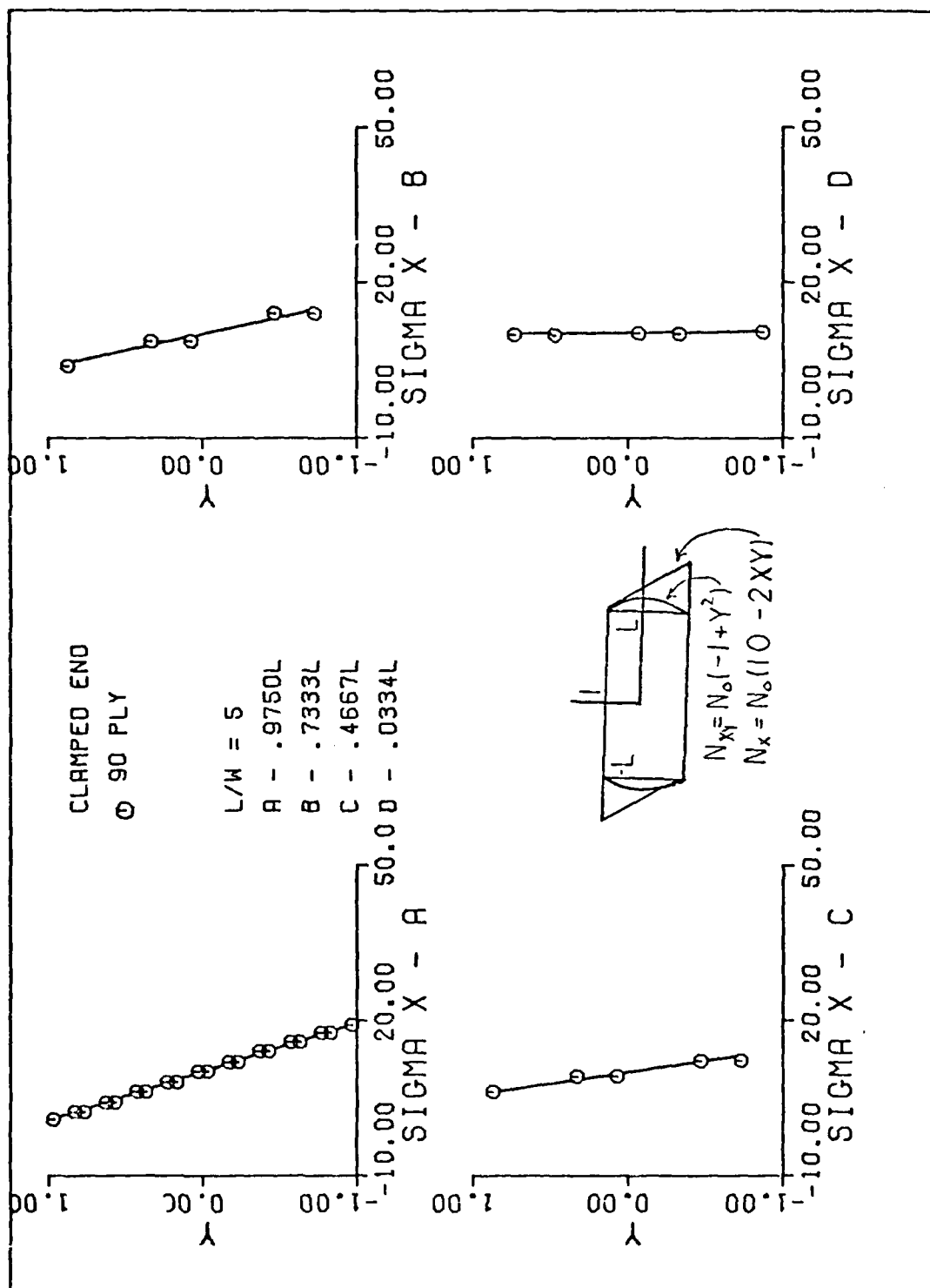


Fig C-3. Single 90 Degree Fiber Oriented Plate SIGMAX Results for Aspect Ratio of Five

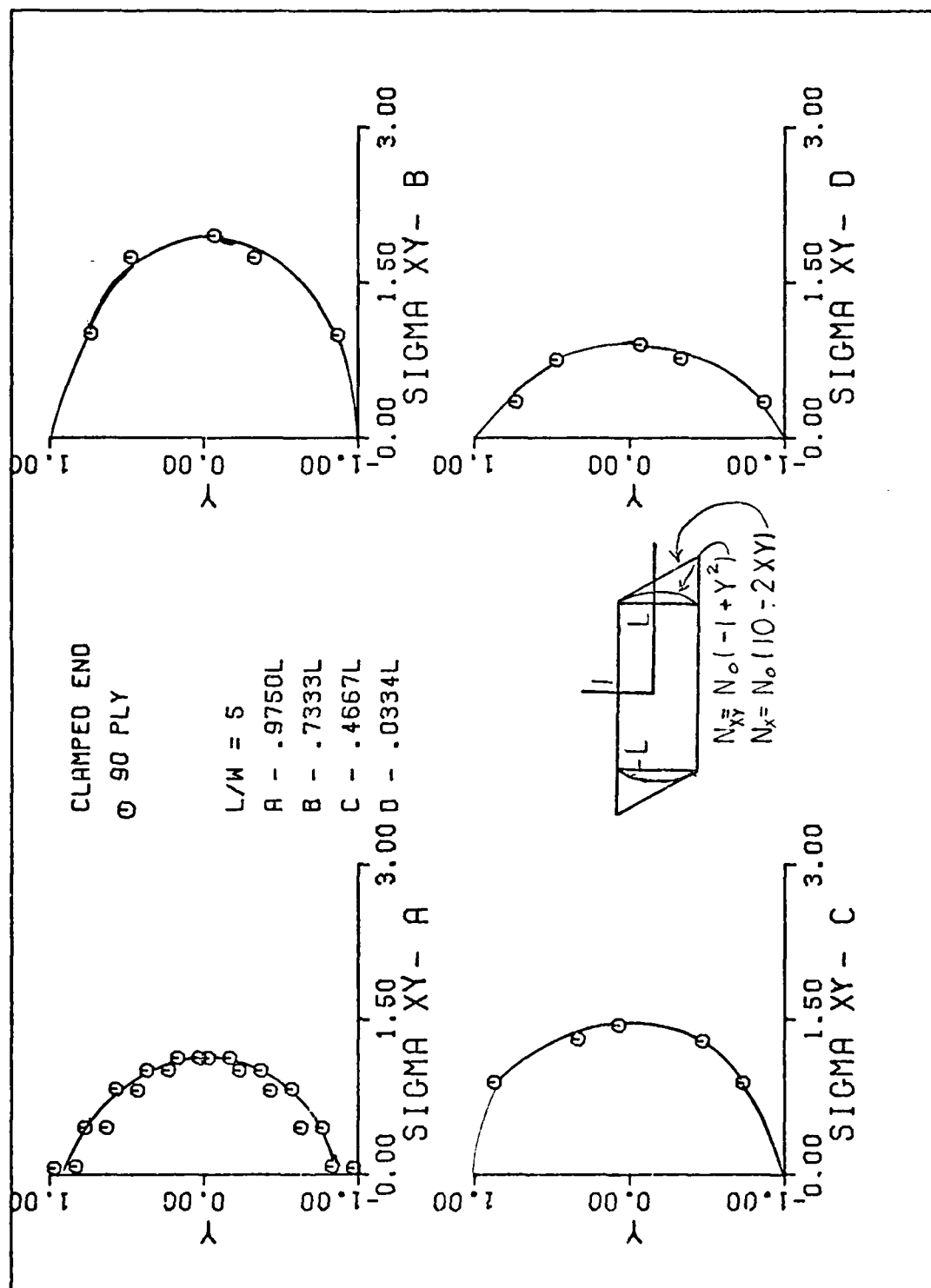


Fig C-4. Single 90 Degree Fiber Oriented Plate SIGMAXY Results for Aspect Ratio of Five

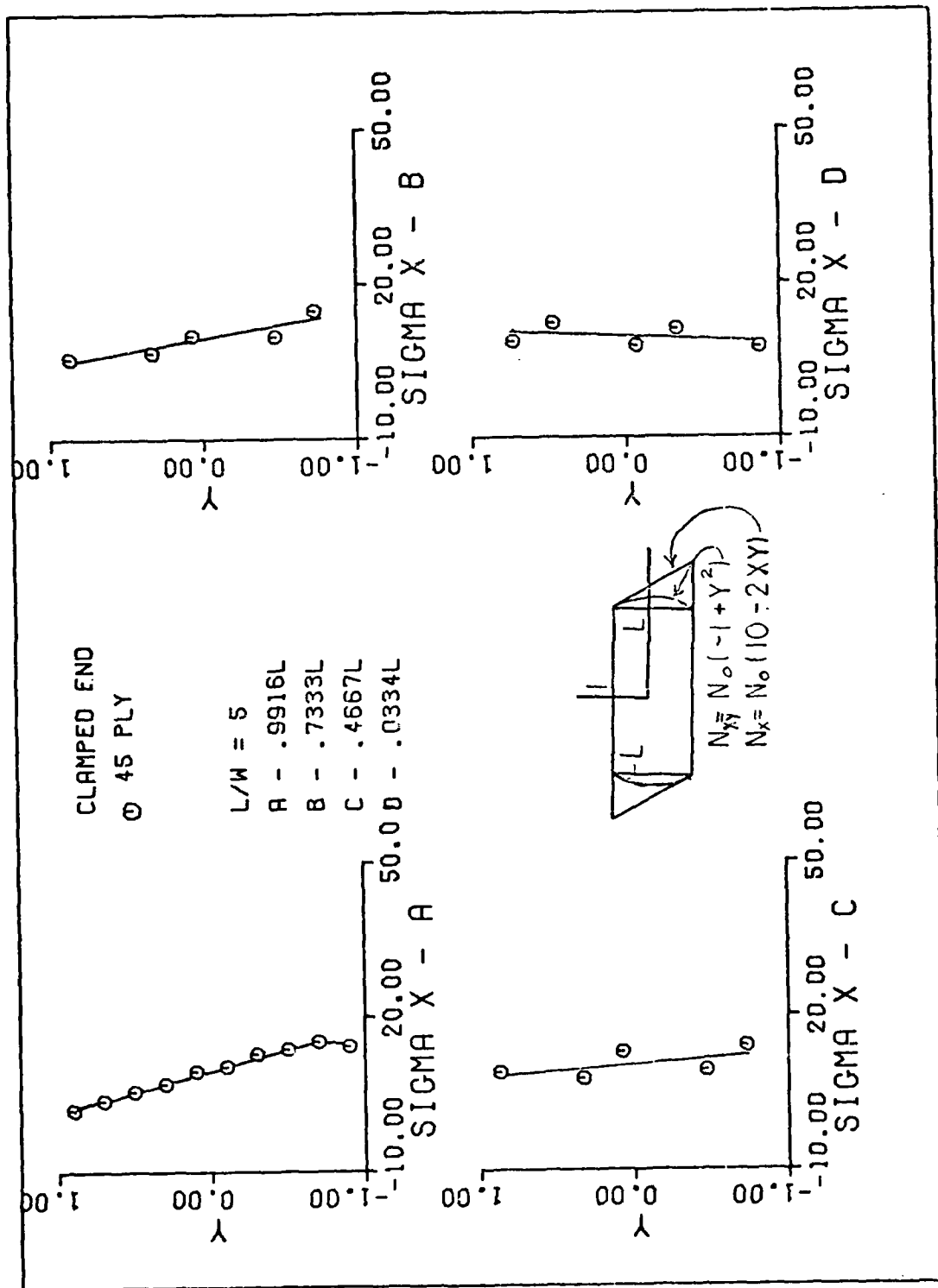


Fig C-5. Single 45 Degree Fiber Oriented Plate SIGMAX Results
 for Aspect Ratio of Five

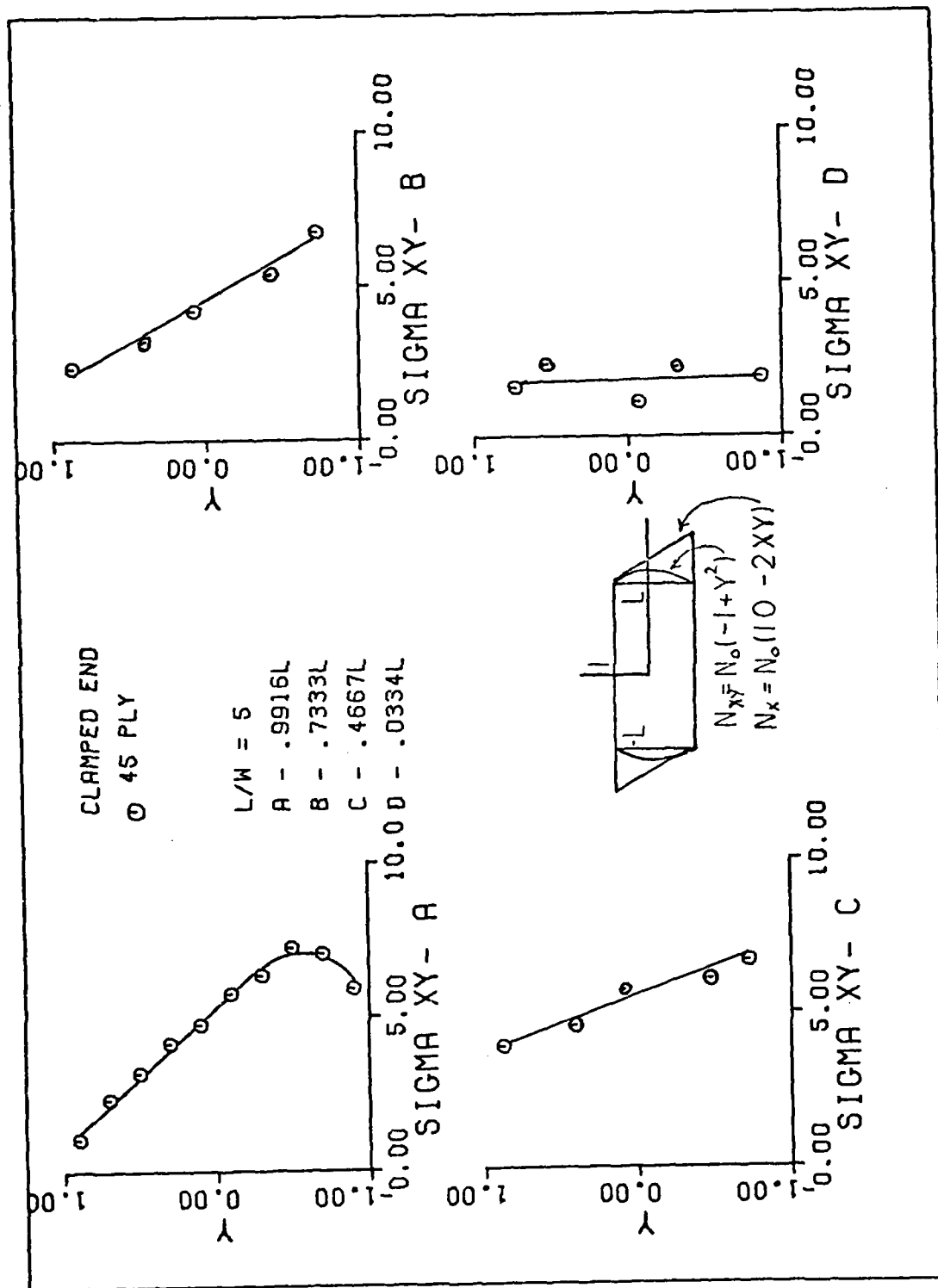


Fig C-6. Single 45 Degree Fiber Oriented Plate SIGMAXY Results for Aspect Ratio of Five

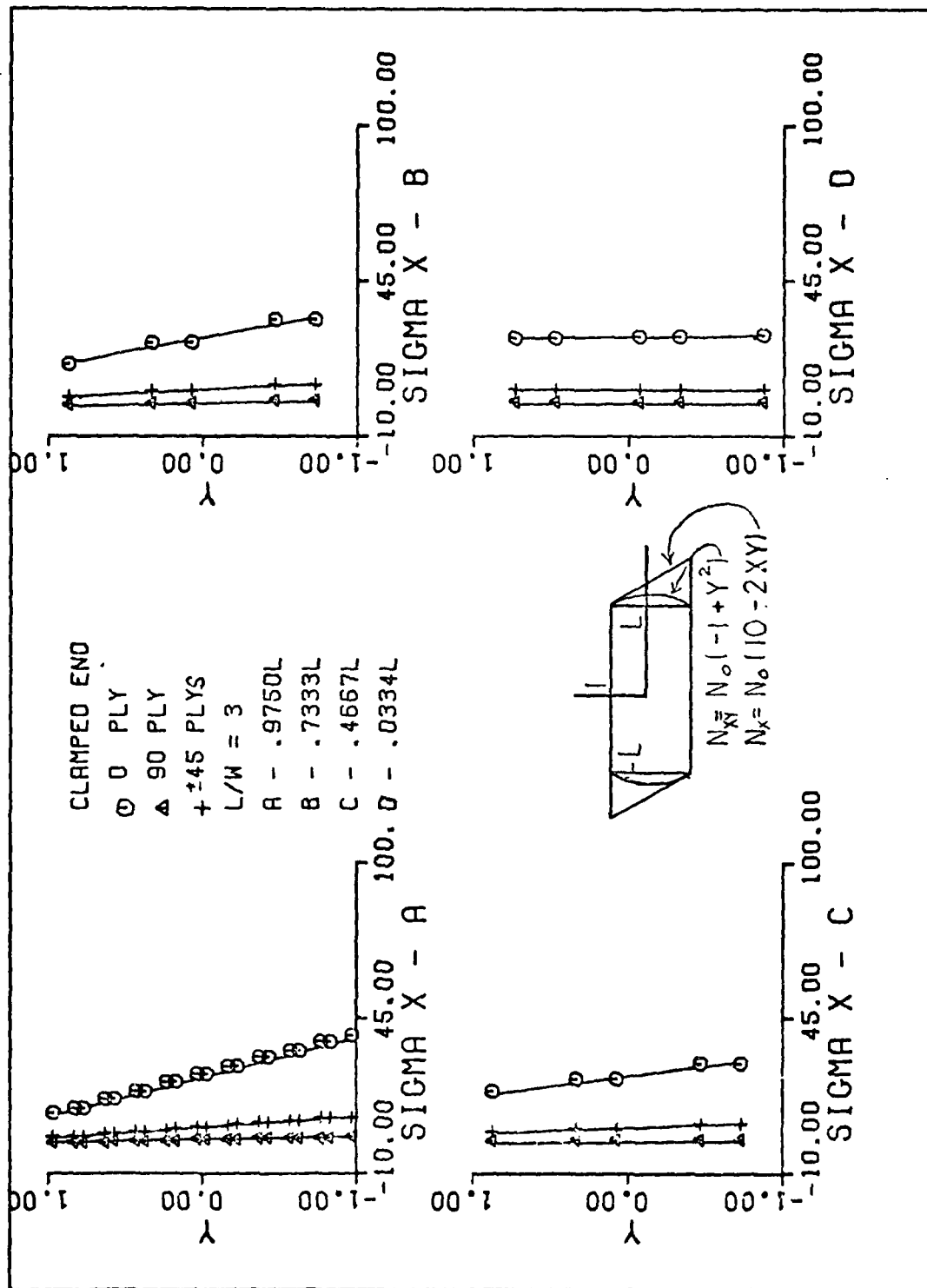


Fig C-7 (0, ±45, 90)s Plate SIGMAX Results
 for Aspect Ratio of Three

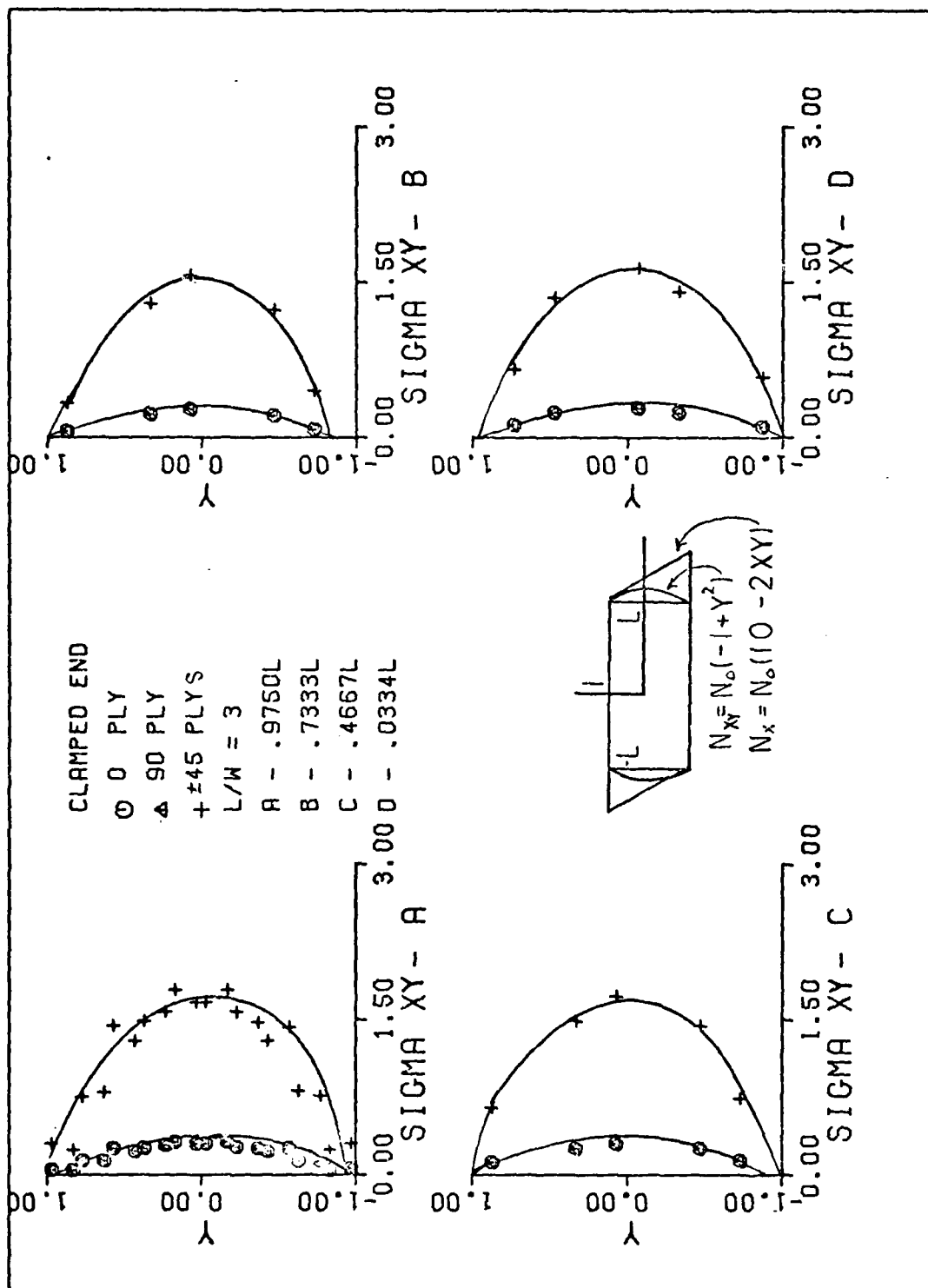


Fig C-8. (0, ±45, 90)s Plate SIGMAXY Results
 for Aspect Ratio of Three

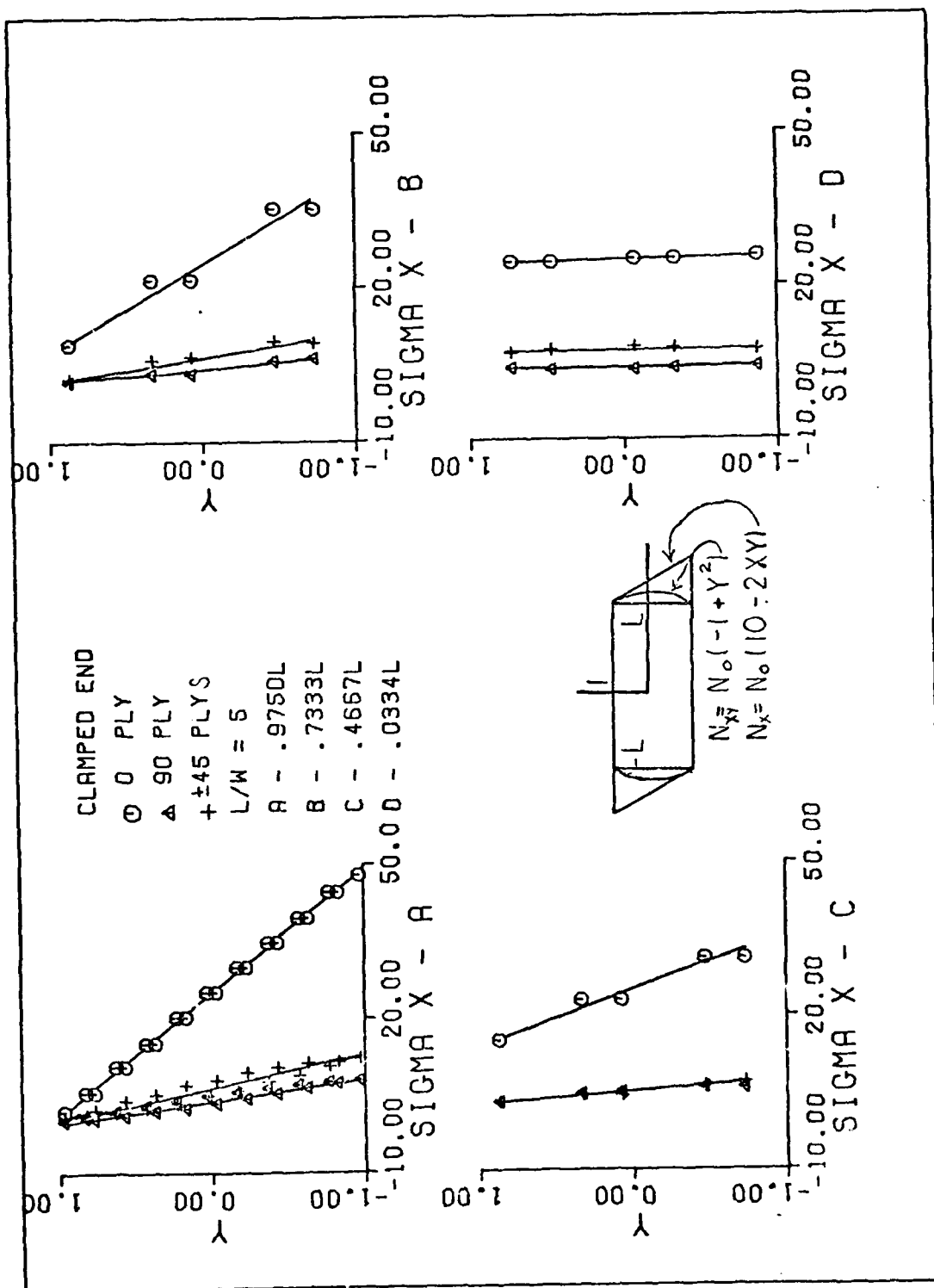


Fig C-9. (0, 45, 90)s Plate SIGMAX Results
 for Aspect Ratio of Five

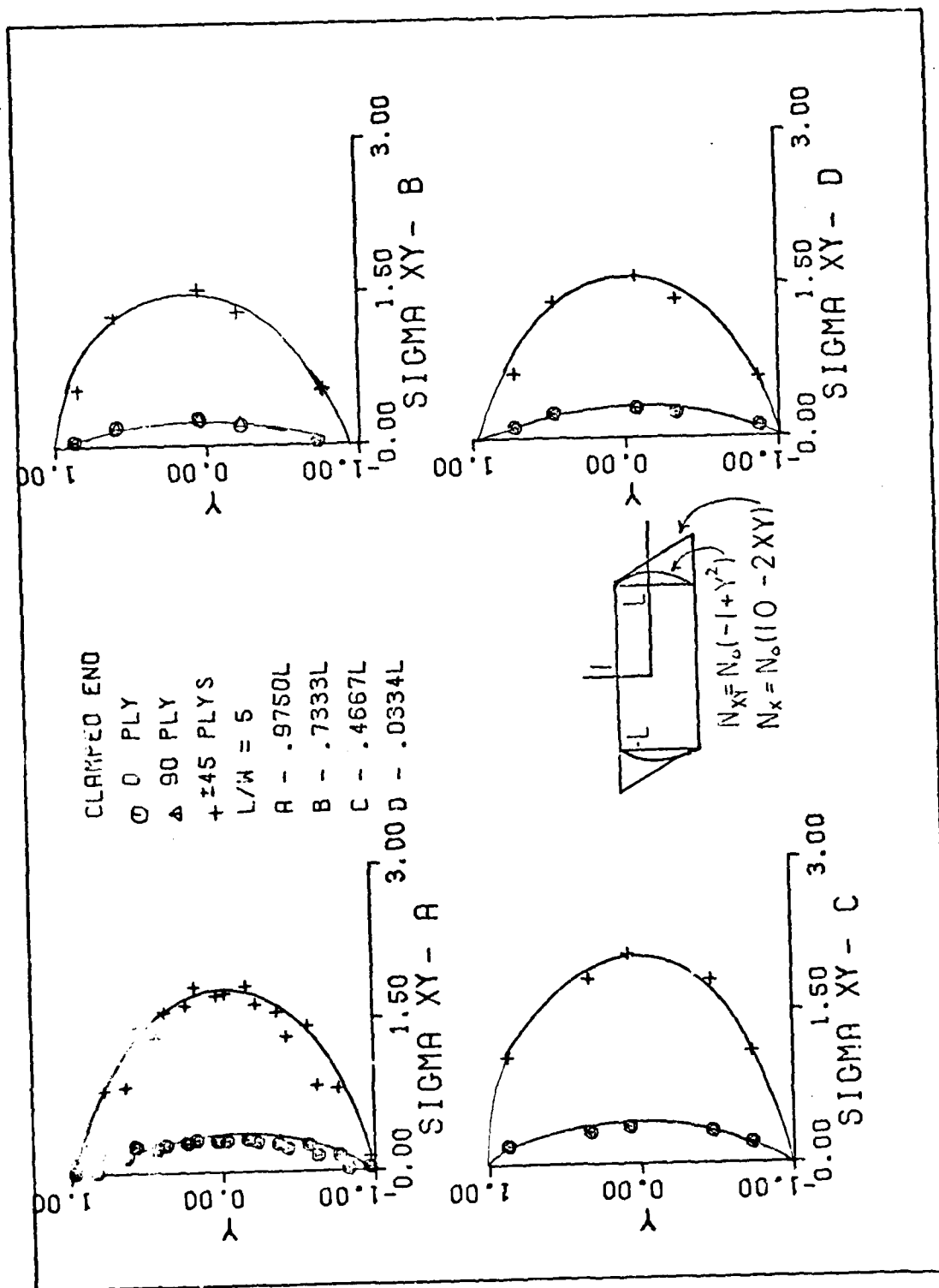


Fig C-10. (0, 45, 90)s Plate SIGMAXY Results
 for Aspect Ratio of Five

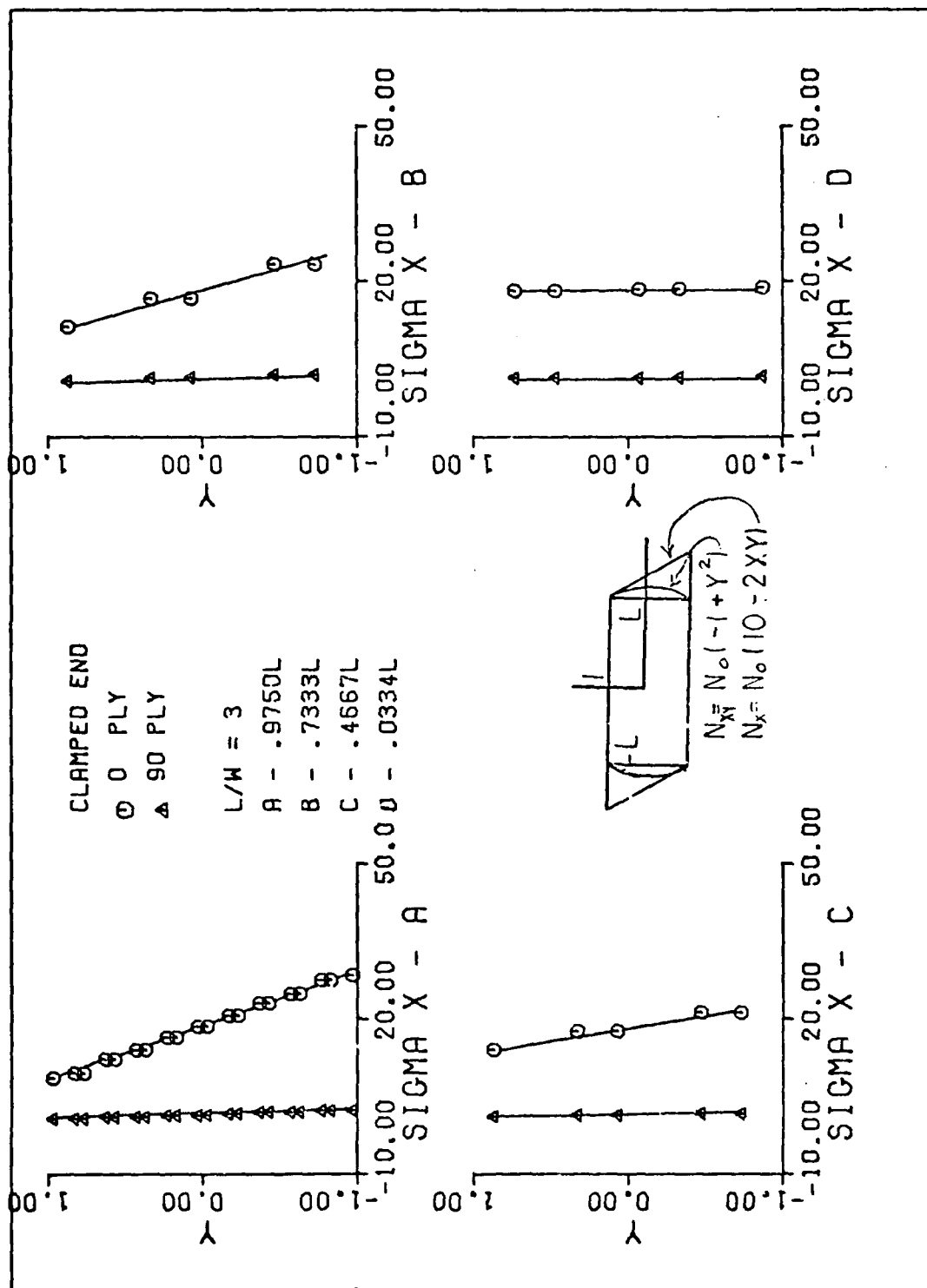


Fig C-11. (0, 90)s Plate SIGMAX Results
for Aspect Ratio of Three

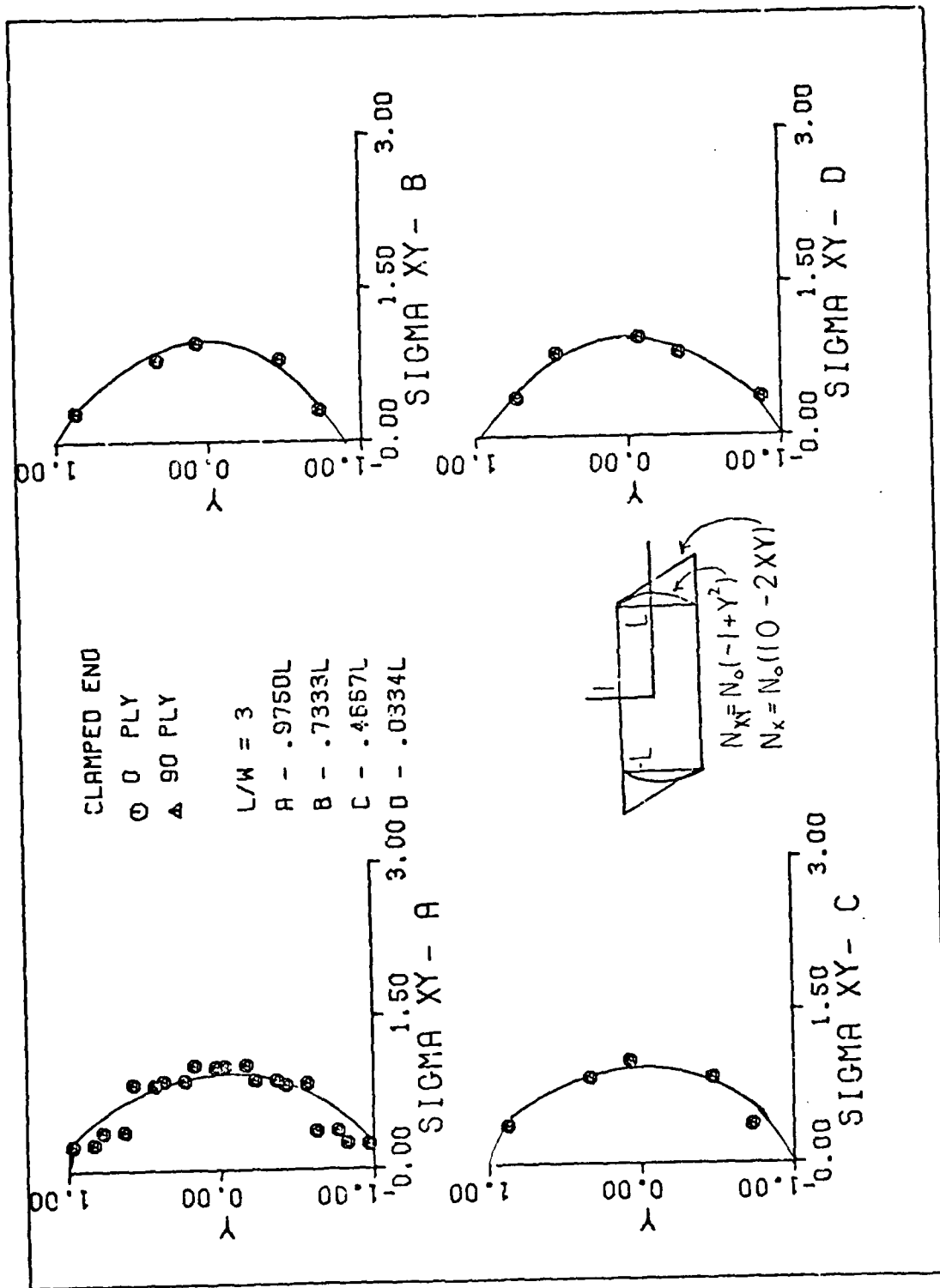


Fig C-12. (0, 90)s Plate SIGMAXY Results
for Aspect Ratio of Three

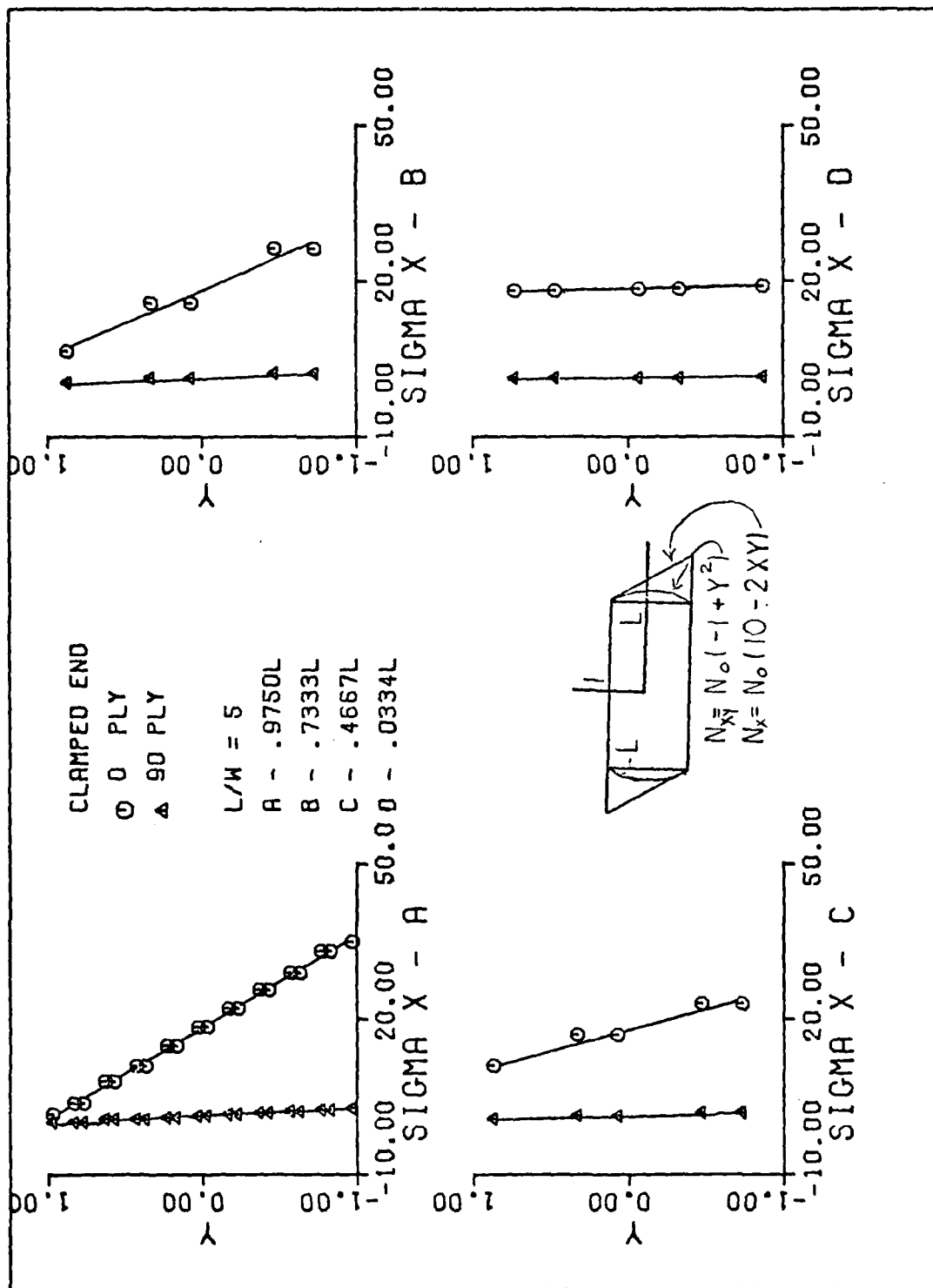


Fig C-13. (0, 90)s Plate SIGMAX Results
 for Aspect Ratio of Five

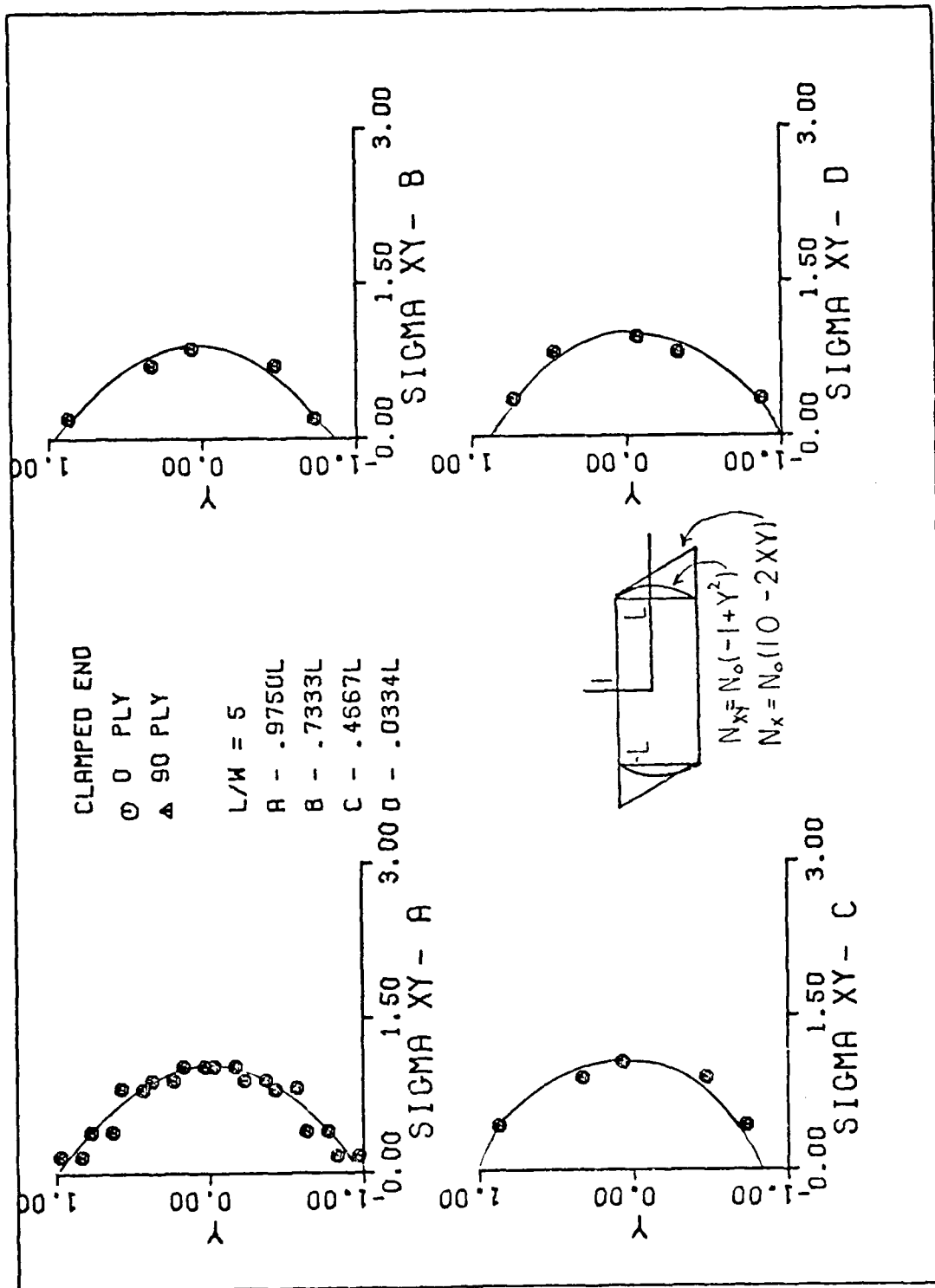


Fig C-14. (0, 90)s Plate SIGMAXY Results
for Aspect Ratio of Five

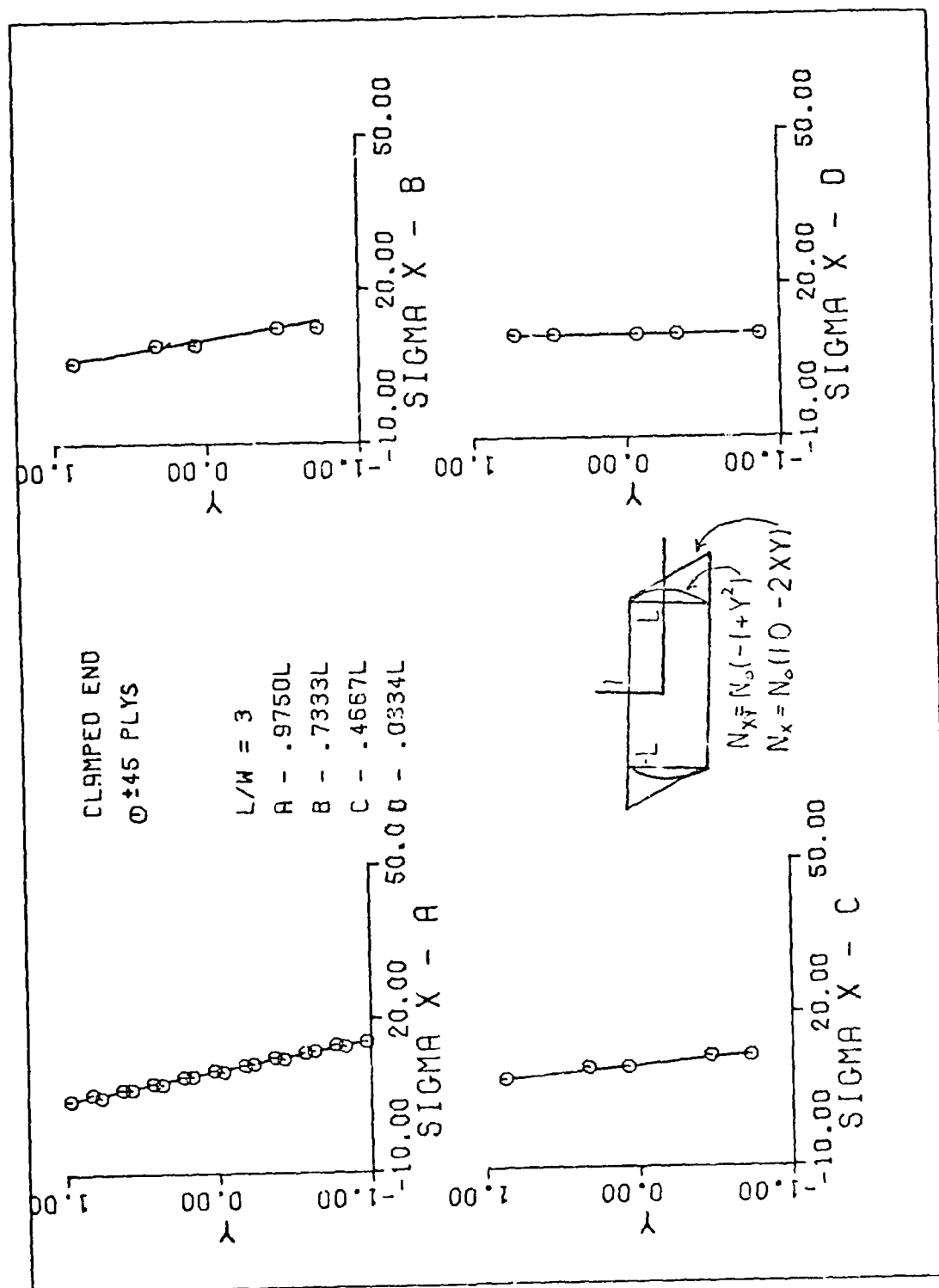


Fig C-15. (±45)s Plate SIGMAX Results for Aspect Ratio of Three

AD-A081 908

AIR FORCE INST OF TECH WRIGHT-PATTERSON AFB OH SCHOO--ETC F/6 11/4
INVESTIGATION OF SAINT VENANT'S PRINCIPLE AS RELATED TO LAMINAT--ETC(U)
DEC 78 S R SMITH
AFIT/0AE/AA/780-13

UNCLASSIFIED

NC

2 of 2

AD-A081 908



END

DATE

FORMED

4-80

DTIC

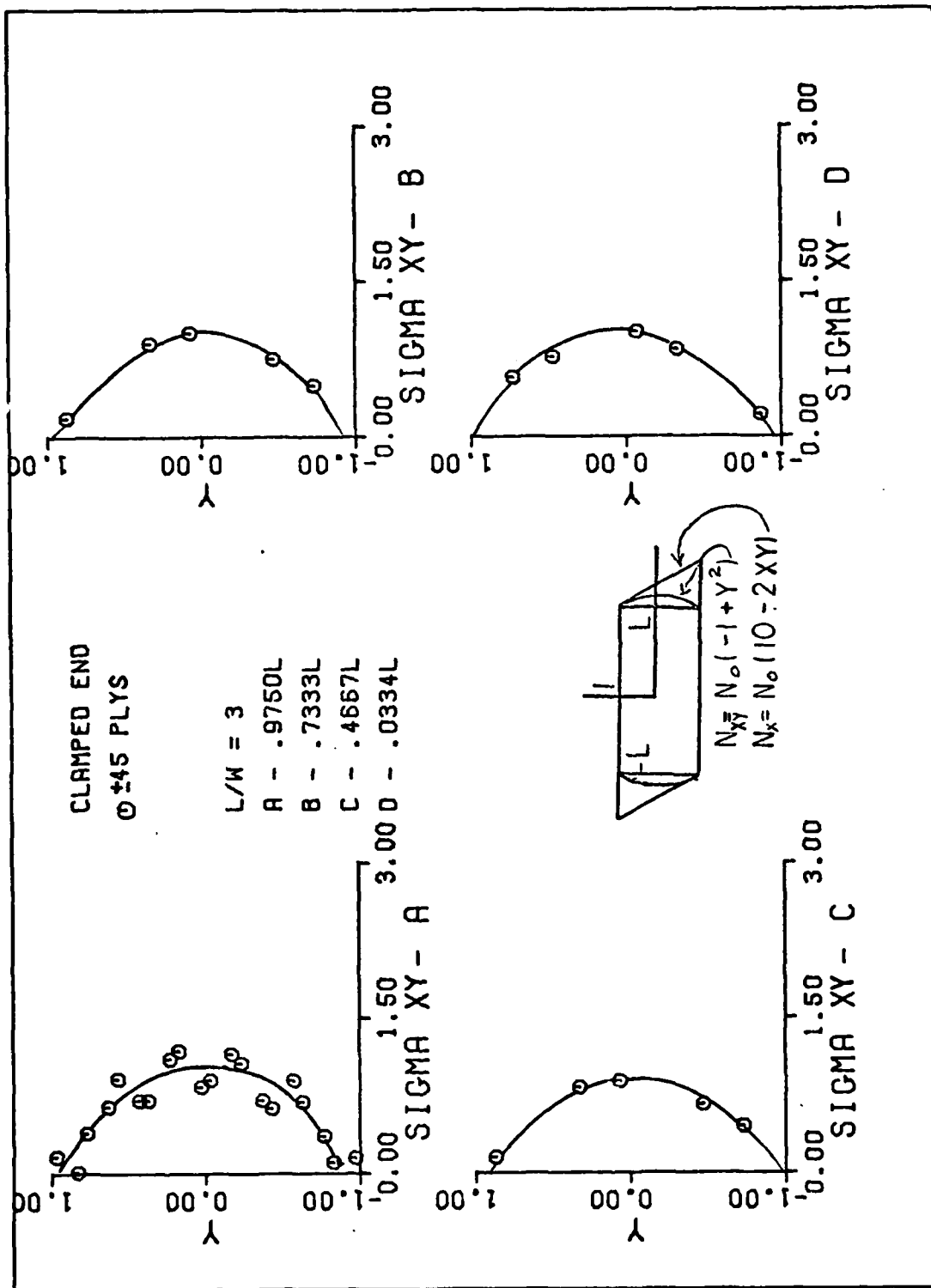


Fig C-16. $(\pm 45)_s$ Plate SIGMAXY Results for Aspect Ratio of Three

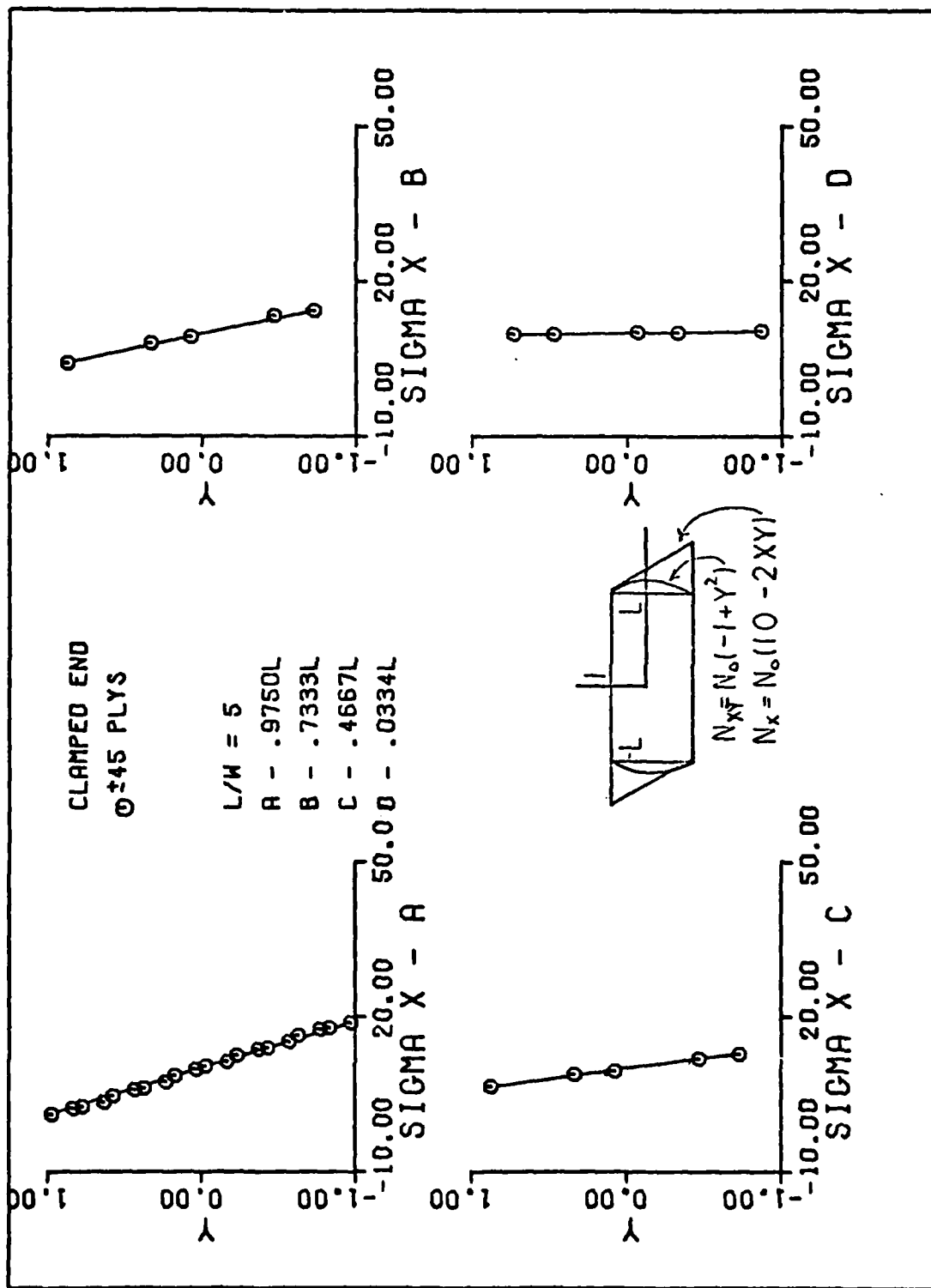


Fig C-17. (± 45) s Plate SIGMAX Results for Aspect Ratio of Five

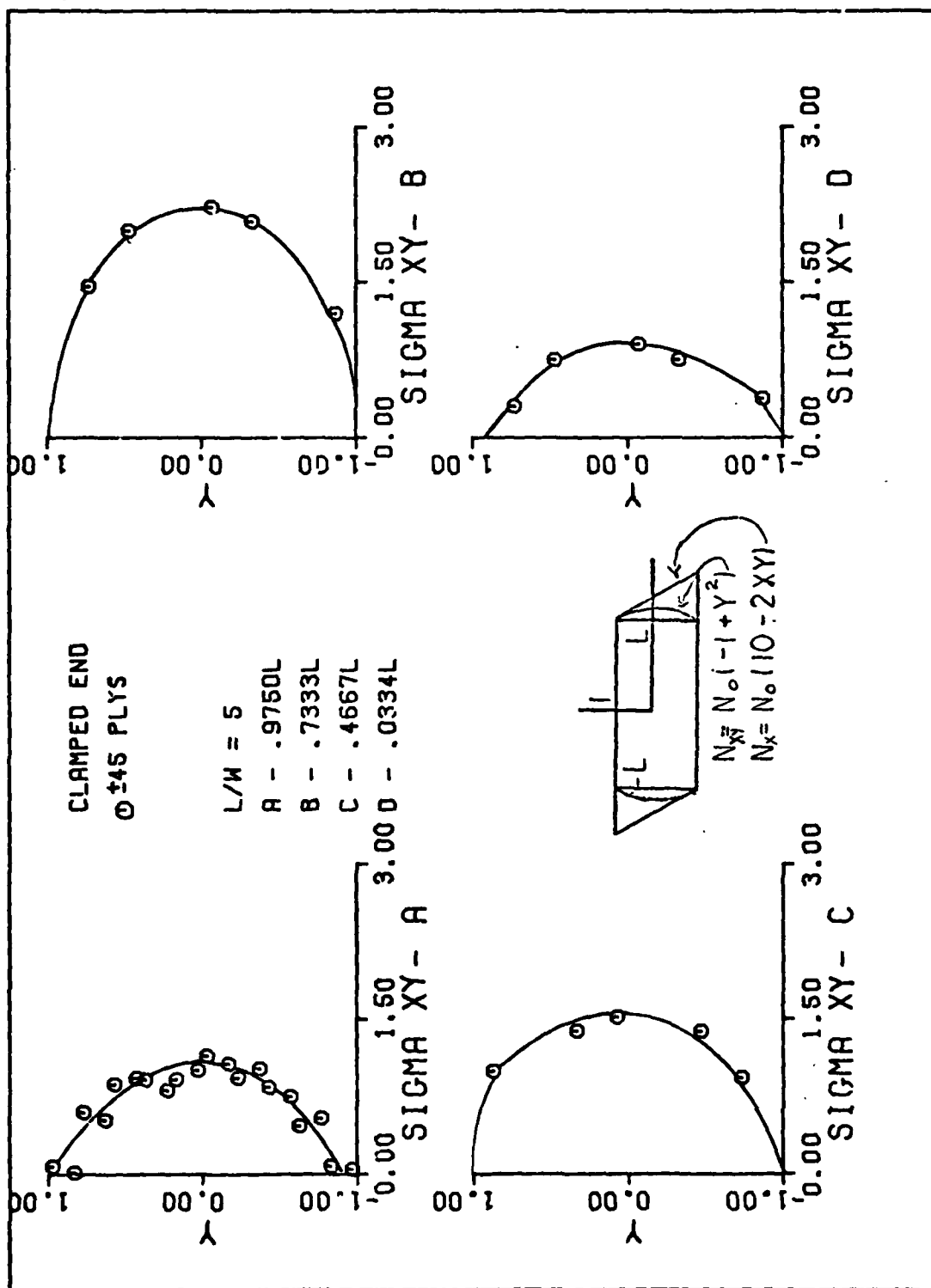


Fig C-18. (± 45) s Plate SIGMAXY Results for Aspect Ratio of Five

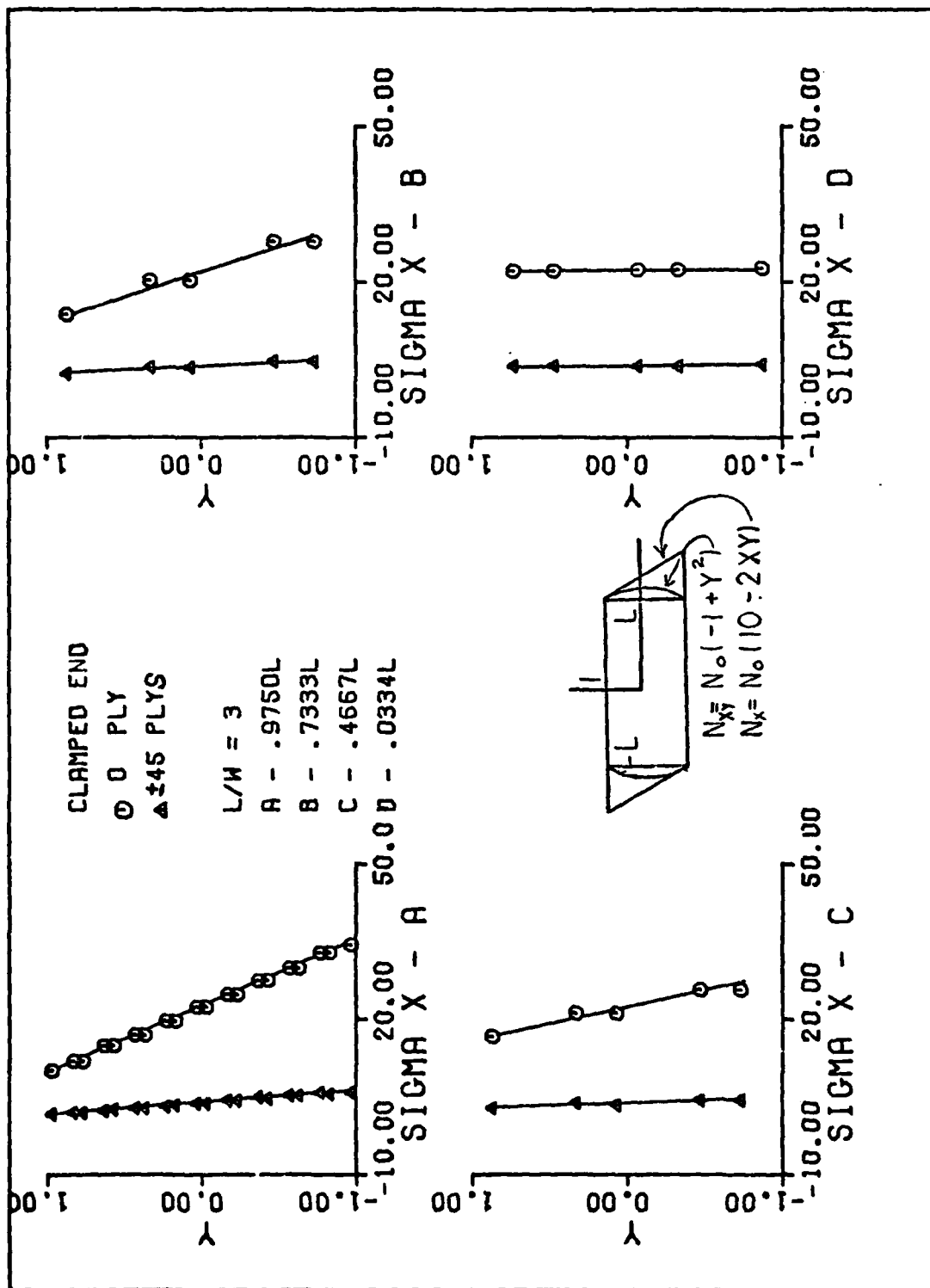


Fig C-19. (0, ±45)s Plate SIGMAX Results for Aspect Ratio of Three

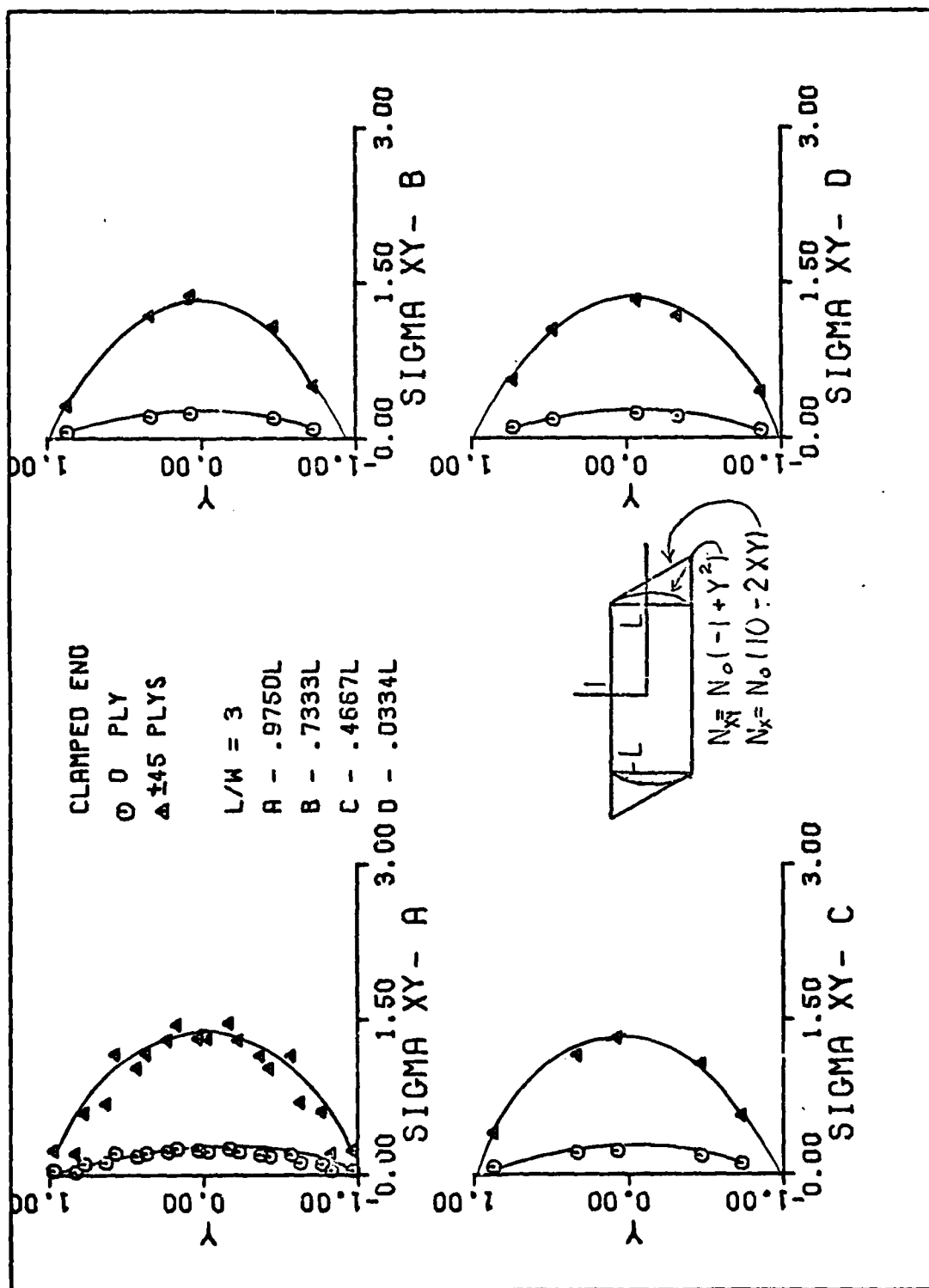


Fig C-20. (0, ±45)s Plate SIGMAXY Results for Aspect Ratio of Three

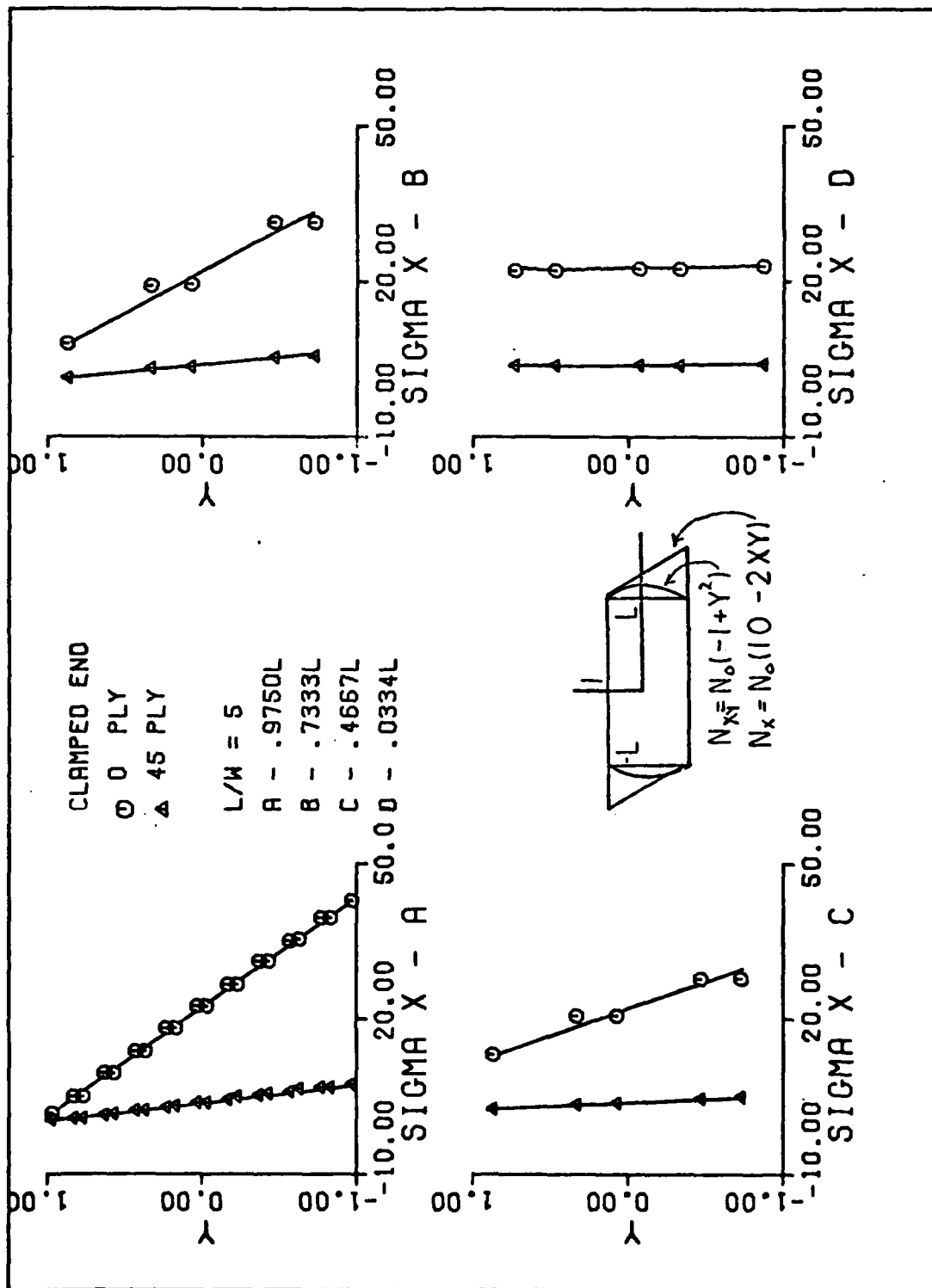


Fig C-21. (0, +45)s Plate SIGMAX Results for Aspect Ratio of Five

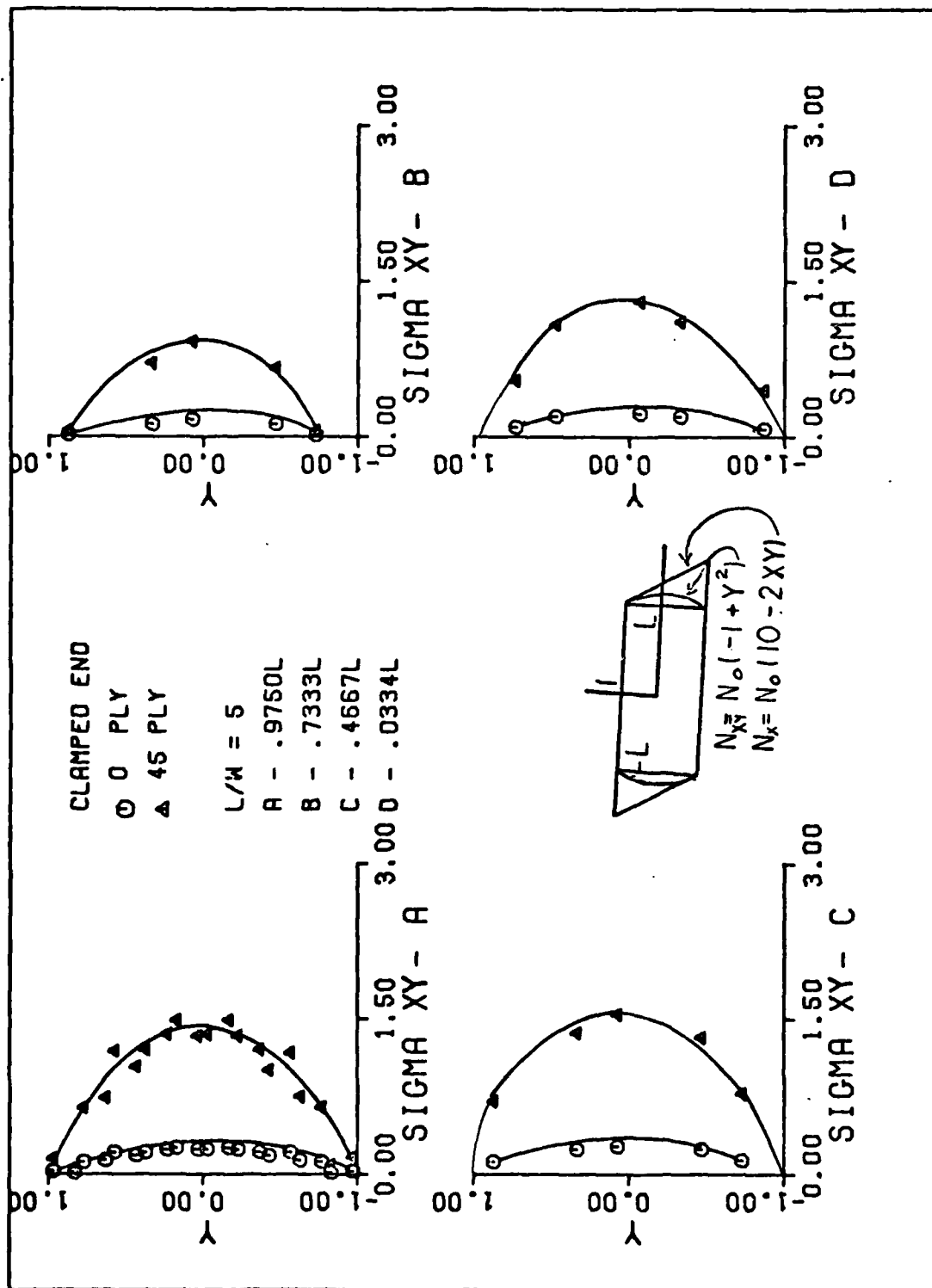


Fig C-22. $(0, \pm 45)$ s Plate SIGMAXY Results for Aspect Ratio of Five

Appendix D

Analytic Solution for the Orthotropic Plate

The following mathematical development follows the analytic solution presented by Choi and Horgan. An approach similar to this can be followed if laminate plate material properties are considered in place of constitutive constants. The development for the 0deg ply is presented here for completeness. For further details, Reference 6 should be consulted.

The strains for a plate in a state of plane strain are as follows:

$$2e_{ij} = U_{i,j} + U_{j,i} \quad (D-1)$$

where u is the displacement. The strains can also be written in terms of the in-plane stresses as follows

$$\begin{aligned} e_{11} &= \beta_{11}\tau_{11} + \beta_{12}\tau_{22} + \beta_{16}\tau_{12} \\ e_{22} &= \beta_{21}\tau_{11} + \beta_{22}\tau_{22} + \beta_{26}\tau_{12} \\ 2e_{12} &= \beta_{61}\tau_{11} + \beta_{62}\tau_{22} + \beta_{66}\tau_{12} \end{aligned} \quad (D-2)$$

where the subscripts on the stresses and strains represent the planes of symmetry in the material and the β 's form the compliance matrix. The elastic constants (β 's) are assumed to be such that the strain energy density is positive-definite, and

$\beta_{ij} = \beta_{ji}$. The positive-definite condition yields the condition

$$\begin{aligned} & \beta_{11}\beta_{22}\beta_{66} + 2\beta_{16}\beta_{26}\beta_{12} - \beta_{11}\beta_{26}^2 \\ & - \beta_{22}\beta_{16}^2 - \beta_{66}\beta_{12}^2 > 0 \\ & \beta_{11} > 0, \quad \beta_{11}\beta_{22} - \beta_{12}^2 > 0 \end{aligned} \tag{D-3}$$

The Airy stress functions used are

$$\sigma_x = \phi_{yy}, \quad \sigma_y = \phi_{xx} \quad \text{and} \quad \tau_{xy} = -\phi_{xy} \tag{D-4}$$

where the subscripts denote differentiation.

The compatibility relations yield

$$\begin{aligned} & \beta_{22}\phi_{xxxx} - 2\beta_{26}\phi_{xxxy} + (2\beta_{12} + \beta_{66})\phi_{xxyy} \\ & - 2\beta_{16}\phi_{xyyy} + \beta_{11}\phi_{yyyy} = 0 \end{aligned} \tag{D-5}$$

The equilibrium conditions are identically satisfied by the stress functions. A solution of Eq (D-5) is sought in the form

$$\phi = e^{-\gamma x} F(y) \tag{D-6}$$

where γ is a constant.

The lateral boundary conditions are

$$F(\pm 1) = 0 \quad F'(\pm 1) = 0 \tag{D-7}$$

for a plate loaded in tension.

Substituting the above stress function into the compatibility relation (D-5) yields:

$$\begin{aligned} \beta_{11} F_{,yyyy} + 2\beta_{16} \gamma F_{,yyy} + (2\beta_{12} + \beta_{66}) \gamma^2 F_{,yy} \\ + 2\beta_{26} \gamma^3 F_{,y} + \beta_{22} \gamma^4 F = 0 \end{aligned} \quad (D-8)$$

where the subscripts on F indicate differentiation.

Eqs (D-7) and (D-8) form an eigenvalue problem for the ordinary differential Eq (D-8). A solution of Eq (D-8) is sought in the form of

$$F(y) = e^{\omega y} \quad (D-9)$$

or

$$\begin{aligned} \phi &= e^{-\gamma x} e^{\omega y} \\ &= e^{\omega y - \gamma x} \end{aligned} \quad (D-10)$$

Eq (D-8) becomes

$$\begin{aligned} \beta_{11} \omega^4 + 2\beta_{16} \gamma \omega^3 + (2\beta_{12} + \beta_{66}) \gamma^2 \omega^2 + 2\beta_{26} \gamma^3 \omega \\ + \beta_{22} \gamma^4 = 0 \end{aligned} \quad (D-11)$$

We now let $\omega = \mu \gamma$ where ω and μ are complex numbers.

Eq (D-11) becomes

$$\begin{aligned} \beta_{11} \mu^4 + 2\beta_{16} \mu^3 + (2\beta_{12} + \beta_{66}) \mu^2 \\ + 2\beta_{26} \mu + \beta_{22} = 0 \end{aligned} \quad (D-12)$$

From the positive-definite strain energy density conditions, it can be shown that the roots of μ are complex or purely imaginary.

The conjugate pairs of roots are

$$\omega_{1,2} = (p_1 \pm iq_1)\gamma \quad \delta_{3,4} = (p_2 \pm iq_2)\gamma \quad (D-13)$$

$$\text{where} \quad \mu = P \pm iq \quad (D-14)$$

Using the Eqs (D-9) and D-13), the complete solution is

$$F(y) = A_1 e^{(P_1 \pm iq_1)\gamma y} + A_2 e^{(P_2 \pm iq_1)\gamma y} \quad (D-15)$$

$$F(y) = e^{P_1 \gamma y} (C_1 \cos q_1 \gamma y + C_2 \sin q_1 \gamma y) \\ + e^{P_2 \gamma y} (C_3 \cos q_2 \gamma y + C_4 \sin q_2 \gamma y) \quad (D-16)$$

where A_i and C_i are arbitrary constants.

For the orthotropic case, $\beta_{16} = 0$ and $\beta_{26} = 0$ and three cases of the solution (D-16) can be considered.

$$\text{Case A: } (2\beta_{12} + \beta_{66})^2 - 4\beta_{11}\beta_{22} > 0$$

$$\text{Case B: } (2\beta_{12} + \beta_{66})^2 - 4\beta_{11}\beta_{22} < 0 \quad (D-17)$$

$$\text{Case C: } (2\beta_{12} + \beta_{66})^2 - 4\beta_{11}\beta_{22} = 0$$

For Boron Epoxy:

$$\beta_{12} = .227$$

$$\beta_{66} = 24.2$$

$$\beta_{11} = .722$$

$$\beta_{22} = 13.6$$

$$\begin{aligned}
& (2\beta_{12} + \beta_{66})^2 - 4\beta_{11}\beta_{22} \\
& = [2(.227) + 24.2]^2 - 4(.722)(13.6) > 0
\end{aligned}$$

\therefore Case A applies

when Case A holds

$$P_1 = P_2 = 0, \quad \omega \text{ is purely imaginary}$$

$$\omega_{1,2} = \pm q_1 \gamma, \quad \omega_{3,4} = \pm q_2 \gamma$$

The even eigenfunctions of Eq (D-8) are

$$Fe(y) = \frac{\cos \gamma q_1 y}{\cos \gamma q_1} - \frac{\cos \gamma q_2 y}{\cos \gamma q_2} \quad (D-18)$$

where γ is a root of

$$q_1 \tan \gamma q_1 - q_2 \tan \gamma q_2 = 0$$

The odd eigenfunctions of Eq (D-8) are

$$Fe(y) = \frac{\sin \gamma q_1 y}{\sin \gamma q_1} - \frac{\sin \gamma q_2 y}{\sin \gamma q_2} \quad (D-19)$$

where γ is a root of

$$q_1 \cot \gamma q_1 - q_2 \cot \gamma q_2 = 0$$

From the Airy stress functions and Eq (D-6), we get

$$\sigma_x = e^{-\gamma x} F'', \quad \sigma_y = \gamma^2 e^{-\gamma x} F, \quad \tau_{xy} = +\gamma e^{-\gamma x} F', \quad (D-20)$$

The total stress can be found by taking a summation of the individual solutions or

$$\begin{aligned}
 \phi &= \sum_{k=1}^{\infty} C_k e^{-\gamma_k x} F_k(y) \\
 \sigma_x &= \sum_{k=1}^{\infty} C_k e^{-\gamma_k x} F_k''(y) \\
 \sigma_{xy} &= \sum_{k=1}^{\infty} C_k \gamma_k^2 e^{-\gamma_k x} F_k(y) \\
 \tau_{xy} &= \sum_{k=1}^{\infty} C_k \gamma_k e^{-\gamma_k x} F_k'(y)
 \end{aligned}
 \tag{D-21}$$

where C_k is an arbitrary constant determined from the end condition. Using the relationship

$$e^z = 2(\cosh z + \sinh z) \tag{D-22}$$

Eq (17) becomes

$$\begin{aligned}
 \phi &= \sum_{k=1}^{\infty} (a_k \cosh \gamma_k x + b_k \sinh \gamma_k x) F_k(y) \\
 \sigma_x &= \sum_{k=1}^{\infty} (a_k \cosh \gamma_k x + b_k \sinh \gamma_k x) F_k''(y) \\
 \sigma_y &= \sum_{k=1}^{\infty} \gamma_k^2 (a_k \cosh \gamma_k x + b_k \sinh \gamma_k x) F_k(y) \\
 \tau_{xy} &= \sum_{k=1}^{\infty} \gamma_k (a_k \sinh \gamma_k x + b_k \cosh \gamma_k x) F_k'(y)
 \end{aligned}
 \tag{D-23}$$

where a_k and b_k are arbitrary constants determined from the end conditions and orthogonality conditions.

Vita

Steven Robert Smith was born 19 May 1950, in Washington, Indiana. He graduated from Boonville High School of Boonville Indiana in 1968. After receiving a Bachelor of Science in Engineering from the University of Evansville, Indiana in 1973, he was commissioned through the Reserve Officers' Training Corps. From June 1973 to June 1977, he served as a Range Development Engineer and was involved in aircraft flight testing at Edwards AFB, California. In June, 1977, he entered the Air Force Institute of Technology in the Graduate Aeronautical Engineering Program.

Permanent Address: Route 1
Boonville, Ind. 47601

REPORT DOCUMENTATION PAGE		READ INSTRUCTIONS BEFORE COMPLETING FORM
1. REPORT NUMBER AFIT/GAE/AA/78D-13	2. GOVT ACCESSION NO.	3. RECIPIENT'S CATALOG NUMBER
4. TITLE (and Subtitle) Investigation of Saint Venant's Principle as Related to Laminated Composite Plates		5. TYPE OF REPORT & PERIOD COVERED MS Thesis Jun 77 - Dec 78
7. AUTHOR(s) Steven R. Smith Capt. USAF		6. PERFORMING ORG. REPORT NUMBER
9. PERFORMING ORGANIZATION NAME AND ADDRESS Air Force Institute of Technology AFIT/EN, WPAFB, Ohio 45433		8. CONTRACT OR GRANT NUMBER(s)
11. CONTROLLING OFFICE NAME AND ADDRESS		10. PROGRAM ELEMENT, PROJECT, TASK AREA & WORK UNIT NUMBERS
14. MONITORING AGENCY NAME & ADDRESS (if different from Controlling Office)		12. REPORT DATE December 1978
		13. NUMBER OF PAGES 108
		15. SECURITY CLASS. (of this report) unclassified
		15a. DECLASSIFICATION/DOWNGRADING SCHEDULE
16. DISTRIBUTION STATEMENT (of this Report) Approved for public release; distribution unlimited		
17. DISTRIBUTION STATEMENT (of the abstract entered in Block 20, if different from Report)		
18. SUPPLEMENTARY NOTES Approved for public release; IAW AFR 190-17 Joseph P. Hipp, Maj. USAF Director of Information		
19. KEY WORDS (Continue on reverse side if necessary and identify by block number) composites finite elements		
20. ABSTRACT (Continue on reverse side if necessary and identify by block number) The structural stiffness properties of composite laminated plates are experimental information needed in order to design aircraft components manufactured with composite materials. A common test used to obtain the necessary moduli is to apply a tension load on the ends of the specimen. Little study, if any, has been reported relating the application of the Saint Venant's		

1
principle within a multi-ply laminated plate.

Previously, researchers have shown that routine application of Saint Venant's principle in problems involving a single composite lamina is not generally justified. This study offers justification for using Saint Venant's principle in commonly laid-up graphite epoxy plate specimens. The boundary conditions considered are attempts at modeling varying end supports for an in-plane loading. The analysis has been carried out using a finite element model considering three aspect ratios: 3, 5, and 10.